In compliance with the
Canadian Privacy Legislation
some supporting forms
may have been removed from
this dissertation.

While these forms may be included
in the document page count,
their removal does not represent
any loss of content from the dissertation.

**University of Alberta**

# Applications of Solid Phase Peptide Synthesis and Computer Modeling to Drug Delivery

by

Gary Hugh Van Domselaar 

A thesis submitted to the Faculty of Graduate Studies and Research in partial fulfillment of the requirements for the degree of Doctor of Philosophy

in

Pharmaceutical Sciences

Faculty of Pharmacy and Pharmaceutical Sciences

Edmonton, Alberta

Fall 2003

*Your file Votre référence*
*ISBN: 0-612-88061-3*
*Our file Notre référence*
*ISBN: 0-612-88061-3*

**University of Alberta**

**Library Release Form**

**Name of Author:** Gary Hugh Van Domselaar

**Title of Thesis:** Applications of Solid Phase Peptide Synthesis and Computer Modeling to Drug Delivery

**Degree:** Doctor of Philosophy

**Year this Degree Granted:** 2003



SEPTEMBER 29, 2003

**University of Alberta**

**Faculty of Graduate Studies and Research**

The undersigned certify that they have read, and recommend to the Faculty of Graduate Studies and Research for acceptance, a thesis entitled "Applications of Solid Phase Peptide Synthesis to Drug Delivery" submitted by Gary Hugh Van Domselaar in partial fulfillment of the requirements for the degree of Doctor of Philosophy in Pharmaceutical Sciences.

Dr. David S. Wishart

Dr. Mavanur R. Suresh

Dr. Afsaneh Lavasanifar

Dr. Robert S. Hodges

Dr. Paul G. Scott

SEPT 25, 2003

## Abstract

Polymer-based drug delivery systems improve the performance of a variety of therapeutic drugs by increasing efficacy and reducing side effects. Most of these delivery systems rely on traditional homopolymer formulations synthesized using traditional polymer chemistries. Peptide synthesis is a promising alternative strategy for nano-engineering polymeric drug delivery systems, in that it affords fine control over the polymer composition, can incorporate a diverse array of amino acid subunits, and provides a simple and readily accessible chemical protocol for the peptide and polymer synthesis. Two studies were conducted to investigate the feasability of using solid phase peptide synthesis (SPPS) in constructing drug delivery systems. The first study investigated the ability to construct, entirely using SPPS, a $^{99m}$Tc-chelator-peptide system for diagnostic radioimaging. A combination of a benzoyl-protected triglycine bifunctional chelator linked to a triproline spacer could be assembled on to the N-terminii of peptides during the peptide synthesis. The final constructs chelated $^{99m}$Tc with high efficiency and high purity while retaining receptor binding capability. The second study investigated the ability to engineer poly(ethylene oxide)-*block*-polypeptide (PEO-*b*-peptide) block copolymers for use as micelle-based drug delivery systems. Micelle-forming block copolymers were prepared using a synthetic strategy of SPPS for construction of the peptide block followed by solution phase condensation with the PEO block. A variety of PEO-peptide block copolymers were synthesized and their micellization properties examined. One construct in particular [$PEO_{5000}$-*block*-poly(tyrosine)$_{15}$] was found to have suitable properties for drug delivery. The significant amount of trial-and-error encountered in optimizing these peptide-based polymer

therapeutics prompted an investigation in to the *in silico* modeling of nonionic amphipathic block copolymer micelle formation. Micelle simulations were performed in a 40x40x40 cubic lattice on a system of 200 amphipathic unimers using a Monte Carlo energy minimization algorithm. The model successfully simulated micelle formation and critical micellization temperature. These experiments show that peptides and SPPS may be successfully applied to the engineering of drug delivery systems, and that computer modelling of micelle behaviour may eventually lead to a reduction in the amount of experimentation involved in designing and optimizing these systems.

**Acknowlegements**

I would like to thank past and present members of the Wishart lab, especially David Wishart, for providing an outstanding research environment. Alan Gibbs, Paul Stothard, Lena Andrew, Alex Nip, Haiyan Zhang, Diane Jette, Yunjun Wang, Trent Bjorndahl, Scott Watson, and Subee Okarvi were a tremendous help, always eager to share their expertise, knowledge, and encouragement. Ryan de los Angeles, Dong Luo, Steve Neal, Anuj Ranjan, Ian Forsythe, Wei Xia, Yi Zhang, Hassan Monzavi, Bahram Habibi-Nazhad, Steve Neal, Kathy Wang, Xiaoli Dong, Albert Leung, Nelson Young, Kavoos Basmenji, Zhan Chang, Rajarshi Maiti, Shan Sundaraj, Anchi Guo, Sudeepa Bhattacharyya, Godwin Amegbey, Scott Ellerbeck, Ping Li, Ashenafi Abera, Imke Gronwald, Michael Madlansacay, Yamini Ramamoorthy, Anuj Ranjan, Caspar Zhang, Robert Yang, and Dan Tzur were a source of good advice, clever ideas, and stimulating conversation.

Numerous researchers outside the lab have made my time at the University of Alberta enjoyable and productive, including committee members John Samuel, Mavanur Suresh, and Glen Kwon; professors Robert Hodges, Afsaneh Lavasanifar, and James Diakur; graduate students Donald Husereau, Rodney Gagne, and Mesfin Fanta; and researcher Kevin Morin.

I thank my friends Markle Verhagen, Amy Nugent, Thaddius Welch, Lorne Burke, and Jack Moore for their support over the years. I also thank especially my parents Lynn and Michael Taylor, and Gary Van Domselaar, Sr., and my siblings James, Barbara Jane, and Desiree. They have always supported me at all times of my life, good and bad.

I dedicate this thesis to the people who are no longer in my life, but will always have a place in my heart: Jane Anne Nagel and Daniel John Van Domselaar.

## Table Of Contents

## List of Tables

## List of Figures

## List of Abbreviations

| | |
|---|---|
| AADT | amine-amide-dithiol |
| AmB | amphotericin |
| BBB | blood-brain barrier |
| BFCA | bifunctional chelating agent |
| Boc | Nα tert butyloxycarbonyl |
| Caco | colon adenocarcinoma |
| CDDP | cis-diammine-dichloroplatinum, cisplatin |
| CDR | complementarity determining region |
| CMC | critical micelle concentration |
| CMT | critical micelle temperature |
| DADT | diaminedithiol |
| DDAVP | 1-deamino-8-D-arginine vasopressin, desmopressin |
| DHT | dihydroxytestosterone |
| DMF | N,N-dimethylformamide |
| DTT | dithiothreitol |
| EPR | enhanced permeation and retention |
| ESMS | electrospray mass spectrometry |
| Fmoc | 9-fluorenylmethoxycarbonyl |
| GRP | gastrin releasing peptide |
| HBTU | O benzotriazole N,N,N',N' tetramethyluronium hexafluorophosphate |
| HPLC | high performance liquid chromatography |
| IMC | indomethacin |
| mAb | monoclonal antibody |

| | |
|---|---|
| MAG3 | mercaptoacetyltriglycine |
| MAPT | amino-phenoxyethane |
| MBHA | methylbenzhydrylamine |
| MDR | multi-drug resistance |
| MFT | mean field theory |
| MRP | multi-drug resistance - associated protein |
| MTX | methotrexate |
| MUC-1 | tumor associated antigen polymorphic endothelial mucin core protein |
| NGF | nerve growth factor |
| NMM | N-methyl morpholine |
| PCL | poly ($\epsilon$-caprolactone) |
| PEO-*b*-PAsp(DOX) | doxorubicin conjugated PEO b poly($\alpha$,ß-aspartic acid) |
| PEO-*b*-PBLA | Poly(ethylene oxide)-block-poly(ß-benzyl L-aspartic acid) |
| PEO-*b*-PS | poly(ethylene oxide)-block-polystyrene |
| PEO | poly(ethylene oxide) |
| Pgp | P-glycoprotein |
| PHAA | PEO-*b*-poly(2-hydroxyethyl aspartamide) |
| Pic | picolinic acid |
| PLGA | polylactide-co-glycolide |
| PLLA | poly (L-lactic acid) |
| PPO | poly (propylene oxide) |
| PSA | preformed symmetric anhydride |
| RCP | radiochemical purity |
| RES | reticuloendethelial system |
| SCF / SCFT | self-consistent field theory |
| SCLC | small cell lung carcinoma |
| SEC | size exclusion chromatography |

| | |
|---|---|
| SPC | solution-phase condensation |
| SPOC | solid phase organic chemistry |
| SPPS | solid phase peptide synthesis |
| TB | target-to-background |
| TEM | transmission electron microscopy |
| TFA | trifluoroacetic acid |
| WBC | white blood cell |

# CHAPTER 1. INTRODUCTION

## 1.1. Application of Synthetic Peptides in Drug Targeting and Drug Delivery

### 1.1.1. Preamble

Since its introduction in the 1960s, solid-phase peptide synthesis (SPPS) has become an indispensable technology in the fields of medicine and biology. Today, synthetic peptides are routinely used in many areas of research and industry. For instance, to better understand peptide-receptor interactions from a pharmacological and biochemical perspective, structure-function studies have been conducted on synthetic versions of many biologically important peptides including gastrin [1], oxytocin [2], vasopressin [2], glucagon [3], gonadotropin releasing hormone [4], somatostatin [5], angiotensin [6], α-melanotropin [7], and δ-opioid [8] peptides. Synthetic peptides are used to determine the substrates of many proteinases, an important class of proteins involved in many critical aspects of bodily functioning such as food digestion, blood coagulation, blood pressure regulation, phagocytosis, peptide hormone regulation, neuromodulation, and regulation of peptide-messengers [9]. Synthetic peptides are used extensively in immunology for the study of antigen-antibody interactions, epitope mapping, and production of monoclonal and polyclonal antibodies for diagnostic and therapeutic purposes [10]. Synthetic peptides play an important role as therapeutics as well. Some prominent examples of available synthetic peptide drugs include calcitonin [11], desmopressin (also known as DDAVP) [12], octreotide [13], and vasopressin [14]. Synthetic peptides offer much promise as vaccines, where they are easier and cheaper to

prepare, and cause fewer side effects than conventional vaccine technologies (i.e. live attenuated and inactive vaccines). Promising synthetic peptide vaccine candidates currently in clinical trials include the *GP100*:209-217 (210) antigen against melanoma [15], and an anti HIV peptide based on the HIV-1 gag V3 loop [16]. A brief introduction to SPPS is given in Section 1.2 of this chapter.

An emerging use for synthetic peptides is in the field of drug delivery and drug targeting. In fact, synthetic peptides possess many qualities that make them especially well suited to this application. Foremost is the ability to control their composition and thus their function. This feature allows researchers to engineer synthetic peptides with custom behaviors. Another important feature of synthetic peptides for drug delivery is their targetability. Synthetic peptides can be made to bind the receptors of their naturally produced analogs. By conjugating drugs or drug delivery vehicles to these targeting peptides, synthetic peptides can be used to pilot drugs from their site of administration to their site of action [17]. Finally, peptides are biocompatible and biodegradable, and through proper design one can modulate their biological activity, making them safe for use in drug formulation. These factors combine to make synthetic peptides versatile materials for the engineering of drug delivery vehicles.

This dissertation focuses primarily on the application of SPPS in two areas of advanced drug delivery: peptide-based radiopharmaceutical delivery and block copolymer micelle-based drug delivery. Peptide-based radiopharmaceutical delivery involves the targeting of a therapeutic or diagnostic radionuclide to a specific target by attaching the radionuclide to a peptide that binds to a receptor that is overly or exclusively expressed by the target tissue or pathogen. Peptide-based

radiopharmaceuticals are discussed in Section 1.3 of this chapter and are the subject of Chapter 2. Amphipathic block copolymer micelles are supramolecular aggregates formed from polymers comprised of alternating hyrdrophobic and hydrophilic segments that form spontaneously when exposed to a solvent that is selective for one segment of the block copolymer but not the other. Amphipathic block copolymers have been studied in detail for their ability to deliver hydrophobic small molecule drugs that have low solubility *in vivo* [18]. An introduction to the use of block copolymer micelles as drug delivery vehicles is given in Section 1.4 of this chapter. Peptide-based block copolymer micelles for drug delivery are the subject of Chapter 3.

Modeling block copolymer micelle behaviour is a field of study more closely related to physical chemistry than to drug delivery, yet it is still quite relevant to drug delivery in that it attempts to predict micelle behaviours such as formation, stability, solubization, and interactions at interfaces. Assessing these problems empirically is a labour-intensive and time-consuming process, therefore any information that can help decide which block copolymer-drug formulations are worth pursuing from a physicochemical standpoint is welcome information indeed. An introduction and overview of nonionic, amphipathic block copolymer modeling is presented in Section 1.5 of this chapter. Chapter 4 describes some early work on Monte Carlo simulations of block copolymer formulation.

## 1.2. Introduction to Solid Phase Peptide Synthesis

Solid phase peptide synthesis (SPPS) was first introduced by Bruce Merrifield in 1963 [19]. Since that time, this revolutionary technology has now become by far the

most common strategy for the chemical synthesis of peptides and their derivatives. The SPPS methodology provides biological researchers with the means for quick, efficient, and even automated chemical construction of peptides and small proteins. As a result, there has been an explosive growth in the research and in the medicinal application of this fundamentally important class of biomolecules. SPPS technology has since been applied to the construction of oligonucleotides and more recently, to solid phase organic chemistry (SPOC), also called "combinatorial chemistry": the construction of small molecule libraries. In recognition of the contribution of SPPS to the advancement of science, Dr. Merrifield was awarded the 1984 Nobel Prize in Chemistry.

The general idea of SPPS is illustrated in Figure 1.1. Central to SPPS is the concept of synthesis on a solid support. The solid support allows the attached peptide to be easily removed from the byproducts of synthesis by a simple filtering process. Multistep reactions can be performed on the solid support without the need for laborious and inefficient purification steps during the intermediate stages of peptide synthesis, as is required using conventional solution-phase chemical synthesis techniques. As a consequence of this technology, several important advantages over solution phase synthesis have been realized. Practical peptide lengths achievable by SPPS have been extended to approximately 35 residues (versus approximately 10 residues using classical solution phase synthesis), and there are reports of the successful SPPS of very large peptides or small proteins using the stepwise solid phase approach, including: insulin (51 residues) [20], Lysozyme (129 residues) [21], Interferon-γ1 (166 residues) [22], and an analog of growth hormone (188 residues) [23]. Prior to the introduction of SPPS, the effort required to synthesize even a small (under 10 residue) peptide often was enormous,

typically involving the coordinated efforts of several highly trained chemists and many months or even years of work. For example, the synthesis of oxytocin, a 9-residue cyclic disulfide peptide by du Vigneaud and coworkers in 1953 took a half-dozen chemists nearly a year to synthesize [24]. The achievement contributed significantly to du Vigneaud's award of the Nobel Prize in Chemistry in 1955. Today, a single lab technician operating a modern peptide synthesizer can reasonably produce high-purity (>95%) peptides of up to 35 residues in under a week.

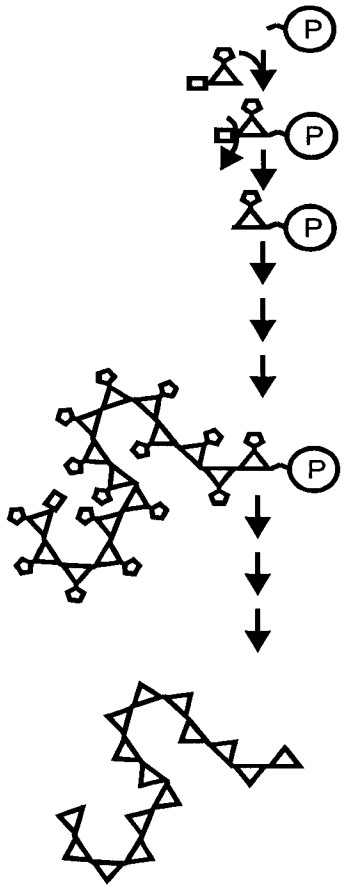


Figure 1.1. General concept of SPPS. The open circle labeled 'P' represents the functionalized solid support. Triangles represent amino acids with Nα-protection (open squares) and side-chain protection (open hexagons). Protected amino acids are assembled stepwise on to the solid support. Upon completion of synthesis, side-chain protection and the solid support are removed to yield the crude peptide.

SPPS involves four main steps (see Figure 1.2): 1) assembly of the protected peptide on the solid support; 2) removal of the protecting groups and cleavage of the peptide from the solid support; 3) purification of the crude peptide product; and 4) characterization of the resulting peptide. Although many variations exist for the synthesis, cleavage, deprotection, purification, and characterization of peptides, a "standard set" of operations for SPPS have been adopted. For peptide construction, two main strategies exist, identified by the amino acid protection scheme: the acid-labile $N^{\alpha}$-tert-butyloxycarbonyl (Boc) [19] strategy and the base-labile 9-fluorenylmethoxycarbonyl (Fmoc) strategy [25]. Boc chemistry relies on the graduated acid lability of the side chain and Na-protecting group. The Na-boc group is removed by treatment with the 'weak' organic acid TFA, whereas the side-chain protecting groups are removed only by treatment with a strong mineral acid such as hydrofluoric acid. Fmoc chemistry uses a base labile Nα-protecting group and base-insensitive side chain protection. Side chain protecting groups are removed after synthesis by treatment with acid, such as TFA.

There also exist several classes of amino acid activation and coupling methods: the preformed symmetric anhydride (PSA) approach, the active ester-based approach, and the use of uronium and phosphonium salts. Cleavage and side-chain deprotection of the completed peptide-resin is carried out by exposure to a mixture of "cleavage cocktail" in strong acid such as hydrofluoric acid (HF) for Boc chemistry or trifluoroacetic acid (TFA) for Fmoc chemistry. For purification of crude peptides, preparative reversed-phase high-performance liquid chromatography (RP-HPLC) is used almost universally. For

peptide characterization, a combination of analytical RP-HPLC (for purity determination) and mass spectrometry (for composition verification) are used routinely.

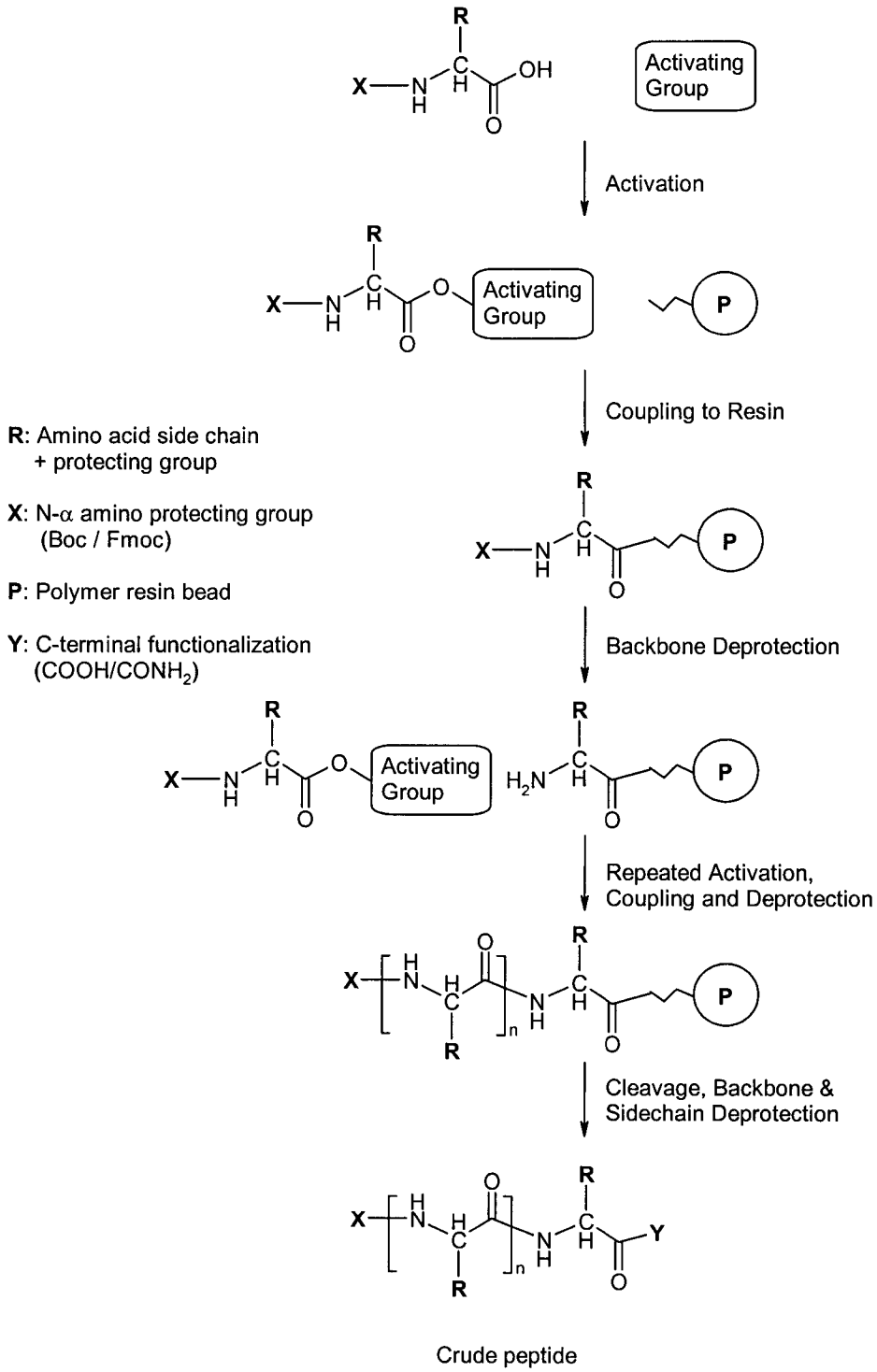


Figure 1.2. General scheme of solid phase peptide synthesis.

## 1.3. Review of $^{99m}$Tc-based Peptide Radiopharmaceuticals

### 1.3.1. Preamble

Peptide-based radioimaging agents are a very active subject of research due largely to their ability to produce high quality radioimages. This superior imaging ability is most ably demonstrated by the clinical use of [$^{111}$In]DTPA-Octreotide, currently the most commonly used radiopharmaceutical for lymphoma tumour imaging [26]. Peptides have been labeled with various radioisotopes, including $^{123}$I, $^{125}$I, $^{131}$I, $^{111}$In, $^{99m}$Tc, and others (albeit to a lesser degree) [27]. Of these, $^{99m}$Tc is ideally suited for diagnostic nuclear medicine, for three main reasons. First, $^{99m}$Tc is a $\gamma$-emitter; it does not emit $\alpha$ or $\beta$ particles that would expose a high dose of dangerous radiation to the patient. Also, the half-life of $^{99m}$Tc is 6 h, which is long enough to allow for the preparation of the radiopharmaceutical, but short enough to avoid a harmful radiation dose to the patient. Second, $^{99m}$Tc is readily obtained from simple $^{99}$Mo/$^{99m}$Tc generators (a column containing the parent radionuclide, $^{99}$Mo and its decay product $^{99m}$Tc). This eliminates the need for an on-site nuclear reactor or particle accelerator, making $^{99m}$Tc the least expensive radionuclide available. Finally, as a transition metal located at the center of the periodic table, $^{99m}$Tc can exist in several oxidation states (from –1 to +7); consequently, $^{99m}$Tc possesses a diverse chemistry which allows for many different approaches in developing $^{99m}$Tc-based radiopharmaceuticals. Nearly 80% of all radiopharmaceuticals used in nuclear medicine are $^{99m}$Tc labeled compounds [28]. This section presents the medical and chemical considerations for this important class of radiopharmaceuticals, and reviews the more important technetium-labeled radiopharmaceutical peptide constructs developed to date.

### 1.3.2. Requirements for $^{99m}$Tc-based Peptides

In the development of $^{99m}$Tc-based peptides for clinical use, a number of issues must be addressed. First, the $^{99m}$Tc-labeled peptide must be biologically efficacious: it must have high uptake in the target organ, a high target-to-background (TB) ratio, and favorable pharmacokinetics. Second, the labeled peptide must have high radiochemical purity (RCP), at least 90% is required to qualify for clinical use [28]. Finally, because of the short half-life of $^{99m}$Tc, the labeled peptide must be amenable to kit formulation. A kit contains the peptide to be labeled along with all the other components required for radiolabeling, such as a reducing agent, a bulking agent, and a transfer agent if necessary.

### 1.3.3. Technetium Chemistry

Technetium is eluted from the $^{99}$Mo/$^{99m}$Tc generators in the form of pertechnetate $[^{99m}TcO_4]^-$. No effective chemistry exists for attaching pertechnetate to peptides, and so it must first be reduced from $^{99m}$Tc(VII) to a lower oxidation state and then attached to the peptide by chelation. The final oxidation state of $^{99m}$Tc after reduction depends on the reducing agent, reagents, and the chelating ligand present. The $[TcO]^{3+}$ core is stable in the presence of a strong chelating ligand and has therefore become the most frequently used core for radiopharmaceutical purposes [12]. $[TcO]^{3+}$ forms a square pyramidal oxotechnetium complexes with tetradentate ligands such as the $N_4$ propylene amine oxime, the $N_3S$ triamidethiols, $N_2S_2$ monoamidemonoaminedithiols, and $N_2S_2$ diaminedithiols. An alternate technetium core used in radiopharmaceuticals is the $[TcO_2]^+$ core. $[TcO_2]^+$ forms octahedral complexes with polydentate ligands containing phosphine P donor atoms [29] or N/thioether S donors [30]. This technetium

core has been used as a heart imaging agent [31], and has been used in $^{99m}$Tc labeling of a somatostatin analog [32].

### 1.3.4. The Bifunctional Chelating Agent

Peptides for technetium labeling are designed as conjugates of the targeting peptide and a technetium chelator (termed a BiFunctional Chelating Agent or BFCA). Sometimes the BFCA and peptide are joined through a linker in order to prevent them from interfering with each other. BFCAs for chelation with $[TcO]^{3+}$ are typically tetradentate, and therefore occupy all of the available coordination sites on the $[TcO]^{3+}$ core. Many ligands are available for chelating the $[TcO]^{3+}$ core and are characterized by the donor atoms involved: the $N_4$ triamineoxime [33], the $N_3S$ triamidethiols [34], the $N_2S_2$ diaminedithiols [35], and the $N_2S_2$ monoamidemonoaminedithiols [36]. One notable exception to the use of tetradentate ligands is hydrazinonicotinamide (HYNIC). Unlike the tetradentate ligands, HYNIC coordinates "naked" technetium through a single amide moiety and therefore a coligand (such as tricine) is required to complete the square pyramidal coordination sphere. The use of the HYNIC group as a BFCA is especially attractive because it labels very easily and efficiently, and is easily incorporated into peptides. It has been used for the radiolabeling of chemotactic peptides [37] and somatostatin analogs [38]. A diagram depicting ligand binding to the technetium core is provided in Figure 1.3.

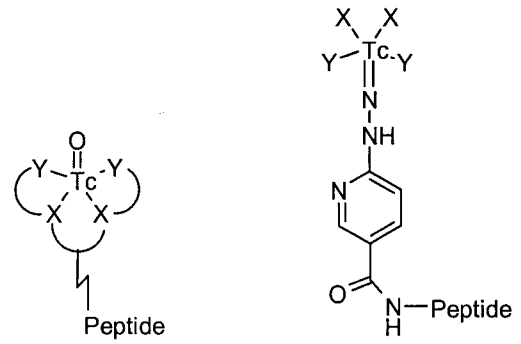


Figure 1.3. Technetium cores and chelating ligands used in peptide radiolabeling.

One important aspect of technetium chelation is isomerism. Given that both the $[TcO]^{3+}$ core and the [Tc]HYNIC core possess a square pyramidal geometry, ligand coordination can give rise to a number of different isomers. Ligands containing a single chiral centre will form epimers, due to the *syn* and *anti* binding to the technetium core. In a similar fashion ligands with two or more chiral centres will form diastereomers, and even achiral ligands will form enantiomers because of the asymmetric bonding to the technetium core. These isomers can potentially have different lipophilicities and biodistributions. In the specific case of $^{99m}$Tc peptide radiopharmaceuticals however, the physical and biological properties are a function of both the technetium chelate and the peptide. When the peptide size is much larger than the chelate, as is often the case, the contribution of the technetium chelate to overall biodistribution and lipophilicy is small relative to the targeting peptide. As a result, for Tc-BFCA-peptide constructs, the difference in lipophilicities and biodistribution attributable to the different forms of overall construct tends to be minimal.

### 1.3.5. Radiolabeling

Three main approaches exist for radiolabeling proteins and peptides: 1) direct labeling, 2) the preformed chelate approach, and 3) indirect labeling [39]. The direct approach involves the use of a reducing agent to convert disulfide bonds to free thiols, which bind technetium. Although simple to carry out, the direct labeling method has little control over the technetium binding specificity, and is generally not applicable for peptides as they typically do not possess a disulfide bond or else the disulfide bond is too critical to the biological activity of the peptide to be reduced. The preformed chelate approach involves the chelation of technetium to the BFCA followed by attachment of the BFCA-Tc chelate to the peptide. In this approach the chemistry is better defined than for the preformed chelate and does not expose the peptide to the sometimes quite harsh conditions required for chelation. The preformed chelate approach has been applied to radiolabeling studies of platelet IIb/IIIa receptor antagonists for thrombus imaging [18], however the conjugation is complex and time consuming to carry out, and therefore are generally not suitable for clinical use. In the indirect labeling approach, the BFCA is attached to the peptide through the N-terminus, C-terminus, or through a reactive group on a side-chain. Radiolabeling is effected by reduction of $^{99m}TcO_4^-$ in the presence of the BFCA-peptide conjugate or a transfer ligand such as $^{99m}$Tc glucoheptonate. Because of the well-defined chemistry and efficient, straightforward labeling, the indirect labeling approach is the most practical for peptide radiopharmaceutical development.

### 1.3.6. $^{99m}$Tc-Based Radiopharmaceutical Peptides

The spectrum of pathological conditions for which peptide radiopharmaceuticals are suitable is subject to several restrictions. Chief among these is

that the therapeutic target must differentially or exclusively express a receptor for which the peptide can bind with high affinity and specificity. This requirement is necessary in order to achieve a sufficient target-to-background (TB) ratio for radioimaging. Another important consideration concerns the accessibility of the pathological condition to the radiopharmaceutical peptide. Soluble peptides generally cannot cross biological membranes such as the blood-brain barrier unless specifically designed to interact with a specialized transport mechanism [40]. Because of this, pathological conditions that require the radioimaging agent to traverse one or more membrane barriers in order to reach their target receptor generally are not good candidates for peptide-based radioimaging. Additionally, upon administration peptides are exposed to numerous proteolytic enzymes and can be degraded quite quickly. The combination of rapid peptide degradation and short $^{99m}$Tc half-life greatly restricts the time available for the labeled peptide to accumulate at the target site (on the order of hours). Hence the target site must be quickly accessible to allow for sufficient accumulation before the labeled peptide degrades or loses too much activity. The targets that best meet these requirements for $^{99m}$Tc-peptide based imaging and therapy are: 1) either blood-borne or accessible by extravasation, and 2) targets that sufficiently overexpress a peptide receptor so that the pathological target can be adequately imaged or treated. To date, three pathological conditions have been identified that fit these requirements: thrombus imaging, infection / inflammation imaging, and tumour imaging.

*1.3.6.1. Thrombus Imaging*

A thrombus is a blood clot that forms in the heart or blood vessels. Thrombus formations are common and potentially life threatening events. Current estimates suggest

that in North America over 5 million cases of deep vein thrombosis occur per year and that over 500 000 cases of pulmonary embolism occur, resulting in over 100 000 deaths [41]. Current technologies for radioimaging thrombi include $^{111}$In-labeled platelets [42], antiplatelet antibodies [43], radiolabeled fibrinogen [44], $^{125}$I- and $^{111}$In-labeled antifibrin antibodies [45], and $^{99m}$Tc-labeled peptides [46].

A thrombus is primarily comprised of fibrinogen and aggregates of red blood cells and platelets. Fibrinogen mediates the aggregation by binding to the GPIIb/IIIa receptor expressed by active platelets via the tripeptide sequence Arg-Gly-Asp (RGD). A number of peptide analogs derived from the RGD sequence have been studied for their potential as $^{99m}$Tc-based radioimaging peptides for imaging thrombi.

Carroll *et al.* have evaluated the thrombus imaging properties of cyclic RGD analogs with a variety of different chelators including amino-phenoxylethane (MAPT) amine-amide-dithiol (AADT), and HYNIC (Figure1.4) [47,48]. The peptide and BFCA are conjugated through a 6-aminocaproic acid linker in order to preserve the biological activity of the targeting peptide upon $^{99m}$Tc labeling. Using a canine arteriovenous shunt model, Carroll's group reported high thrombus uptake and thrombus-to-background ratios for the $^{99m}$Tc labeled peptide [48].

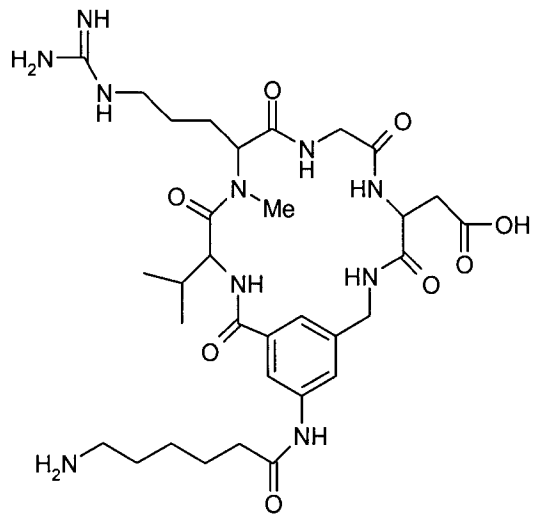

Figure 1.4 Structure of thrombus imaging peptide (cyclo) (D-Val)-(N-Me-Arg)-Gly-Asp-Mamb (Mamb = meta-aminomethylbenzoic acid) with 6-aminocaproic acid linker for BFCA conjugation.

Lister-James *et al.* have also developed a $^{99m}$Tc-labeled IIb/IIIa receptor binding peptide for thrombus imaging [49]. The receptor binding peptide, termed bipapcitide, is a dimer of two identical cyclic 13-residue peptides (apcitide) linked at their C-terminus. Apcitide contains an -Apc-Gly-Asp- sequence that acts as a mimetic of the RGD sequence (Apc is S-aminopropylcysteine, an arginine surrogate). Apcitide also contains a Cys(Acm)-Gly-Cys(Acm)- sequence for chelating technetium. $^{99m}$Tc labeling is performed by ligand exchange with $^{99m}$Tc[glucoheptonate]. $^{99m}$Tc-labeled bipapcitide gives excellent images of thrombus. The FDA approved bipapcitide in September 1998 for the detection and localization of acute venous thrombosis in the lower extremities [50].

*1.3.6.2. Infection / Inflammation Imaging*

The ability to image the focal site of an infection or inflammation is important for elucidating the cause of disease and for determining an appropriate therapeutic

regimen. Existing technologies for imaging the infection and inflammation include X-ray computed tomography, ultrasound, conventional radiography, magnetic resonance imaging, and radiography. Currently approved technologies for radioimaging of inflammation and infection include [$^{67}$Ga]citrate, $^{111}$In-labeled white blood cells (WBCs), and $^{99m}$Tc-labeled nonspecific polyclonal IgG's [51]. More recently researchers have been investigating the use of $^{99m}$Tc-labeled chemotactic peptides for imaging infection and inflammation.

The chemotactic peptide (N-formyl)-Met-Leu-Phe (fMLF) has been studied by Fischmann and colleagues for imaging infection and inflammation [52]. fMLF is a bacterial peptide that induces the migration of neutrophils to sites of inflammation by binding to high-affinity receptors on inflammatory cells. Fischman's group modified the fMLF C-terminus with HYNIC for technetium chelation. Radiolabeling was carried by ligand exchange with [$^{99m}$Tc]glucoheptonate. Imaging studies were conducted on rabbits induced with deep thigh *E. coli* infections using the radiolabeled peptide and $^{111}$In-labeled WBCs for comparison. They reported greater accumulation and a superior T/B ratio with radiolabeled fMLF compared to $^{111}$In-labeled WBCs after 18 h. They attribute their findings to the peptide's greater ability to diffuse into sites of infection.

A 23-residue peptide with the sequence Ac-Lys-Lys-Lys-Lys-Lys-Cys-Gly-Cys-Gly-Gly-Pro-Leu-Tyr-Lys-Lys-Ile-Ile-Lys-Lys-Leu-Leu-Glu-Ser has been investigated for its infection and inflammation imaging potential by Dean and coworkers [53]. This peptide, termed P483, is based on the C-terminal sequence of human platelet factor 4, a 29 kDa protein that binds to receptors on a number of different cell types including monocytes, hepatocytes, fibroblasts, and endothelial cells. P483 binds $^{99m}$Tc

via its -Cys-Gly-Cys- sequence. The N-terminal pentalysine sequence is intended to promote renal clearance. Using a rabbit infection model, $^{99m}$Tc-labeled P483-heparin complex was reported to bind to WBCs and showed superior uptake to sites of infection and a higher T/B ratio compared to [$^{111}$In]oxine-WBCs [52].

Tuftsin is a 4-residue chemotactic peptide (Tyr-Lys-Pro-Arg) derived from the constant fragment of IgG. Tuftsin promotes chemotaxis of neutrophils. Pollak's group used a $^{99m}$Tc-labeled tuftsin receptor antagonist (Pic-Ser-Cys(Acm)-Gly-Thr-Lys-Pro-Pro-Arg, Pic = Picolinic acid) for imaging inflammation [54]. The N-terminal Pic-Ser-Cys(Acm)-Gly unit was used for chelating $^{99m}$Tc via ligand exchange with [$^{99m}$Tc]glucoheptonate. They reported an excellent T/B ratio of 16.2 after 17 h post-injection in an infected rat model.

*1.3.6.3. Tumour Imaging*

Probably the most suitable application for radiolabeled peptides is in the area of target-specific tumour imaging agents. Currently, most research in this area has focused on the use of radiolabeled monoclonal antibodies (mAbs). Radiolabeled monoclonal antibodies target a specific antigen expressed by the tumour cell. They have proven to be quite effective in this regard and a number of them are used clinically, including: [$^{111}$In]Satumomab Pendetide for imaging of colorectal and ovarian carcinomas [55], [$^{99m}$Tc]Nofetumomab Merpentan for detection of small cell lung carcinoma [56], [$^{99m}$Tc]Arcitumomab for use in colorectal and ovarian carcinoma [57], and [$^{111}$In]Capromab Pendetide for imaging of pelvic lymph nodes [58].

Peptide-based radioimaging agents have shown clinical utility as well, and have several advantages over mAbs. Their smaller size allows for greater uptake at the tumour

site, and their more rapid clearance results in higher T/B ratios with less time [28]. One of the most commonly used radiopharmaceuticals in tumour imaging is [$^{111}$In]DTPA-Octreotide, a 13-residue analog of somatostatin used for the detection of somatostatin receptor-positive tumours including neuroendocrine cancer, carcinoid, and lymphoma [60]. However, the long half-life of $^{111}$In ($t_{1/2}$ = 67 h) and high cost are less desirable than that of $^{99m}$Tc for diagnostic imaging. As a consequence, numerous investigations are under way to develop [$^{99m}$Tc]peptide radiopharmaceuticals for tumour imaging [60].

Most investigations have focused on conjugating somatostatin analogs with various BFCAs including the $N_2S_2$ diamidedithiols [16], $N_3S$ triamidethiols [61,53,54], HYNIC [62], and propyleneamine oxime [63]. Of these, two $N_3S$-type chelators have shown considerable promise. P587 contains a Gly-Gly-Cys sequence that chelates technetium as an $N_3S$ triamidethiol [52]. P829 chelates technetium as an $N_3S$ aminediamidethiol using the sequence ($\beta$-Dap)-Lys-Cys ($\beta$-Dap = 2,6-diaminopimelic acid) [53,54]. Both P587 and P829 contain a Tyr-(D-Trp)-Lys-Val sequence for somatostatin receptor binding. Imaging studies conducted using a CA20948 somatostatin-positive pancreatic tumour-bearing rat model showed favorable tumour uptake for these $^{99m}$Tc-labeled somatostatin receptor-binding peptides compared to [$^{111}$In]DTPA-octreotide [53].

Receptors for the gastrin-releasing peptide (GRP) are over-expressed by a number of malignant tumours, including small cell lung, prostate, breast, and colon cancer [55,63-65]. Bombesin, a 14-reside peptide isolated from frog skin, is a close analog of GRP and binds with high affinity and specificity to the GRP receptor. Several

analogs of bombesin have been investigated as $^{99m}$Tc-labeled radioimaging agents by members of Wagner's lab [66] (John Hopkins University, Baltimore MD), and Volkerts group[67] (University of Missouri-Columbia, Columbia MO).

Wagner's group investigated the bombesin analogue (PyroGlu)-Gln-Lys-Leu-Gly-Asn-Gln-Trp-Ala-Val-Gly-His-Leu-Met-$NH_2$ ($Lys^3$-bombesin) [66]. They derivatized the $Lys^3$ sidechain with diaminedithiol (DADT) chelating agents. $^{99m}$Tc labeling was carried out using a glucoheptonate transfer ligand. An *in vitro* binding assay using rat brain membranes showed [$^{99m}$Tc]DADT-$Lys^3$-bombesin to have a comparable dissociation constant ($K_i$ = 4.3 ±1.0 nM) to that of [$^{125}$I]$Tyr^4$-bombesin (Ki = 0.5 nM).

Volkert's group studied novel dithiaphosphine ($P_2S_2$) based BFCAs using a 8-residue bombesin analog with the sequence Gln-Trp-Ala-Val-Gly-His-Leu-Met-$NH_2$ extended at the N-terminus with a 5-aminovaleric acid linker [67] . $^{99m}$Tc labeling was carried out using the preformed chelate approach with yields of ~60%. A high binding value ($IC_{50}$ = 0.8 ±0.4 nM) was determined by competitive binding to the GRP receptors on Swiss 3T3 mouse fibroblast cells using non-radioactive Re-labeled $P_2S_2$-bombesin and [$^{125}$I]$Tyr^4$-bombesin as the competitive bombesin analogue. Biodistribution studies with [$^{99m}$Tc]$P_2S_2$-bombesin showed rapid, predominantly renal clearance from the blood pool and nontargeted tissues, due presumably to the relatively hydrophilic $P_2S_2$ BFCA.

### 1.3.7. Development of an All-SPPS Methodology to Construct Radiopharmaceutical Peptides

The field of radiopharmaceutical peptide imaging systems has developed as a branch of 'traditional' radiopharmacy, where the focus has been primarily on radiolabeling with small chelators using traditional organic and inorganic chemistry.

Most radiopharmaceutical peptide synthetic strategies adopt this approach to design the chelator and linker, using SPPS exclusively for the construction of the targeting peptide. Excellent progress has been made using this approach, however, these synthetic strategies can be laborious, and can require a great deal of expertise in the design of a single construct. This need not be the case. The flexibility and engineerability inherent in SPPS can in principle be applied to the construction of the entire BFCA-linker-targeting peptide. An all SPPS approach would have the advantages of being biocompatible, automatable, and easy to construct.

In Chapter 2 of this thesis I describe the design, synthesis, preparation, and initial testing of a $^{99m}$Tc-labeled bombesin analog linked to a MAG3 chelator through a triproline linker (Figure 1.5) . This construct exhibits high $^{99m}$Tc-binding, resistance to transchelation, and minimal loss of receptor-binding capability. The entire BFCA-linker-peptide is easily constructed by SPPS, making this synthetic approach attractive and applicable for the construction of many other BFCA-peptide constructs for radioloabeling with $^{99m}$Tc.

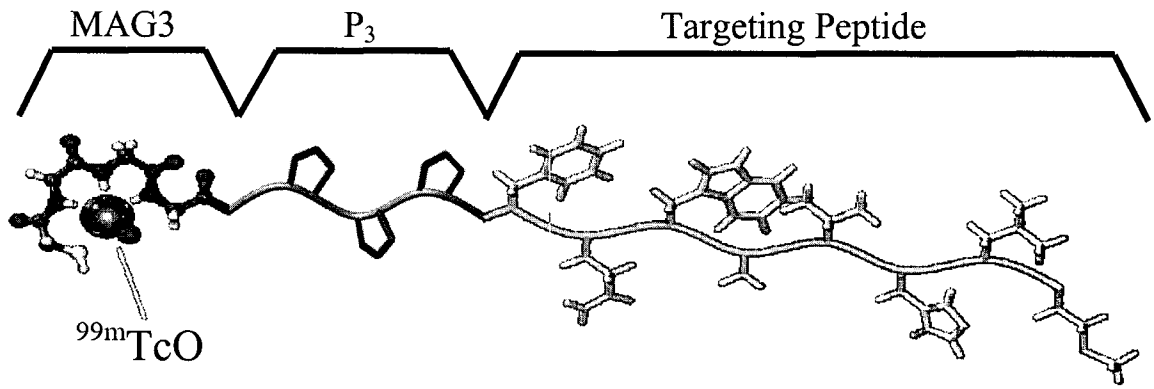


Figure 1.5 Design of MAG3-$P_3$-targeting peptide.

## 1.4. Review of Block Copolymer Micelles as Drug Delivery Vehicles

### 1.4.1. Preamble

Block copolymer micelles fall into the class of drug delivery systems known as nanoscopic drug carriers. Other members of this class include liposomes, cyclodextrins, antibody conjugates, lipoprotein particles, and viruses. Drug carriers at this scale (less than ~200 nm) are small enough to escape detection and elimination by the reticuloendothelial system (RES), yet are large enough (greater than ~10 nm) to avoid renal excretion. As a consequence, nanoscopic drug carriers have the very desirable property of being able to circulate in the vasculature for extended periods of time. Their small size also allows them to extravasate through leaky vasculature and, where lacking a lymphatic system, accumulate at the target site. This is known as Enhanced Permeation and Retention or EPR effect, a phenomenon associated with inflammation and often found in solid tumours. Thus, this type of delivery system is said to be "passively" targetable to these classes of disease, with the exception of MAb-drug conjugates. MAb-drug conjugates, by their nature, have the potential to selectively target any pathological conditions possessing the mAb's antigen and thus are "actively" targetable. A great deal of research is currently being conducted to impart active targetability to the other members of the nanoscopic drug carrier class by attaching targeting moieties to the drug carrier surface.

Block copolymer micelle-based nanoscopic drug carrier systems are receiving an increasing amount of attention, due to their ability to load hydrophobic small molecule drugs, long circulation times *in vivo*, and targetability [68,69]. Over the last two decades, the study and development of block copolymer micelles have since made tremendous

progress, due largely to the work of Kataoka, Kwon, Kabanov, Eisenberg, and their coworkers (for reviews, see [18,68-70]). This section describes the essential features of block copolymer micelles and their relevance to drug delivery, the technical aspects of their synthesis and characterization, and concludes with a review of recent developments of block copolymer micelles as drug delivery systems.

### 1.4.2. Compositional and Structural Aspects of Block Copolymer Micelles

Block copolymer micelles for drug delivery are based on amphipathic *AB*- and *ABA*-type block copolymers, i.e. polymers composed of alternating segments of hydrophilic (*A*) blocks and hydrophobic (*B*) blocks (Figure 1.6a). In aqueous environments, block copolymers can form micelles with a dense hydrophobic core surrounded by a dilute hydrophilic shell (Figure 1.6b).

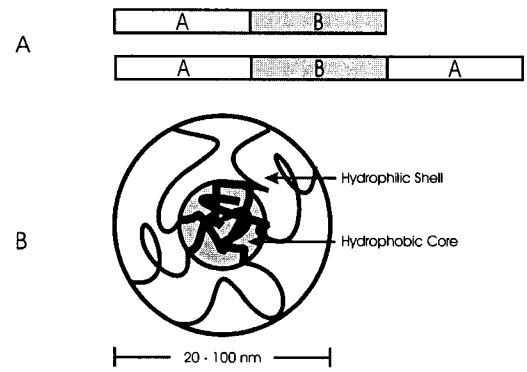


Figure 1.6. A) Diagram depicting the structure of amphipathic *AB* and *ABA* block copolymers. B) Cartoon diagram of a block copolymer micelle.

#### *1.4.2.1. The Hydrophilic Shell*

In a block copolymer meicelle, the micelle shell interacts with the outer environment and therefore determines the micelle's pharmacokinetics, biodistribution, and largely determines the micelle's physical and biological stability [69]. For drug

delivery applications, poly(ethylene oxide) (PEO) is used almost exclusively for the block copolymer hydrophilic shell-forming block because it is non-immunogenic, biocompatible, and amenable to synthesis at a variety of polymer lengths with high purity and low polydispersity. Additionally, PEO's high degree of hydration and large excluded volume induce repulsive forces between the chains at the polymeric density present at the core-shell interface. This repulsive force imparts a steric stability to the micelle by immobilizing the chains, essentially anchoring them to the core[71]. This repulsive force also results in the PEO chains stretching away from the interface to form a "polymeric brush". The brush adsorbs water molecules, effectively presenting an 'aqueous-like' surface to the biological environment. This imparts biological stability to the micelle by preventing opsonization, thereby enhancing evasion of the RES [72]. Block copolymer micelle-based drug delivery systems that incorporate hydrophilic blocks other than PEO are used for special applications, such as poly(*N*-isoproylacrylamide) for thermoresponsiveness [73] and pH-responsiveness [74], or poly(acrylic acid) for bioadhesiveness [75].

*1.4.2.2. The Hydrophobic Core*

The hydrophobic micelle core provides the driving force for micellization and serves as the drug reservoir, thus the core determines the micelle's drug loading capacity, release rate, and to a large extent determines the micelle's physico-chemical properties. One of the defining features of polymeric micelles is their unusually high selectivity for the drug (or other small molecule) that it is intended to solubilize [76]. For maximum drug-loading capability the composition of the hydrophobic block and the drug must be similar, thus there is a much greater need for compositional variety for the hydrophobic

core-forming segment. Consequently, a much larger range of compositions have been synthesized and studied for core-forming segments compared to shell-forming segments, including as representative examples, polymers based on poly($\epsilon$-caprolactone) [77, 78], poly(lactide-*co*-glycolide) (PLGA) [79,80], poly(propylene oxide) (PPO) [81,82], and poly(aspartic acid) [18,83,84]. A common structural design of the core-forming block involves the covalent modification of the polymer segment with the chosen drug, a concept first proposed by Ringsdorf and coworkers [85]. These drug conjugates are designed either to increase the micelle core compatibility for physically loading the drug, or to release the conjugated drug upon micelle dissociation. An additional requirement for the core-forming block arises from the fact that upon administration *in vivo*, the drug-loaded block copolymer micelle is diouted in the blood compartment to concentrations below its critical micelle concentration (CMC). To prevent immediate dissociation into unimers (single unaggregated polymers), the combination of length and hydrophobicity of the core-forming block must be sufficient to form a solid or glass-like core upon micellization (i.e. the glass-transition temperature ($T_g$) of the micelle core must be above body temperature).

*1.4.2.3. The Hydrophilic Block / Hydrophobic Block Ratio*

For nonionic amphipathic diblock copolymers, the size ratio of the core-forming block to that of the shell-forming block is important for micelle formation and morphology. The hydrophilic block should have a higher molecular weight than the hydrophobic block in order to impart water solubility [86]. As the molecular weights between the segments become approximately equal, micelle structure becomes disordered [87] and can result in considerable variability in micelle size and

morphology, whereas a uniform size and narrow distribution of micelle size are crucial for controlling disposition in the body [88]. When ionic hydrophilic blocks are used as the micelle shell-forming segments, small hydrophilic block / hydrophobic block ratios (less than 0.5—known as "crew-cut" micelles) can form water-soluble micelles with well defined morphologies and narrow polydispersities [88]. The ionic character of the micelle corona is sufficiently polar to solubilize much longer core-forming blocks (upwards of 30 times larger); however it should be noted that micelle morphology and polydispersity are highly sensitive to the pH and ionic strength of the external medium, which is not the case for block copolymers with nonionic shell-forming blocks [88].

#### *1.4.2.4. Micelle Size Distribution*

Micelle size distribution describes the variation in diameter within a population of micelles. As mentioned earlier, a narrow size distribution is desirable for block copolymer micelles intended for drug delivery, and the same can be said of nanoscopic drug carriers in general. Particulate size determines RES recognition and tissue penetration (especially where an EPR effect is involved). As a result, nanoscopic delivery systems with large size distributions may undergo undesirable size-sieving during the disposition process in the body [89]. Polymeric micelles can have considerably narrow size distributions, comparable to viruses and lipoproteins, so the potential for size-sieving is minimal [90]. Indeed, the small size distribution, core/shell architecture, nanoscopic diameter, and ability to transport lipophilic substances in aqueous media make polymeric micelles structural and functional analogues of lipoproteins [91].

*1.4.2.5. Micelle Stability*

When developing micelle-based drug delivery systems, consideration of micelle stability is of fundamental importance. Micelle stability is characterized by two properties: static stability and dynamic stability. Static stability is a measure of the driving force of micellization, i.e. the free energy change between free unimers and micelles. Static stability is characterized by the critical micelle concentration (CMC): the minimum concentration of polymer required to spontaneously form micelles. The relationship between CMC and the Gibbs free energy change ($\Delta G$) is given by

$$\Delta G = -\ln RT \times CMC \tag{1.1}$$

The CMC is the most fundamental measure of micelle stability; however, from the perspective of drug delivery, micelle *dynamic* stability is more important. Micelle dynamic stability refers to the ability of a micelle to resist decaying into free unimers when diluted below their CMC, such as when they are introduced into the blood compartment [92]. Micelles are thermodynamically unstable below the CMC and will decay into free unimers. Micelle cores with a $T_g$ at or below the ambient temperature and only weak intramolecular cohesive forces exist in "open association", i.e. in equilibrium with free unimer [93]. Dilution of these micelles below their CMC results in an instant (on the order of milliseconds) decay into free unimers. Micelle cores with a $T_g$ that is significantly higher than ambient temperature, or cores with strong intramolecular cohesive forces exist in "closed association", i.e. in a "frozen" state [93]. These micelles dissociate slowly (hours or days) upon dilution below their CMC. For the purposes of drug delivery, polymer micelles must decay slowly under sink conditions, thus good dynamic stability is an absolute requirement.

*1.4.2.6. Block Copolymer Synthesis*

The route of synthesis chosen in the construction of a block copolymer is guided predominantly by the desired composition for each block and type of block copolymer (*AB*, *ABA*, *ABC* etc.). A well-established and widely practiced synthetic technique that is applicable to the construction of many block copolymer types and compositions involves the derivatization of one or both ends of an existing homopolymer with a polymerization initiator. The homopolymer is introduced into a solution containing the second monomer and initiates the polymerization of the second block copolymer on to the terminal end(s) of the first block. This synthetic scheme is depicted in Figure 1.7.

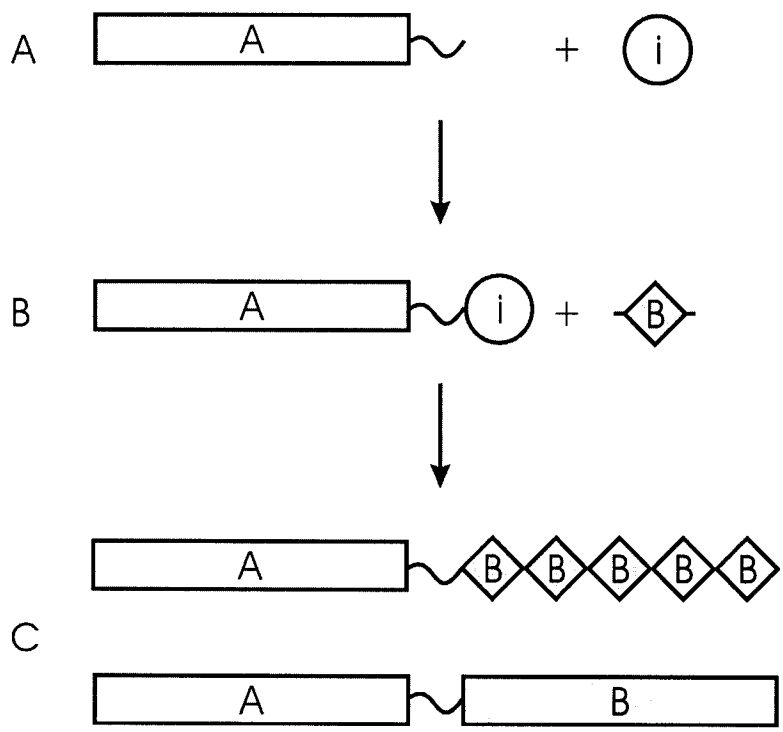


Figure 1.7. Synthesis of block copolymer by polymerizing one block to the terminus of the another. A) Homopolymer *A* is derivatized with an initiator *i* for the polymerization of the second block *B*. B) Introduction of the derivatized *A* block into a solution containing the *B* monomer initiates polymerization of *B* block on to the end of the *A* block, forming the *AB* block copolymer C).

An illustrative example of how block copolymers are constructed using this strategy can be found in the synthesis of the *AB* block copolymer PEO-*b*-poly(β-benzyl L-aspartic acid) (PEO-*b*-PBLA) [94]. For this construct, the primary amine of α-methyl-ω-amino-poly(ethylene oxide) is used to initiate the ring-opening polymerization of β-benzyl L-aspartate *N*-carboxyanhydride monomer to yield the PEO-*b*-PBLA block copolymer (Figure 1.7).

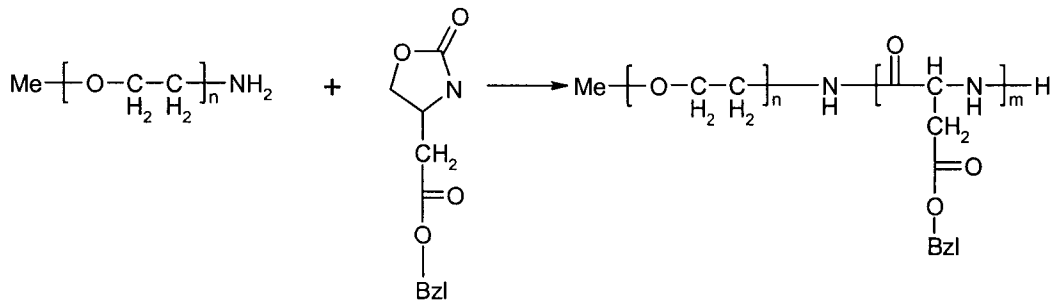

Figure 1.8. Synthesis of PEO-*b*-PBLA by ring opening polymerization of β-benzyl L-aspartate *N*-carboxyanhydride monomer with of α-methyl-ω-amino-poly(ethylene oxide).

An alternate method for block copolymer preparation involves the conjugation of preexisting end-functionalized homopolymers. Because each of the homopolymers can be synthesized under its own optimal conditions, the conjugation technique rivals the technique of polymerizing one block on to the end of another for its potential to create well-defined block copolymers with low polydispersity. The conjugation technique has been applied in the synthesis of PEO-*b*-polystyrene (PEO-*b*-PS) for optoelectronic applications [95], and in the synthesis of both PEO-*b*-poly(ε-caprolactone) and PEO-*b*-poly(DL-lactide) for controlled drug release formulation [96]. Copolymer block conjugation has also been applied to the construction of PEO-*block*-peptide micelles for drug delivery (this work, Chapter 3).

*1.4.2.7. Micelle Formation and Drug Loading*

Block copolymers form micelles when dissolved in a selective solvent, i.e. a solvent in which one block is soluble but the other block is insoluble. Where amphipathic, nonionic block copolymers for drug delivery are concerned, the aqueous environment of the body provides the selective solvent. Micellization is normally a spontaneous, entropically driven process, however, for micellization to occur the free block copolymer chains must initially exist as in an unaggregated state known as *unimers*. Simply adding dry block copolymer to an aqueous solution may not be sufficient for micellization if the hydrophobic block is sufficiently large and lipophilic to prevent the block copolymer from entering the solution. Instead, most block copolymers are first dissolved in a non-selective solvent (a solvent that can dissolve both blocks). Dissolution in non-selective solvent provides the necessary initial condition for micellization. The dissolved block copolymer is then introduced to the selective solvent where micellization occurs. In the field of drug delivery, two techniques have been widely adopted for the micellization of amphipathic, nonionic polymers: oil-in-water emulsion (o/w emulsion), and dialysis. The o/w emulsion technique uses a water-immiscible, volatile non-selective solvent to initially dissolve the block copolymer, such as chloroform. The solution is added to the selective (aqueous) solvent, with stirring, and the block copolymer partitions between the two phases. As the nonselective solvent evaporates, more block copolymer partitions into the aqueous phase with the formation of micelles until the nonselective solvent is completely gone. In the dialysis technique, a water-miscible nonselective solvent such as dimethylacetamide is used to dissolve the block copolymer. The selective solvent is gradually added. The solvent mixture becomes increasingly selective, inducing

the block copolymers to micellize. The micelle solution is then dialyzed against the final aqueous solution until the nonselective solvent is completely removed and micellization is complete.

The preferred method for loading hydrophobic drugs into block copolymer micelles is to noncovalently incorporate the drug into the micelle (physical loading) during the micelle formation step. The drug and block copolymer are coincubated in a nonselective solvent that is also a good solvent for the drug. The mixture is then added to the aqueous solvent and micellization allowed to proceed by o/w emulsification or dialysis. The hydrophobic small molecule drug initially partitions between the nonselective and selective solvent, with preference for the nonselective solvent. As the nonselective solvent concentration decreases and micellization proceeds, the drug partitions with increasing preference into the micelle core. When micellization is complete, an aqueous solution of drug-loaded micelles remains.

As an alternative to physical loading, drugs can instead be conjugated to the block copolymer, usually to the core-forming block. First introduced by Ringsdorf and coworkers [85], this method of drug loading involves the covalent attachment of drug to the side-chain of the core-forming block using a hydrolytically or enzymatically sensitive bond such as an ester or amide. Sufficiently hydrophobic drugs can be attached directly to provide the driving force for micellization, otherwise, the drug can attached through a hydrophobic linkage. Drug release is presumed to occur as the micelle degrades into free polymer chains and exposes the drug-polymer bond to the biological milieu. Interestingly, at least one study comparing the tumour reducing ability of drug-conjugated block copolymer micelles to drug-loaded, drug-conjugated micelles has been

performed. These workers showed high *in vivo* antitumour activity for the physically loaded system, whereas the drug-conjugated polymer micelle had negligible *in vivo* activity [97]. These results imply that drug-conjugated block copolymers may be better used to enhance the solubilization of physically loaded drug rather than serve as the single source of drug.

### 1.4.3. Review of Block Copolymer Micelle-Drug Systems

#### *1.4.3.1. PEO-b-poly(Aspartic Acid) Micelles*

Kataoka and Kwon have performed extensive studies on micellar drug delivery systems based on PEO-*b*-poly(aspartic acid) (for a review, see [98]). The most extensively studied system is based on doxorubicin-conjugated PEO-*b*-poly($\alpha,\beta$-aspartic acid) [PEO-*b*-PAsp(DOX)] (Figure 1.9). Doxorubicin, an antineoplastic with a broad spectrum of activity, is conjugated at the primary glycosidic amino group to the carboxyl side chains of the PAsp block. The PAsp(DOX) block of PEO-*b*-PAsp(DOX) is sufficiently hydrophobic to form micelles in an aqueous solvent. The intramolecular $\pi$-$\pi$ stacking of the DOX planar anthracene side-chain increases the cohesive forces in the core, which improves the micelle dynamic stability and accommodates the loading of free DOX into the micelle core [97, 99]. In a mouse tumour model, PEO-PAsp(DOX) micelles with chemically and physically bound DOX demonstrated prolonged circulation in blood and accumulation in solid tumour [100]. When compared to free DOX, PEO-*b*-PAsp(DOX) demonstrated reduced toxicity (5%), and higher antitumour activity.

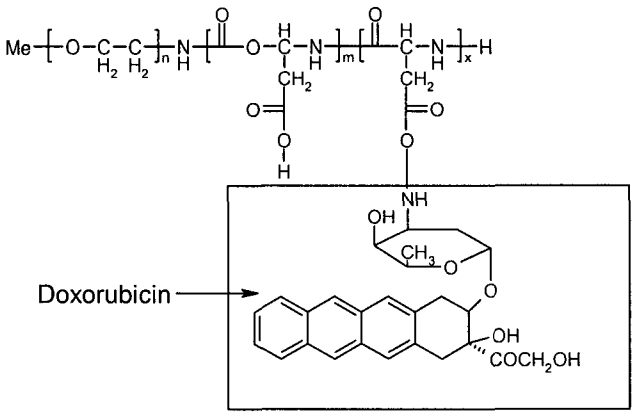


Figure 1.9. Structure of poly(ethylene oxide)-*b*-poly(α,β-aspartic acid)-doxorubicin conjugate.

These same researchers have investigated a similar system composed of PEO-*b*-poly(β-benzyl aspartic acid) (PEO-*b*-PBLA) for the purpose of developing a polymeric micelle system for the delivery of doxorubicin using only physical loading of drug [89]. PEO-*b*-PBLA was prepared via ring-opening polymerization of β-benzyl aspartate N-carboxyanhydride using α-methoxy-ω-amino-poly(ethylene glycol) as an initiator. Doxorubicin was loaded using the o/w emulsion method. Their studies showed DOX/PEO-*b*-PBLA micelles had a narrow size distribution (50–70 nm), high drug loading level (15 to 20 w/w %), and improved blood circulation relative to free DOX. DOX/PEO-*b*-PBLA micelles also showed significantly higher antitumour activity versus free DOX against the C26 mouse colon adenocarcinoma cell line.

PEO-*b*-PBLA has also been studied for its ability to load and release other drugs as well. In one study, PEO-*b*-PBLA micelles were investigated for their ability to physically load and release indomethacin (IMC), a powerful nonsteroidal anti-inflammatory drug and analgesic used in the treatment of fever, pain, and inflammation caused by rheumatoid arthritis [101]. IMC/PEO-*b*-PBLA was

characterized as having a narrow size distribution (19-29 nm) and a low CMC (18 mg/L). The release rate of IMC was found to be dependant on the pH of the medium, indicating that the release rate of IMC from the micelles is controlled by the partition coefficient of IMC based on the pH of the medium and interaction between IMC and the hydrophobic portion of the micelles.

Amphotericin B (AmB), a membrane active drug used in the treatment of systemic fungal diseases, has also been loaded into PEO-*b*-PBLA in an attempt to increase its solubility and lower its high potential systemic toxicity [102]. Compared to Fungizone (amphotericin deoxycholate), AmB/PEO-*b*-PBLA micelles showed reduced hemolytic activity (15 μg/ml AmB/PEO-*b*-PBLA required to initiate hemolysis compared to 1 μg/ml for Fungizone), and increased antifungal activity (4 to 8 times higher minimal inhibitory concentration compared to Fungizone). In a similar study, Lavasanifar *et al.* studied the AmB-loading properties of a PEO-*b*-PAsp derivative, using stearic acid esters of poly(ethylene oxide)-*b*-poly(hydroxyethyl L-aspartamide) [103]. Their studies showed that fatty acid derivatives of PEO-*b*-PAsp could ably load AmB, and could effect hemolysis. They also noted that the hemolytic activity of the AmB-loaded PEO-*b*-PAsp was strongly dependant on the level of stearate ester substitution: AmB-loaded micelles with 11% stearic acid substitution were able to induce hemolysis, whereas AmB loaded micelles with stearic acid substitution levels above 50% were completely non-hemolytic. A later study on the *in vivo* efficacy of AmB-loaded micelles showed that these formulations exhibited reduced *in vitro* hemolysis but retained potent *in vivo* antifungal activity, similar to that of Fungizone [104].

Other derivatives of PEO-*b*-PAsp have been studied as polymeric micelle-based drug carriers as well. Cisplatin (CDDP), a potent antineoplastic drug, has been chelated to PEO-*b*-PAsp by ligand exchange to form PEO-*b*-PAsp(CDDP) drug conjugate [105]. In a comparison with free CDDP, PEO-*b*-PAsp(CDDP) micelles showed approximately 20% reduced toxicity *in vitro*. *In vivo* studies using a mouse tumour model (MKN 45 human gastric cancer xenograft) showed higher and more sustained CDDP levels in tumour tissue, similar antitumour activity, and reduced renal damage compared to free CDDP.

A drug conjugate of PEO-*b*-poly(2-hydroxyethyl aspartamide) (PHAA) and the anticancer drug methotrexate (MTX) has been recently prepared and initial studies performed [106]. These MTX conjugate micelles were shown to self-assemble with average diameters of 14 nm as judged by transmission electron microscopy (TEM) analysis. Gradual release of MTX was observed to occur by ester hydrolysis. Micelle stability was found to increase by increasing the level of substitution of the core-forming block with the hydrophobic MTX, thereby increasing the hydrophobicity of the micelle core.

*1.4.3.2. PEO-b-Polyester Micelles*

Block copolymers with core forming blocks made from biocompatible polyesters such as poly(ε-caprolactone) (PCL), poly(L-lactic acid) (PLLA), and polylactide-*co*-glycolide (PLGA) comprise a major class of block copolymers for drug delivery (Figure 1.10). Homopolymers of PLLA, PCL, and PLGA have been studied extensively as structural materials for biomedical devices such as implants, sutures, and prosthetics. They have also been used in the preparation of biodegradable microspheres

for controlled release [92]. These medically important polymers contain hydrolytically sensitive ester bonds within the polymer backbone. The mechanism of micelle degradation for this class of polymers includes both dissociation into unimers as well as degradation of the polymer backbone from exposure to aqueous solvent.

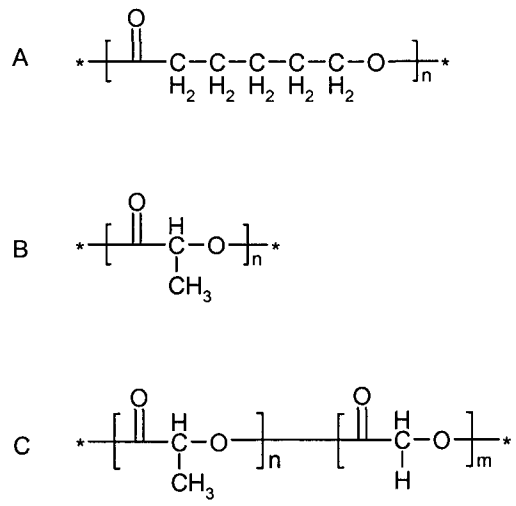


Figure 1.10. Chemical structures for A) poly(ε-caprolactone), B) poly(L-lactide), and C) polylactide-*co*-glycolide.

Eisenberg and coworkers have studied PEO-*b*-PCL diblock copolymer micelles loaded with the neurotrophic and immunosupressant drug FK506, and its structural analog, L-685-818 [107]. The drug was physically loaded into the micelles by dialysis from DMF to water. The drug-loaded micelles were compared to free drug for their ability to potentiate the ability of nerve growth factor (NGF) to promote differentiation of PC 12 rat pheochromocytoma cells. Potentiaton of PC 12 differentiation by NGF was demonstrated for both drug-loaded micelles, although the degree of cell differentiation was not as high as for free drug. The discrepancy was attributed to incomplete drug release from the micelle over the 48 h incubation period. In a later study by the same group, FK506/PEO-*b*-PCL was examined *in vivo* for the ability to repair peripheral nerve

injury [90]. They reported a significant increase in the rate of functional recovery of injured nerve when using micellar FK506.

Testosterone is a steroidal drug used in androgen replacement therapy. Currently available testosterone preparations have been found to have low potency and may be rapidly cleared by the liver, and are possibly hepatotoxic [108]. PEO-*b*-PCL micelles were loaded with the testosterone analog dihydroxytestosterone (DHT) and investigated for their ability to improve DHT's pharmacokinetic profile. An *in vitro* study of on the biological activity of DHT released from the polymeric micelles on HeLa cells bearing androgen receptor showed no appreciable difference from that of DHT alone. Drug release studies showed a sustained release of DHT when incorporated in PEO-*b*-PCL for one month compared to only 3 h for free DHT [108].

Kim and coworkers have studied PEO-*b*-PCL loaded with indomethacin (IMT) [109,110]. They reported high drug loading capabilities of PEO-*b*-PCL with IMT (42 w/w %). The release rate from polymeric micelles was sustained for 15 days. An unusually high range of diameters were reported for their IMT/PEO-*b*-PCL systems (100–160 nm), however, this size range is still possibly small enough to avoid removal from blood circulation by the RES.

Davis and coworkers polymerized lactide to α-methoxy, ω-hydroxy-PEO by ring-opening polymerization using stannous octoate as a catalyst [111]. They reported micelle diameters ranging from 15 to 19 nm. Drug loading studies were conducted using sudan black B and testosterone as model drugs. A large difference in maximum loading levels were observed for the two compounds: 63.9 w/w % for sudan black B versus 0.74

w/w % for testosterone. The large discrepancy is attributed to the much greater hydrophobicity of sudan black B (logP = 7.2) compared to testosterone (logP = 3.2).

Kataoka's group prepared α-aldehyde-PEO-*b*-PLA [112] and then conjugated peptidyl ligands [phenylalanine (Phe) and tyrosyl-glutamic acid (Tyr-Glu)] via reductive amination with $NaBH_3CN$ to condense the α-aldehyde-PEO-*b*-PLA to the peptide N-terminal amino group [113]. Approximately 50% peptidylation was reported for both the Phe and Tyr-Glu derivatized PEO-*b*-PLA block copolymers. Micelles formed from peptide-PEO-*b*-PLA were observed to have a mean diameter of 40 nm with an extremely narrow distribution (±0.4 nm) and low CMC (~3 mg/L). Surface charge measurements correlated well with the amount of conjugated Tyr-Glu, indicating that the Tyr-Glu residues situate on the outer surface of the micelles rather than buried in the micelle interior. The results of this study suggest that active targeting of polymeric micelles can be achieved using peptidic targeting ligands.

Micellar drug delivery systems based on PEO-*b*-polyglycolide (PEO-*b*-PLG) have not been studied in detail, because the relatively hydrophilic PLG block does not provide as high a driving force for micellization as PLA or PCL. Instead, random copolymers of polylactide-*co*-glycolide (PLGA) are used for the hydrophobic block. Indeed, there exists only one relevant drug delivery study involving micelles composed of PEO-*b*-PLG [114]. Kim's group, who studied the drug loading and release characteristics of block copolymers of PEO-*b*-PLG micelles loaded with indomethacin, as a companion study to their previous work with IMC/ PEO-*b*-PCL and IMC/PEO-*b*-PLGA. [109,114]. Interestingly, they found PEO-*b*-PLG micelles to have many favorable properties as a drug delivery vehicle for IMC, including: small size

(<200 nm), low CMC (1.57 x $10^{-7}$ mol/L), high loading capacity (25 w/w %), and slow release (60% IMC release over 12 days in phosphate buffered saline at pH 7.4 and 37 °C).

Kim's group has studied the triblock copolymer PEO-*b*-PLGA-*b*-PEO for its micellization properties, and for is ability to load and release two model drugs: the hydrophilic drug ketoprofin, and the hydrophobic drug spironolactone [116]. They note that specific compositions of PEO-*b*-PLGA-*b*-PEO exist as a free flowing sol at room temperature but becomes a transparent gel at body temperature. This interesting property suggests that drug-loaded PEO-*b*-PLGA-*b*-PEO micelle system may be promising candidate as an injectable drug delivery depot [116,117].

*1.4.3.3. PEO-b-PPO-b-PEO Micelles*

Poly(ethylene-oxide)-*block*-polypropylene-*block*-poly(ethylene oxide) (PEO-*b*-PPO-*b*-PEO), also called poloxamer, is a commercially available block copolymer (Pluronic) with widespread and industrial application as detergents, emulsifiers, and lubricants [118]. The structure of PEO-*b*-PPO-*b*-PEO is provided in Figure 1.11. The poloxamer block copolymer has been studied in some detail for its drug delivery properties [119]. Special attention has focused on exploiting the ability of poloxamer micelle formulations to promote drug penetration across biological barriers including the blood-brain barrier and the small intestine [119]. Other studies examine the effect of poloxamer micelle formulations for the treatment of multi-drug-resistant tumours [120-122]. Following is a brief review of the significant research conducted on poloxamer-formulated drug delivery systems.

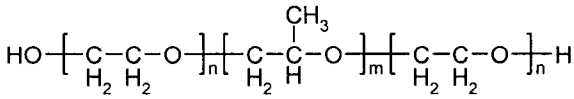

Figure 1.11. Chemical structure of triblock copolymer PEO-*b*-PPO-*b*-PEO.

Cells from multidrug-resistant (MDR) tumors overexpress "efflux proteins" that act to pump drugs out of a cell [121]. The MDR effect seriously complicates chemotherapy, making these tumours among the most difficult types to treat. Several studies have demonstrated that PEO-*b*-PPO-*b*-PEO block copolymer-drug formulations sensitize resistant cells, resulting in an increase of two to three orders of magnitude the cytotoxic activity of the drug on MDR tumours, including murine leukemias (P388, P388-Dox), subcutaneous murine myelomas (Sp2/0, Sp2/0-Dnr), intravenous and subcutaneous lewis lung carcinoma (3LL-M27), subcutaneous human breast carcinomas (MCF-7, MCF-7ADR), and human head and neck carcinoma (KBv) [122-126]. Pluronic was not observed to alter the drug uptake in non-MDR tumours, or P-glycoprotein (Pgp) independent MDR tumours, but was shown to inhibit the efflux mechanism in Pgp-based MDR tumours, allowing increased drug uptake and resulting cytotoxicity [121]. This evidence suggests that the poloxamer inhibits the Pgp efflux pump system specifically. Several mechanisms have been suggested to account for this behaviour. Studies by Venne *et al.* [122] examined doxorubicin localization in the MDR breast cancer cell line MCF-7. In these cells, free doxorubicin is sequestered in cytoplasmic vesicles. Following incubation with Pluronic block copolymer, the drug is released from the vesicles and accumulates primarily in the nucleus. Other studies suggest that an energy depletion phenomenon may contribute to lowered multi-drug resistance. Pluronic block copolymers are known to affect mitochondrial function in non-MDR cells by acting as $K^+$

ionophores and by directly inhibiting the NADH dehydrogenase complex by interacting with the hydrophobic sites of this complex in the mitochondrial membrane [123]. Because drug efflux is an energy driven process, it is likely that the inhibiting effect of Pluronic on cellular energy metabolism contributes to reduced drug resistance in MDR tumour cell lines.

Pluronic block copolymers have been shown to have dramatic effects on the microviscosity of cell membranes as a result of adsorption to the lipid bilayer [124]. It appears that this effect is different for some normal and cancerous cells. Regev and coworkers [125] observed that the membranes of cancerous cells became 'fluidized' upon treatment with Pluronic, whereas normal cells became 'solidified'. Multi-drug resistance is lowered by membrane fluidizers by abolishing Pgp ATPase activity and hence loss of Pgp-mediated drug efflux.

The effect of poloxamer on Pgp and the related transporter protein MDR-associated Protein (MRP) has been linked to the ability of poloxamer to penetrate biological membranes such as the blood-brain barrier (BBB) and intestinal membrane. Both Pgp and MRP are expressed in these membranes and are known to outwardly efflux drugs [126,127]. Batrakova *et al.* [128] performed studies on the effect of poloxamer on the permeability of a broad range of compounds (rhodamine 123, doxorubicin, digoxin, ritonavir, taxol, and vinblastine) using the a bovine brain endothelial cell (BMEC) monolayer as an *in vitro* model of the BBB. Increased permeability (from 1.3x to 20x) in the apical to basolateral direction was observed for these compounds in the presence of Pluronic block copolymer. Kabanov *et al.* [129] showed in an *in vivo* mouse model, increased delivery of haloperidol in insulin or antibody conjugated Pluronic block

copolymer micelles. Batrakova *et al.* [130] published a similar study examining the brain uptake of Pluronic formulations of doxorubicin and the Pgp-dependent drug, digoxin, using an *in vivo* mouse model. Consistent with previous findings on poloxamer's ability to inhibit Pgp-dependent efflux, increased levels of digoxin were found in the CNS over doxorubicin. These studies demonstrate that Pluronic block copolymers can be effective in increasing the absorption of drugs across the BBB by inhibiting drug efflux systems.

The same efflux mechanisms found for MDR have been proposed to exist for outwardly effluxing drugs from in intestinal epithilial cells [131]. *In vitro* studies performed by Batrakova *et al.* [132] on the effect of rhodamine permeability to human colon adenocarcinoma cells (Caco-2) cells found that the Pluronic block copolymers inhibited the Pgp efflux system in Caco-2 monolayers, significantly increasing the uptake of the absorption of the rhodamine probe. This and other studies show that Pluronic block copolymers can be useful in increasing the oral bioavailability select drugs by inhibiting drug efflux systems in intestinal epithelial cells.

### 1.4.4. Application of SPPS to the Construction of Block Copolymer Micelles for Drug Delivery

Block copolymers for drug delivery rely on conventional polymerization chemistry for their synthesis. An SPPS approach to their construction would in principle have several advantages over conventional methodologies. One of the most important advantages of SPPS chemistry lies in its ability to generate well defined polymers. Ideally, all manufactured drug substances should be homogeneous and composed of a single, defined species. Polymers generated using conventional technologies are inherently heterogeneous and as such present challenges for their characterization.

Heterogeneity can also have indeterminate effects on biological activity such as toxicity and pharmacokinetics. These problems are alleviated by the use of SPPS because of its demonstrated ability to produce monodisperse polymers.

Another important advantage of SPPS is that it greatly expands the preparative capabilities of these polymers compared to conventional NCA-based chemistries. SPPS permits construction of the core-forming block in a directed, stepwise fashion, allowing the researcher to incorporate any of the 20 available naturally occurring amino acids, as well as literally hundreds of "specialty" amino acids into any position within the polymer.

In Chapter 3 of this thesis I describe a combined SPPS method for constructing core-forming blocks followed by solution phase condensation of the core forming block with the shell-forming block. Using this methodology a number of different constructs were prepared and examined their micellization and drug delivery qualities.

## 1.5. Review of Computer Simulations of Nonionic Block Copolymer Micelles

### 1.5.1. Preamble

The field of micelle modeling deals with the prediction of micelle behavior. In this regard, micelle modeling can be an important aid reducing the amount of trial and error involved in determining which block copolymer constructs may work best for a specific application. Two distinct approaches exist for modeling micelle behavior: analytical modeling [134-143] and computer simulations [145-149]. The analytical models have achieved considerable predictive accuracy, although they make assumptions on micelle shape and size, most do not include intermicellar interactions, and they can be

quite complex to carry out. In contrast, computer simulations utilizing stochastic algorithms (such as the Monte Carlo algorithm), have also achieved good qualitative predictive success, make no *a priori* assumptions about micelle size or shape, can provide information on intermicellar interactions, and are simple to compute. This section reviews the developments in the field of nonionic block copolymer micelle modeling.

### 1.5.2. Analytical Modeling of Block Copolymer Micelles

Analytical models of micelle formation have been quite successful in quantitatively predicting many aspects of their behavior. This is due, in part, to the numerous analytical models that have been proposed to explain micellization behavior. The predominant models differ strikingly in their approach to model micelle formation, from phenomenological models to spherical lattice models to statistical-thermodynamic treatments. Consequently these models tend to predict different aspects of micelle behavior, although there is some overlap. This section provides an overview of the different models that have been proposed to explain and predict non-ionic block copolymer micelle behavior.

#### *1.5.2.1. Phenomenological Models*

Phenomenological models predict micelle behavior by accounting for the free energy differences associated with the physicochemical processes that occur during micellization. Most of these models restrict the composition of the block copolymer to the *AB* type. These models adopt the Flory-Huggins mean-field model, i.e. the micelle core and shell are treated as homogeneous phases [133]. The equilibrium values of the independent variables in the system are determined by minimizing the free energy of the system with respect to that variable.

de Gennes [134] pioneered the theory of formation of diblock copolymer micelles in selective solvents. The micelle cores were treated as solvent-excluded melts surrounded by a solvated corona of shell blocks. The shell was assumed to have a constant density, independent of micellar size. The free energy was expressed as a function of the core-solvent interfacial free energy, the free energy of deformation of elastic chains in the micelle, and the free energy of mixing the solvent molecules with the chains in the micelle corona. Equilibrium values were determined by minimizing the free energy per molecule of an isolated micelle with respect to the aggregation number. The shell block was considered not to have any influence on the micellar characteristics.

Leibler [135] established a theory of CMC for block copolymers in "solutions" of homopolymers. Munch and Gast [136] applied this theory to block copolymer micelles in regular solutions. These models were used to predict the behavior of the CMC with the degree of incompatibility of the core-forming block and solvent ($\chi_{AS}$), block length, and solvent size. One of the important advancements in these theories over that of de Gennes' is that the free energy of the entire system is included, instead of an isolated micelle. It has been known for some time that micelles above the $T_g$ exist in equilibrium with their isolated unimer counterparts, and that this behavior is fundamental to predicting the CMC. A serious shortcoming of these theories, however, is their assumption of monodisperse micelle aggregation numbers. This assumption prevents any analysis of micelle polydispersity.

Nagarajan *et al.* [137] formulated a theory of block copolymer formation (extending the work of Leibler and de Gennes) by treating aggregation number as an independent variable, related to the core and shell volumes. They found that the most

important factor in micelle formation was the contribution of the free energy in the state of dilution of the core-forming block, and that the major limiting factor in micellization was the core-solvent interface. Nagarajan extended this theory to account for small hydrophobic molecule solubilization, and compared the predictions to earlier experiments [138,139]. Their prediction of the dramatic sensitivity of solute-loading to the interaction parameter between the solvent was in excellent agreement with the experimental data, however a lack of data on solubilized micelle size and dispersity prevented any direct comparison on these aspects of micelle behavior. Their theory predicted a narrow dispersity for both aggregation number and degree of solubilization, and these predictions have generally been borne out by experimental observation.

*1.5.2.2. Self-Consistent Mean-Field Lattice (SCF) Theory*

SCF theory uses a conformational approach to model micellar behavior [140]. Like the Monte Carlo simulations and other thermodynamic models, a lattice is used to describe the system. In SCF theory the lattice consists of concentric, equidistant shells, each of which is further divided into lattice cells. A first-order Markov approximation is used to enumerate the conformations of the molecules, as a result, the chains are modeled as self-intersecting walks. Each conformation is weighted by a potential of mean force generated by all other conformations. As a simplifying assumption, this potential field is modeled as a mean field. In this model, fluctuations in size and shape of the micelle are neglected. The polymer and solvent are distributed throughout the lattice and the number of possible configurations of the lattice determined as the configurational entropy contribution to the free energy. The enthalpic contribution to the system free energy—due to interactions between the polymer, solvent, and solute—are characterized by

Flory-Huggins interaction parameters. The total system free energy is minimized with respect to the number of chains in a given conformation to determine the segment density profiles of the micelles. SCF theory does not make any *a priori* assumptions as to micelle shape or size, accordingly, it has been used with good success to explain the morphological dependencies of micelles to polymer architecture (linear, star, *AB*, *ABA*, etc.) and intermicelle interactions.

Scheutjens and Fleer [141] advanced the first formulation of SCF theory for block copolymer micelles. They showed that the interfacial region between the core and the shell is not sharp, as is assumed in the phenomenological models. Later Hurter *et al.* [142] expanded SCF theory to account for solubilization. The predictions of this theory were tested against the experimental observations of Hurter *et al.* [142]. Because of its ability to produce segmental density profiles, SCF theory can predict the localization of solute in the micelle. In this study, naphthalene was predicted to localize almost entirely within the core of the micelle. The theory also quantitatively predicted the observed effect of the relative composition of core block to shell block to the partition coefficient of the solute between the micelle and water. Not considered in this work are the polydispersity or the effect of the interaction parameter on solute loading. It is worth noting that one of the assumptions of this theory is the use of that a lattice site to represent equally a solvent molecule, a solute molecule, or a polymer Kuhn segment. Deviations in the molecular volumes of the real system to that of the model reduces the quantitative accuracy of the predictions.

*1.5.2.3. Statistical Thermodynamic Theory*

The ability of the phenomenological and SCF models to describe micelle solution phase behavior is limited at best, due in large part to their limited ability to model intermicellar interactions. In order to account for the effects of intermicellar interactions on micelle shape, size, and size distribution, Zoeller *et al.* [143] proposed a statistical-thermodynamic theory to model nonionic micellar solutions, using the McMillan-Mayer theory of multicomponent solutions as a starting point.

The SCF and mean-field theories assume the 'solvent' to be in many ways like a vacuum, whereas statistical-mechanical analyses account for the presence of solvent when calculating the Gibbs free energy. The McMillan-Mayer theory provides a link between the two, and as a result, the thermodynamic properties of a system in a vacuum can be used to predict the behavior of a system in a continuum solvent. The independent variables in the McMillan Mayer theory are the temperature, total volume of solution (at temperature $T$), the chemical potential of the pure solvent, and the volume fraction of polymer in the solvent.

Zoeller *et al.* [143] used their statistical-thermodynamic theory to examine the limit of micelle growth, micellar solution phase separation, CMC, and size distribution. Their analysis was carried out only for spherocylindrical micelle behavior, which is not applicable for drug delivery systems, although it is worth mentioning that the predictions of this model for CMC values and the variance of micelle size with temperature are in extremely good agreement with the experimentally obtained values. The validation of this theory by its predictive accuracy, and the generality of its design make this an attractive theory to extend for micelle solubilization predictions.

### 1.5.3. Monte Carlo Simulations of Block Copolymer Micelle Formation.

Polymer simulations adopt many of the same simplifying assumptions as those used by Flory to successfully describe the thermodynamics of polymer behavior [133]. The system is modeled as a three-dimensional simple cubic lattice. Each node in the lattice is occupied by a solvent molecule, or copolymer "unit." No lattice node may be doubly occupied. Each unit interacts with its neighbors via a predetermined interaction energy, $E_{ij}$ where $i$ and $j$ represent the various components within the matrix, specifically, the hydrophobic block, the hydrophilic shell, solvent, or solute. The copolymer is usually restricted to the *AB* type. The total energy of the system is determined, and then minimized, typically by the Monte Carlo method using the Metropolis rules [144].

Cifra and co-workers [145] were among the first to attempt computer simulations of nonionic copolymers, although limitations on computing power limited these simulations to two dimensions. These same researchers later produced the first three-dimensional simulation of copolymer interactions [146]. Their system simulated the behavior of a block copolymer / homopolymer blend (with the homopolymer composition matching one end of the *AB*-type block copolymers). They compared the behavior of their simulation to the predictions of mean-field theory (MFT) of de Gennes [134]. A reasonable fit was found for the predicted and simulated behavior of the net interaction parameter of the blend and the copolymer compositional variable $x$, where $x$ is the degree-of-polymerization ratio of the *A* block to the *B* block.

Mattice's group [147,148] expanded on the early work of Cifra *et al.* to produce a popular model for simulating micelle formation of nonionic micelles. Mattice's simulations demonstrated a strong dependence on critical micelle concentration (CMC)

with the Flory-Huggins interaction parameters (a measure of how well a polymer will dissolve in a given solvent) between the core-forming block and solvent $\chi_{AS}$. Specifically, a linear relationship between the CMC and $\chi_{AS}N_A$ was observed, where $N_A$ is the number of nodes comprising the hydrophobic block. Interestingly, the simulated micelle structures matched nearly exactly with the predicted segmental density profiles from self-consistent mean-field lattice theory of Scheutjens and Fleer [123].

Recently the phenomenon of micellar "contaminant" entrapment was simulated by Talsania *et al.* [149]. The results of their simulations predicted an average aggregation-number polydispersity index (the variation in the average number of polymers in a micelle) of 1.5 for empty micelles. A contaminant concentration-dependent polydispersity was found for loaded micelles, from approximately 2 (for low contaminant concentrations) to less than 1.4 for high loading. No data was presented for the variation of solubilizate population within micelles of fixed aggregation number. Some interesting findings from this set of simulations include: the solubilization of organic contaminants is enthalpically driven; the contaminant is localized into the micelle core; and addition of contaminant increases micelle size and decreases the CMC.

Except for the work of Talsania, there is very little research in the field of polymer micelle simulations with practical utility for polymer micelle-based drug delivery systems. Instead, simulations tend to explore more elementary micellization behaviour. The work presented in Chapter 4 of this thesis was motivated by a desire to develop a micelle simulation system that might be able to predict some of the more complicated phenomenae of interest to researchers in drug delivery. A system for

modelling micellization behaviour using Monte Carlo energy minimization was developed and some preliminary investigations conducted to compare the simulations to the results obtained in Chapter 3 of this thesis.

## 1.6. References


1. Khalid P., Chaturvedi S., Khan M.M., Rastogi A.K., Kundu B., Ahmad F., Mathur K.B., Kidwai J.R. (1989) Effect of some novel synthetic analogues of CCK-4 on insulin and glucagon secretion. *Acta Diabetol. Lat.* **26**:203-209.

2. Wang J., Breslow E., and Sykes B.D. (1996) Differential binding of desmopressin and vasopressin to neurophysin-II. *J. Biol. Chem.* **2**: 31354-3139.

3. Unson C.G., Wu C.R., Jiang Y., Yoo B., Cheung C., Sakmar T.P., and Merrifield R.B. (2002) Roles of specific extracellular domains of the glucagon receptor in ligand binding and signaling. *Biochemistry* **41**:11795-11803.

4. Spetzler J.C., Meldal M., Meinjohanns E., Steinaa L., Mouritsen S., and Bock K. (1997) Synthetic hFSH peptide constructs in the evaluation of previous studies on the hFSH receptor interaction. *J.Pept. Sci.* **3**:397-414.

5. Rajeswaran W.G., Hocart S.J., Murphy W.A., Taylor J.E., and Coy D.H. (2001) N-Methyl scan of somatostatin octapeptide agonists produces interesting effects on receptor subtype specificity. *J. Med. Chem.* **44**:1416-1421.

6. Howl J., Wheatley M. (1996) Molecular recognition of peptide and non-peptide ligands by the extracellular domains of neurohypophysial hormone receptors. *Biochem J.* **317 ( Pt 2)**:577-582.

7. Haskell-Luevano C., Lim S., Yuan W., Cone R.D., and Hruby V.J. (2000) Structure activity studies of the melanocortin antagonist SHU9119 modified at the 6, 7, 8, and 9 positions. *Peptides* **21**:49-57.

8. Okada Y., Fukumizu A., Takahashi M., Shimizu Y., Tsuda Y., Yokoi T., Bryant S.D., and Lazarus L.H. (2000) Synthesis of stereoisomeric analogues of endomorphin-2, H-Tyr-Pro-Phe-Phe-NH(2), and examination of their opioid receptor binding activities and solution conformation. *Biochem Biophys. Res. Commun.* **276**:7-11.

9. Wilk S. and Chen W.E. (1997) Synthetic peptide-based activators of the proteasome. *Mol. Biol. Rep.* **24**:119-124.

10. Van Regenmortel M.H. (2001) Antigenicity and immunogenicity of synthetic peptides. *Biologicals* 29:209-213.

11. Prestwood K.M. and Raisz L.G. (2002) Prevention and treatment of osteoporosis. *Clin. Cornerstone* **4**:31-41.

12. Djurhuus J.C. and Rittig S. (2002) Nocturnal enuresis. *Curr. Opin. Urol.* Jul;12(4):317-20.

13. Froidevaux S. and Eberle A.N. (2002) Somatostatin analogs and radiopeptides in cancer therapy. Biopolymers **66**:161-183.

14. Costello-Boerrigter L.C., Boerrigter G., and Burnett J.C. Jr. (2003) Revisiting salt and water retention: new diuretics, aquaretics, and natriuretics. *Med. Clin. North. Am.* **87**:475-491.

15. Panelli M.C.,Wunderlich J., Jeffries J., Wang E., Mixon A., Rosenberg S.A., and Marincola F.M. (2000) Phase 1 study in patients with metastatic melanoma of immunization with dendritic cells presenting epitopes derived from the melanoma-associated antigens MART-1 and gp100. *J. Immunother.* **23**:487-498.

16. Edgeworth R.L., San J.H., Rosenzweig J.A., Nguyen N.L., Boyer J.D., and Ugen K.E. (2002) Vaccine development against HIV-1: current perspectives and future directions. *Immunol. Res.* **25**:53-74.

17. Duncan R. (2003) The dawning era of polymer therapeutics. *Nat. Rev. Drug. Discov.* **2**:347-360.

18. Kwon G.S. and Okano T. (1996) Polymeric micelles as new drug carriers. *Adv. Drug Deliv. Rev.* **21**:107-116.

19. Merrifield R.B. (1963) Solid phase peptide synthesis. 1. The synthesis of a tetrapeptide. *J. Am. Chem. Soc.* **85**:2149-2154.

20. Marglin A. and Merrifield R.B. (1966) The synthesis of bovine insulin by the solid phase method. *J. Am. Chem. Soc.* **88**:5051-5052.

21. Barstow L.E., Cornelius D.A., Hruby V.J., Shimoda T., Rupley J.A., Sharp J.S., Robinson A.B., and Kamen M.D. (1972) *In* "Chemistry and Biology of Peptides" (J. Meinhofer, ed.) pp. 231-233. Ann Arbor Science Publ., Ann Arbor, Michigan.

22. Merrifield R.B. (1983) *In* "Peptides, Structure and Function" (J.J. Hruby and D.H. Rich, eds.) pp. 33-44. Pierce Chemical Co., Rockford, Illinois.

23. Li H.C. and Yamashiro D. (1970) The synthesis of a protein possessing growth-promoting and lactogenic activities. *J. Am. Chem. Soc.* **92**:7608-7609.

24. du Vigneaud V., Ressler C., Swan J.M., Roberts C.W., Katsoyannis P.G., and Gordon S. (1953) The synthesis of an octapeptide amide with the hormonal activity of oxytocin. *J. Am. Chem. Soc.* **75**:4879-4880.

25. Carpin L.A. and Han G.Y. (1972) The 9-Fluorenylmethoxycarbonyl Amino-Protecting Group. *J. Org. Chem.* **37**:3404-3409.

26. Eising E.G., Bier D., Knust E.J., and Reiners C. (1996) Somatostatin-receptor scintigraphy. Methods, indications, results. *Radiologe* **36**:81-88.

27. Fischman A.J., Babich J.W., and Strauss H.W. (1993) A ticket to ride: peptide radiopharmaceuticals. *J. Nucl. Med.* **34**:2253-2263.

28. Liu S., Edward D.S., and Barrett J.A. (1997) $^{99m}$Tc Labeling of Highly Potent Small Peptides. *Bioconjugate Chem.* **8**:621-636.

29. Kelly J.D., Forster A.M., Archer C.M., Booker F.S., Canning L.R., Chiu K.W., Edwards B., Gill H.K., McPartlin M., Nagle K.R., Latham I.A., Pickett R.D., Storey A.E., and Webbon P.M. (1993) Technetium-99m-tetrofosmin as a new radiopharmaceutical for myocardial perfusion imaging. *J. Nucl. Med.* **34**:222-227.

30. Ianoz E., Mantegazzi D., and Lerch P. (1989) Preparation, crystal and molecular structure of trans-dioxo(1,4-dithia-8,11-diazacyclotetradecane)-technetium(V) hexafluorophosphate. *Inorg. Chim. Acta* **156**:235-239.

31. Higley B., Smith F.W., Gemmell H.G., Gupta P.D., Gvozdanovic D.V., Graham D., Hinge D., Davidson J., and Lahiri A. (1993) Tehnetium-99m 1,2-bis[bis(2-ethoxyethyl)]-phosphino[ethane]: human biodistribution, dosimetry and safety of a new myocardial perfusion imaging agent. *J. Nucl. Med.* **34**:30-38.

32. Vallabhajosula S., Moyer B.R., Lister-James J., McBride W.J., Lipsyc H., Lee H., Bastidas D., and Dean R.T. (1996) Preclinical evaluation of tehnetium-99m-labeled somatostatin receptor binding peptides. *J. Nucl. Med.* **37**:1016-1022.

33. Jurisson S., Aston K., Fair C.K., Schlemper E.O., Sharp P.R., and Troutner D.E. (1987) Effect of ring size on properties of technetium amine oxime complexes. X-ray structures of $TcO_2Pent(AO)_2$, which contains an unusual eight-membered chelate ring, and of $TcOEn(AO)_2$. *Inorg. Chem.* **26**:3576-3582.

34. Liu S., Edwards D.S., Looby D.S., Harris A.R., Poirier M.J., Barrett J.A., Heminway S.J., and Carroll T.R. (1996) Labeling a hydrazino nicotinamide-modified cyclic IIb/IIIa receptor antagonist with $^{99m}Tc$ using aminocarboxylates as coligands. *Bioconjugate Chem.* **7**:63-71.

35. Edwards D.S., Cheesman E.H., Watson M.W., Maheu L.J., Nguyen S.A., Dimitre L., Nason T., Watson A.D., and Walovitch R. (1990) Synthesis and characterization of technetium and rhenium complexes of N,N′-1,2-ethylene-diylbis-L-cysteine. Nerolite and its metabolites. *In* "Technetium and Rhenium in Chemistry and Nuclear Medicine 3" (M. Nicolini, G. Banoli, and U. Mazzi, eds.) pp. 431-444. Cortina International, Verona, Italy.

36. Marchi A., Marvelli L., Rossi R., Magon L., Bertolasi V., Ferretti V., and Gilli P. (1992) Nitrido- and oxo-technetium(V) chelate complexes with $N_2S_2$ ligands: synthesis and crystal structures. *J. Chem. Soc. Dalton Trans.* **9**:1485-1490.

37. Babich J.W., Solomon H., Pike M.C., Kroon D., Graham W., Abrams M.J., Tompkins R.G., Rubin R.H., and Fischman A.J. (1993) Technetium-99m-labeled hydrazino nicotinamide derivatized chemotactic peptide analogs for imaging focal sites of bacterial infection. *J. Nucl. Med.* **34**:1967-1974.

38. Macke H.R. and Behe M. (1996) New octreotide derivatives labeled with technetium-99m. *J. Nucl. Med.* **37**:29P (abstract 107).

39. Eckelman W.C., Paik C.H., and Steigman J. (1989) Three approaches to radiolabeling antibodies with $^{99m}$Tc. *Nucl. Med. Biol.* **16**:171-176.

40. Cornford E.M. and Hyman S. (1999) Blood–brain barrier permeability to small and large molecules. *Adv. Drug Deliv. Rev.* **36**:145-163.

41. French J.K. and White H.D. (1999) Glycoprotein IIb/IIIa antagonists in acute coronary syndromes: clinical trials. *Cardiology Review* **16**:43-55.

42. Ezekowitz M.D., Leonard J.C., Smith E.O., Allen E.W., and Taylor F.B. (1981) Identification of left ventricular thrombi in man using indium-111-labeled autologous platelets. *Circulation* **63**:801-810.

43. Proimos G.J. (2001) Platelet aggregation inhibition with glycoprotein IIb-IIIa inhibitors. *Thromb. Thrombolysis* **11**:99-110.

44. Flank C., Kakkar V.V., and Clarke M.B. (1968) The detection of venous thrombosis of the legs using $^{125}$I-labeled fibrinogen. *Br. J. Surg.* **55**:742-747.

45. Khaw B. (1999) Antibodies as delivery systems for diagnostic functions. *Adv. Drug Deliv. Rev.* **37**:63-80.

46. Blum J.E. and Handmaker H. (2000) Role of small-peptide radiopharmaceuticals in the evaluation of deep venous thrombosis. *Radiographics* **20**:1187-1193.

47. Liu S., Edwards D.S., Looby R.J., Poirier M.J., Rajopadhye M., Bourque J.P., and Carroll T.R. (1996) Labeling cyclic glycoprotein IIb/IIIa receptor antagonists with $^{99m}$Tc by the preformed chelate approach: effects of chelators on properties of [$^{99m}$Tc]chelator-peptide conjugates. *Bioconjugate Chem.* **7**:196-202.

48. Harris T.D., Rajopadhye M., Yu K., Glowacka D., Damphousse P.R., Barrett J.A., Heminway S.J., Edwards D.S., and Carroll T.R. (1997) Synthesis, evaluation and Tc-99m complexation of a hydrazinonicotinyl conjugate of a GP IIb/IIIa antagonist cyclic peptide for the detection of deep vein thrombosis. *Bioorg. & Med. Chem. Lett.* **7**:955-960.

49. Lister-James J., Knight L.C., Maurer A.H., Bush L.R., Moyer B.R., and Dean R.T. (1996) Thrombus imaging with a technetium-99m-labeled activated platelet receptor-binding peptide. *J. Nucl. Med* **7**:775-781.

50. Carretta R.F., Streek P.V., and Weiland F.L. (1999) Optimizing images of acute deep-vein thrombosis using technetium-99m-apcitide. *J. Nucl. Med. Technol.* **27**:271-275.

51. McAffe J.G. (1990) What is the best method for imaging focal infections? *J. Nucl. Med.* **31**:413-416 (Editorial).

52. Babich J.W., Graham W., Barrow S.A., Dragotakes C., Tompkins R.H., and Fischman A.J. (1993) Technetium-99m-labeled chemotactic peptides: comparison with Indium-111-labeled white blood cells for localizing acute bacterial infection in the rabbit. *J. Nucl. Med.* **34**:2176-2181.

53. Moyer B.R., Vallabhajosula S., Lister-James J., Bush L.R., Cyr J.E., Snow D.A., Bastidas D., Lipszyc H., and Dean R.T. (1996) Technetium-99m-white blood cell-specific imaging agent developed from platelet factor 4 to detect infection. *J. Nucl. Med.* **37**:673-679.

54. Virgolini I., Leimer M., Handmaker H., Lastoria S., Bischof C., Muto P., Pangerl T., Gludovacz D., Peck-Radosavljevic M., Lister-James J., Hamilton G., Kaserer K., Valent P., and Dean R.T. (1998) Somatostatin receptor subtype specificity and in vivo binding of a novel tumor tracer, $^{99m}$Tc-P829. *Cancer Res.* **58**:1850-1859.

55. Goodbody A.E., Ballinger J., Tran L.L., Sumner-Smit M., Lau F., Meghji K., and Pollak A. (1994) A new Tc-99m labeled peptide inflammation imaging agent. *Eur. J. Nucl. Med.* **21**:790 (Abstract 262).

56. Bohdiewicz P.J. (1998) Indium-111 satumomab pendetide: the first FDA-approved monoclonal antibody for tumor imaging. *J. Nucl. Med. Technol.* **26**:155-163.

57. Breitz H.B., Tyler A., Bjorn M.J., Lesley T., and Weiden P.L. (1997) Clinical experience with Tc-99m nofetumomab merpentan (Verluma) radioimmunoscintigraphy. *Clin. Nucl. Med.* **22**:615-620.

58. Entel R.J. and Weiss B.R. (1998) Diagnosis of inferior vena cava obstruction on Tc-99m Arcitumomab (CEA scan) scintigraphy. *Clin Nucl. Med.* **23**:470-471.

59. Haseman M.K., Rosenthal S.A., and Polascik T.J. (2000) Capromab Pendetide imaging of prostate cancer. *Cancer Biother. Radiopharm.* **15**:131-140.

60. Eising E.G., Bier D., Knust E.J., and Reiners C. (1996) Somatostatin-receptor scintigraphy. Methods, indications, results. *Radiologe* **36**:81-88.

61. Decristoforo C. and Mather S.J. (1999) Preparation, $^{99m}$Tc-labeling, and in vitro characterization of HYNIC and $N_3S$ Modified RC-160 and [Tyr$^3$]Octreotide. *Bioconjugate Chem.* **10**:431-438.

62. Maina T., Stolz B., Albert R., Nock B., Bruns C., and Mäcke H. (1994) Synthesis, radiochemistry and biological evaluation of a new somatostain analogue (SDZ 219-387) labeled with technetium-99m. *Eur. J. Nucl. Med.* **21**:437-444.

63. Moody T.W., Carney D.N., Cuttita F., Quattrocchi K., and Minna J.D. (1985) High affinity of receptors for bombesin/GRP-like peptides on human small cell cancer. *Life Sci.* **37**:105-113.

64. Pinski J., Schally A.V., Halmos G., Yano T., Szepeshazi K., and Groot K. (1994) Somatostatin analogues and bombesin/gastrin releasing peptide antagonist RC-3095 inhibit the growth of glioblastomas *in vitro* and *in vivo*. *Cancer Res.* **54**:5895-5901.

65. Radulovic S., Miller G., and Schally A.V. (1991) Inhibition of growth of HT-29 human colon cancer xenografts in nude mice by treatment with bombesin/gastrin releasing peptide antagonist (RC-3095). *Cancer Res.* **51**:6006-6009.

66. Baidoo K.E., Lin K.S., Zhan Y., Finley P., Scheffel U., and Wagner H.N. Jr. (1998) Design, synthesis, and initial evaluation of high-affinity technetium bombesin analogues. *Bioconjugate Chem.* **9**:218-225.

67. Karra S.R., Schibli R., Gali H., Katti K.V., Hoffman T.J., Higginbotham C., Sieckman G.L., and Volkert W.A. (1999) $^{99m}$Tc-labeling and in vivo studies of a bombesin analogue with a novel water-soluble dithiadiphosphine-based bifunctional chelating agent. *Bioconjugate Chem.* **10**:254-260.

68. Kataoka K., Harada A., and Nagasaki Y. (2001) Block copolymer micelles for drug delivery: design, characterization and biological significance. *Adv. Drug. Deliv. Rev.* **47**:113-131.

69. Allen C., Maysinger D., and Eisenberg A. (1999) Nano-engineering block copolymer aggregates for drug delivery. *Colloids and Surfaces B: Biointerfaces* **16**:3-27.

70. Kabanov A.V., Batrakova E.V., and Alakhov V.Y. (2002) Pluronic block copolymers as novel polymer therapeutics for drug and gene delivery. *J. Control. Rel.* **82**:189-212.

71. Woodle M.C. and Lasic D.D. (1992) Sterically stabilized liposomes. *Biochim. Biophys. Acta* **1113**:171-199.

72. Allen T. (1994) The use of glycolipids and hydrophilic polymers in avoiding rapid uptake of liposomes by the mononuclear phagocyte system. *Adv. Drug Deliv. Rev.* **13**:285-309.

73. Chung J.E., Yokoyame M., Aoyagi T., Sakurai Y., and Okano T. (1998) Effect of molecular architecture of hydrophobically modified poly(*N*-isoproylacrylamide) on

the formation of thermoresponsive core-shell micellar drug containers. *J. Control. Rel.* **53**:119-130.

74. Taillefer J., Jones M.C., Brasseur N., van Lier J.E., and Leroux J.C. (2000) Preparation and characterization of pH-responsive polymeric micelles for the delivery of photosensitizing anticancer drugs. *J. Pharm. Sci.* **89**:52-62.

75. Inoue T., Chen G., Nakamae K., and Hoffman A.S. (1998) An AB block copolymer of oligo(methyl methacrylate) and poly(acrylic acid) for micellar delivery of hydrophobic drugs. *J. Control. Rel.* **51**:221-229.

76. Nagarajan R., Barry M., and Ruckenstein E. (1986) Unusual selectivity in solubilization by block copolymer micelles. *Langmuir* **2**:210-215.

77. Allen C., Yu Y., Maysinger D., and Eisenberg A. (1998) Polycaprolactone-*b*-poly(ethylene oxide) block copolymer micelles as a novel drug delivery vehicle for neurotrophic agents FK506 and L-685,818. *Bioconjugate Chem.* **9**:565-572.

78. Kim S.Y., Shin G.I., Lee Y.M., Cho C.S., and Sung Y.K. (1998) Methoxy poly(ethylene glycol) and ε-caprolactone amphiphilic block copolymeric micelle containing indomethacin. I. Preparation and characterization. *J. Control. Rel.* **51**:1-11.

79. Yoo H.S. and Park T.G. (2001) Biodegradable polymeric micelles composed of doxorubicin conjugated PLGA-PEG block copolymer. *J. Control. Rel.* **70**: 63-70.

80. Peracchia M.T., Gref R., Minamitake Y., Domb A., Lotan L., and Langer R. (1997) PEG-coated nanospheres from amphiphilic diblock and multibock copolymers:

Investigation of their drug encapsulation and release characteristics. *J. Control. Rel.* **46**:223-231.

81. Schmolka I.R. (1991) Poloxamers in the pharmaceutical industry. *In* "Polymers for Controlled Drug Delivery" (P.J. Tarcha, ed.) pp. 189-214. CRC Press, Boca Raton, FL.

82. Liaw J. and Lin Y.C. (2000) Evaluation of poly(ethylene oxide)-poly(propylene oxide)-poly(ethylene oxide) (PEO-PPO-PEO) gels as a release vehicle for percutaneous fentanyl. *J. Control. Rel.* **68**:273-282.

83. Kwon G.S., Naito M., Yokoyama M., Okano T., Sakarai Y., and Kataoka K. (1993) Micelles based on AB block copolymers of poly(ethylene oxide) and poly( β-benzyl L-aspartate). *Langmuir* **9**:945-949.

84. Yokoyama M., Miyauchi M., Yamada N., Okano T., Sakurai Y., Kataoka K., and Inoue S. (1990) Polymer micelles as novel drug carrier: adriamycin-conjugated poly(ethylene glycol)-poly(aspartic acid) block copolymer. *J. Control. Rel.* **11**:269-278.

85. Bader H., Ringsdorf B., and Schmidt B. (1984) Water soluble polymers in medicine. *Ang. Makromol. Chem.* **123/124**:457-485.

86. Kwon G.S. and Kataoka K. (1995) Block copolymer micelles as long-circulating drug vehicles. *Adv. Drug Deliv. Rev.* **16**:295-309.

87. Jada A., Hurtrez G., Siffert B., and Riess G. (1996) Structure of polystyrene-*block*-poly(ethylene oxide) diblock copolymer micelles in water. *Makromol. Chem. Phys.* **197**:3697-3710.

88. Zhang L. and Eisenberg A. (1996) Morphogenic effect of added ions on crew-cut aggregates of polystyrene-*b*-poly(acrylic acid) block copolymers in solutions. *Macromolecules* **29**:8805-8815.

89. Kataoka K., Masumoto T., Yokoyama M., Okano T., Sakurai Y., Fukushima S., Okamoto K., and Kwon G.S. (2000) Doxorubicin-loaded poly(ethylene glycol)-poly(β-benzyl-L-aspartate) copolymer micelles: their pharmaceutical characteristics and biological significance. *J. Control. Rel.* **64**:143-153.

90. Kataoka K., Harada A., and Nagasake Y. (2001) Block copolymer micelles for drug delivery: design, characterization, and biological significance. *Adv. Drug. Deliv. Rev.* **47**:113-131.

91. Li Y. and Kwon G.S. (1999) Micelle-like structures of poly(ethylene oxide)-*block*-(2-hydroxyethyl aspartamide)-methotrexate conjugates. *Colloids and Surfaces B: Biointerfaces* **16**:217-226.

92. Kataoka K., Kwon G.S., Yokoyama M., Okano T., and Sakurai Y. (1993) Block copolymer micelles as vehicles for drug delivery. *J. Control. Rel.* **24**:119-132.

93. Kratochvil P. and Tuzar Z. (1992) Self-association of block copolymers in solution: copolymer micelles. *Polymer Preprints* **41**:135-138.

94. Yokoyama M., Inoue S., Kataoka K., Yui N., and Sakurai Y. (1987) Preparation of adriamycin-conjugated poly(ethylene glycol)-poly(aspartic acid) block copolymer: A new type of polymeric anticancer agent. *Makromol. Chem. Rapid Commun.* **8**:431-435.

95. Francke V. and Iyer V.S. (1997) Synthesis for molecular electronics: rigid rods and discs. *In* "Atomic and Molecular Wires" (C. Joachim and S. Roth, eds.) pp. 61-79. Kluwer Press, Dordrecht, Netherlands.

96. Bae Y.H., Huh K.M., Kim Y., and Park K. (2000) Biodegradable amphiphilic multiblock copolymers and their implications for biomedical applications. *J. Control. Rel.* **64**:3-13.

97. Yokoyama M., Fukushima S., Uehara R., Okamoto K., Kataoka K., Sakurai Y., and Okano T. (1998) Characterization of physical entrapment and chemical conjugation of adriamycin in polymeric micelles and their design for in vivo delivery to a solid tumor. *J. Control. Rel.* **50**:79-92.

98. Lavasanifar A., Samuel J., and Kwon G.S. (2002) Poly(ethylene oxide)-block-poly(L-amino acid) micelles for drug delivery. *Adv. Drug Deliv. Rev.* **54**:169-190.

99. Yokoyama M., Okano T., Sakurai Y., and Kataoka K. (1994) Improved synthesis of of adriamycin-conjugated poly(ethylene oxide)-poly(aspartic acid) block copolymer and formation of unimodal micellar structure with controlled amount of physically entrapped adriamycin. *J. Control. Rel.* **32**:269-277.

100. Yokoyama M., Okano T., Sakurai Y., Ekimoto H., Shibazaki C., and Kataoka K. (1991) Toxicity and antitumor activity against solid tumors of micelle-forming

polymer anticancer drug and its extremely long circulation in blood. *Cancer Res.* **51**:3229-3236.

101. La S.B., Okano T., and Kataoka K. (1996) Preparation and characterization of the micelle-forming polymeric drug indomethacin-incorporated poly(ethylene oxide)-poly(β-benzyl-L-aspartate) block copolymer micelles. *J. Pharm. Sci.* **85**:85-90.

102. Yu B.G., Okano T., Kataoka K., Sardari S., and Kwon G.S. (1998) *In vitro* dissociation of antifungal efficacy and toxicity for amphotericin B-loaded poly(ethylene oxide)-block-poly(β-benzyl-L-aspartate) micelles. *J. Control. Rel.* **56**:285-291.

103. Lavasanifar A., Samuel J., Sattari S., and Kwon G.S. (2000) Block copolymer micelles for the delivery of Amphotericin B. *Pharm. Res.* **19**:418-422.

104. Adams M.L., Andes D.R., and Kwon G.S. (2003) Amphotericin B encapsulated in micelles based on poly(ethylene oxide)-*block*-poly(L-amino acid) derivatives exerts reduced in vitro hemolysis but maintains potent in vivo antifungal activity. *Biomacromolecules* **4**:750-757.

105. Mizumura Y., Matsumura Y., Hamaguchi T., Nishiyama N., Kataoka K., Kawaguchi T., Hrushesky W.J., Moriyasu F., and Kakizoe T. (2001) Cisplatin-incorporated polymeric micelles eliminate nephrotoxicity, while maintaining antitumor activity. *Jpn. J. Cancer Res.* **92**:328-336.

106. Arshady R. (1991) Preparation of biodegradable microspheres and microcapsules: 2. Polylactides and related polyesters. *J. Control. Rel.* **17**:1-22.

107. Allen C., Eisenberg A., Mrsic J., and Maysinger D. (2000) PCL-b-PEO micelles as a delivery vehicle for FK506: assessment of a functional recovery of crushed peripheral nerve. *Drug Deliv. Rev.* **7**:139-145.

108. Wang C. and Swerdloff R.S. (1997) Androgen replacement therapy. *Ann. Med.* **29**:365-370.

109. Shin I.G., Kim S.Y., Lee Y.M., Cho C.S., and Sung Y.K. (1998) Methoxy poly(ethylene glycol) / ε-caprolactone amphiphilic block copolymeric micelle containing indomethacin. I. Preparation and characterization. *J. Control. Rel.* **51**:1-11.

110. Shin I.G., Kim S.Y., Lee Y.M., Cho C.S., and Sung Y.K. (1998) Methoxy poly(ethylene glycol) / ε-caprolactone amphiphilic block copolymeric micelle containing indomethacin. II. Micelle formation and drug release behaviors. *J. Control. Rel.* **51**:13-22.

111. Hagan S.A., Coombes G.A., Garnett M.C., Dunn S.E., Davies M.C., Illum L., and Davis S.S. (1996) Polylactide-poly(ethylene glycol) copolymers as drug delivery systems. 1. Characterizaton of water dispersible micelle-forming systems. *Langmuir* **12**:2153-2161.

112. Kataoka K. (1998) The reactive polymeric micelle based on an aldehyde-ended poly(ethylene glycol)/poly(lactide) block copolymer. *Macromolecules* **31**:1473-1479.

113. Yamamoto Y., Nagasake Y., Kato M., and Kataoka K. (1999) Surface charge modulation of poly(ethylene glycol)-poly(D,L-lactide) block copolymer micelles: conjugation of charged peptides. *Colloids and Surfaces B: Biointerfaces* **16**:135-146.

114. Kim S.Y., Shin I.G., and Lee Y.M. (1999) Amphiphilic diblock copolymeric nanospheres composed of methoxy poly(ethylene glycol) and glycolide: properties, cytotoxicity and drug release behaviour. *Biomaterials* **20**:1033-1042.

115. Jeong B., Bae Y.H., and Kim S.W. (2000) Drug release from biodegradable injectable thermosensitive hydrogel of PEG-PLGA-PEG triblock copolymers. *J. Control. Rel.* **63**:155-163.

116. Jeong B., Bae Y.H, and Kim S.W. (1999) Thermoreversible gelation of PEG-PLGA-PEG aqueous solutions. *Macromolecules* **32**:7064-7071.

117. Alexandridis P. and Hatton T.A. (1995) Poly(ethylene oxide)-block-Poly(propylene oxide)-*block*-Poly(ethylene oxide) Copolymer Surfactants in Aqueous Solutions and at Interfaces: Thermodynamics, Structure, Dynamics, and Modelling. *Colloids Surfaces A: Physicochem. Eng. Aspects* **96**:1-46.

118. Kabanov A.V., Batrakova E.V., and Alakhov V.Y. (2002) Pluronic block copolymers as novel polymer therapeutics for drug and gene delivery. *J. Control. Rel.* **82**:189-212.

119. Kabanov A.V., Batrakova E.V., and Miller D.W. (2003) Pluronic((R)) block copolymers as modulators of drug efflux transporter activity in the blood-brain barrier. *Adv Drug Deliv Rev.* **55**:151-164.

120. Naito S., Yokomizo A., Koga H. (1999) Mechanisms of drug resistance in chemotherapy for urogenital carcinoma. *Int. J. Urol.* **6**:437-439.

121. Alakhov V.Y., Moskaleva E.Y, Batrakova E.V., and Kabanov A.V. (1996) Hypersensitization of multidrug resistant human ovarian carcinoma cells by pluronic p85 block copolymer. *Bioconjugate. Chem.* **7**:209-216.

122. Venne A., Li S., Mandeville R., Kabanov A., and Alakhov V. (1996) Hypersensitizing effect of pluronic L61 on cytotoxic activity, transport, and subcellular distribution of doxorubicin in multiple drug-resistant cells. *Cancer Res.* **56**:3626-9.

123. Brustovetski N.N., Dedukhova V.N., Egorova M.V., Mokhova E.N., and Skulachev V.P. (1996) Uncoupling of oxidative phosphorylation by fatty acids and detergents suppressed by ATP/ADP antiporter inhibitors. *Biochemistry (Moscow)* **56**:1042-1048.

124. Melik-Nubarov N.S., Pomaz O.O., Dorodnych T., Badun G.A., Ksenofontov A.L, Schemchukova O.B., and Arkhazov S.A. (1999) Interaction of tumour and normal blood cells with ethylene oxide and propylene oxide block copolymers. *FEBS Lett.* **446**:194-198.

125. Regev R., Assaraf Y.G., and Eytan G.D. (1999) Membrane fluidization by ether, other anesthetics, and certain agents abolishes P-glycoprotein ATPase activity and modulates efflux from multidrug-resistant cells. *Eur. J. Biochem.* **259**:18-24.

126. Zhang Y., Han H., Elmquist W.F., and Miller D.W. (2000) Expression of various multidrug resistance-associated protein (MRP) homologues in brain microvessel endothelial cells. *Brain Res.* **876**:148-153.

127. Cordon-Cardo C., O'Brien J.P., Casals D., Rittman-Grauer L., Biedler J.L., Melamed M.R., and Bertino J.R. (2000) Multi-drug resistance gene (P-glycoprotein) is

expressed by endothelial cells at blood-brain barrier sites. *Proc. Natl. Acad. Sci. USA* **86**:695-698.

128. Batrakova E.V., Li S., Miller D.W., and Kabanov A.V (1999) Pluronic P85 increases permeability of a broad spectrum of drugs in polarized BMEC and Caco-2 cell monolayers. *Pharm Res.* **16**:1366-1372.

129. Kabanov A.V., Chekhonin V.P., Alakhov V.Y., Batrakova E.V., Lebedev A.S., Melik-Nubarov N.S., Arzhakov S.A., Levashov A.V., Morozov G.V., Severin E.S., *et al.* (1989) The neuroleptic activity of haloperidol increases after its solubilization in surfactant micelles. Micelles as microcontainers for drug targeting. *FEBS Lett.* **258**:343-345.

130. Batrakova E.V., Miller D.W., Li S., Alakhov V.Y., Kabanov A.V., and Elmquist W.F. (2001) Pluronic P85 enhances the delivery of digoxin to the brain: *in vitro* and *in vivo* studies. *J. Pharmacol. Exp. Ther.* **296**:551-557.

131. Hirohashi T., Suzuki H., Chu X.Y., Tamai I., Tsuji A., and Sugiyama Y. (2000) function and expression of multidrug resistance-associated protein family in human colon adenocarcinoma cells (Caco-2). *J. Pharmacol. Exp. Ther.* **292**:265-270.

132. Batrakova E.V., Han H.Y., Miller D.W., and Kabanov A.V. (1998) Effects of pluronic P85 unimers and micelles on drug permeability in polarized BBMEC and Caco-2 cells. *Pharm Res.* **15**:1525-1532.

133. Flory P.J. (1953) "Principles of Polymer Chemistry" Cornell University, Ithaca, NY.

134. de Gennes P.G. (1971) Reptation of a polymer chain in the presence of fixed obstacles. *J. Chem. Phys.* **55**:572-579.

135. Leibler L. (1983) Theory of critical micelle concentration for solutions of block copolymers. *J. Chem. Phys.* **79**:3550-3557.

136. Munch M.R. and Gast A.P. (1988) Block copolymers at interfaces. 1. Micelle formation. *Macromolecules* **21**:1360-1366.

137. Nagarajan R. (1989) Association of nonionic polymers with micelles, bilayers, and microemulsions. *J. Chem. Phys.* **90**:1980-1994.

138. Nagarajan R. and Ruckenstein E. (2000) Molecular Theory of Microemulsions. *Langmuir* **16**:6400-6415.

139. Nagarajan R. and Ganesh K. (1989) Block Copolymer Self-Assembly in Selective Solvents: Theory of Solubilization in Spherical Micelles. *Macromolecules* **22**:4312-4325.

140. Hurter P.N., Scheutjens J.M., and Hatton T.A. (1993) Molecular modeling of micelle formation and solubilization in block copolymer micelles. 1. A self-consistent mean-field lattice theory. *Macromolecules* **26**:5592-5601.

141. Scheutjens J.M. and Fleer G.J. (1979) Statistical theory of the adsorption of interacting chain molecules. 1. Partition function, segment density distribution, and adsorption isotherms *J. Phys. Chem.* **83**:1619-1635.

142. Hurter P.N., Alexandridis P., and Hatton T.A. (1995) *In* "Solubilization in Surfactant Aggregates" (J.F. Scamehorn, ed.) pp. 191-235. Marcel Dekker, New York.

143. Zoeller N., Lue L., and Blankshtein D. (1997) Statistical-Thermodynamic Framework to Model Nonionic Micellar Solutions. *Langmuir* **13**:5258-5275.

144. Metropolis N., Rosenbluth A.W., Rosenbluth M.N., and Teller A.H. (1953) Equation of state calculations by fast computing machines. *J. Chem. Phys.* **21**:1087-1091.

145. Cifra P., Karasz F.E., and MacKnight W.J. (1988) Distribution of interactions in binary polymer mixtures: a Monte Carlo simulation study. *Macromolecules* **21**:446-451.

146. Cifra P., Karasz F.E., and MacKnight W.J. (1989) Computer simulation of copolymer-copolymer and copolymer-homopolymer mixtures with a single interaction energy. *Macromolecules* **22**:3649-3653.

147. Rodrigues K. and Mattice W.L. (1991) Simulation of the steric stabilization of polymer colloids by diblock copolymers. *J. Chem. Phys.* **94**:761-766.

148. Wang Y. and Mattice W.L. (1993) Simulation of the formation of micelles by diblock copolymers under weak segregation. *Langmuir* **9**:66-70.

149. Talsania S.K., Wang Y., Rajagopalan R., and Mohanty K.K. (1997) Monte Carlo Simulations for Micellar Encapsulation. *J. Colloid Int. Sci.* **190**:92-103.

# CHAPTER 2. A SIMPLE AND EFFICIENT METHOD TO PREPARE $^{99m}$Tc-LABELED PEPTIDES[1]

## 2.1. Introduction

Over the last twenty years, researchers in nuclear medicine have endeavored to conjugate receptor-binding peptides to chelators of medicinally important radioisotopes in the interest of developing targetable, pharmacokinetically favorable radioimaging and radiotherapeutic agents [1]. Recent attention has focused on the development of peptide-chelator conjugates for labeling with $^{99m}$Tc: the radionuclide of choice for diagnostic imaging due to its short half-life (6 h), favorable emission energy (140 keV), low cost, and ready availability. The number of peptides currently under investigation as $^{99m}$Tc-based radiopharmaceutical candidates is large and growing rapidly [1-5]. Several of these peptide-chelator conjugates have been demonstrated to bind $^{99m}$Tc while retaining their biological efficacy. As candidates for clinical use however, peptide radiopharmaceuticals for $^{99m}$Tc labeling should also demonstrate amenability to kit formulation, long shelf-life, stability in plasma, resistance to transchelation, high labeling yield (>90%), quick labeling (under 60 min), and high radiochemical purity (>90%) [6]. This latter requirement poses an especially challenging problem. Peptide-chelator conjugates often give rise to multiple isomers upon complexation with $^{99m}$Tc, which typically can be separated only by sophisticated methods such as HPLC. The short

---

[1] Portions of this chapter appear in the Journal of Labelled Compounds and Radiopharmaceuticals: Van Domselaar G.H, Okarvi S.M., Fanta M., Suresh M.R., Wishart D.S.(2000) Synthesis and $^{99m}$Tc-labelling of bz-MAG3-triprolinyl-peptides, their radiochemical evaluation and in vitro receptor-binding. *J. Label. Comp. Radiopharm.* **43**:1193-1204.

half-life of $^{99m}$Tc, however, makes post-labeling HPLC purification impractical in a clinical setting [6]. A major source of this isomerism is believed to arise from the misdirected complexation of $^{99m}$Tc with natural chelating groups on the targeting peptide (amines, amides, thiols, and imidazoles) [7]. An additional source of isomerism originates from the bifunctional chelating agent (BFCA), which, if containing one or more chiral centers (or if the BFCA requires a chiral ancillary ligand), can result in the formation of stereoisomers [8]. Even achiral ligands can produce *syn* and *anti* geometric isomers because of their polydentate binding with the technetium core [9]. One increasingly popular strategy for reducing the number of isomeric species generated when radiolabeling peptides is to incorporate a linker, also known as a pharmacokinetic modifier, between the targeting peptide and the BFCA, thus reducing the potential for misdirected chelation [10,11]. A second strategy is to use an achiral, polydentate BFCA to chelate the technetium core, thus minimizing the potential for generation of isomeric species [6]. Here we describe a convenient solid phase peptide synthesis (SPPS) method that incorporates both of these strategies to produce stable, efficiently labeled (<60 min, >90% labeling yield), and radiochemically pure (>90% as judged by radio-HPLC) technetium-labeled peptide radiopharmceutical complexes.

Specifically, we chose the S-benzoyl protected derivative of mercaptoacetyltriglycine (bz-MAG3) to serve as the sulfhydryl-protected precursor to the achiral, polydentate BFCA. Triproline ($P_3$) was chosen as the non-chelating linker that separates the BFCA from the biologically active peptide (Figure 2.1). We have found that the bz-MAG3-$P_3$ BFCA-linker can be conveniently attached to the N-termini of bioactive peptides using conventional Fmoc-based SPPS. Studies using analogs of

bombesin [12] and αM2 [13], with bz-MAG3-$P_3$ linked to their N-terminus, show that these peptides meet many of the clinical requirements of a $^{99m}$Tc-based peptide radiopharmaceutical, and strongly suggest that this technique can be used to successfully prepare many other $^{99m}$Tc-labeled peptides for diagnostic imaging.

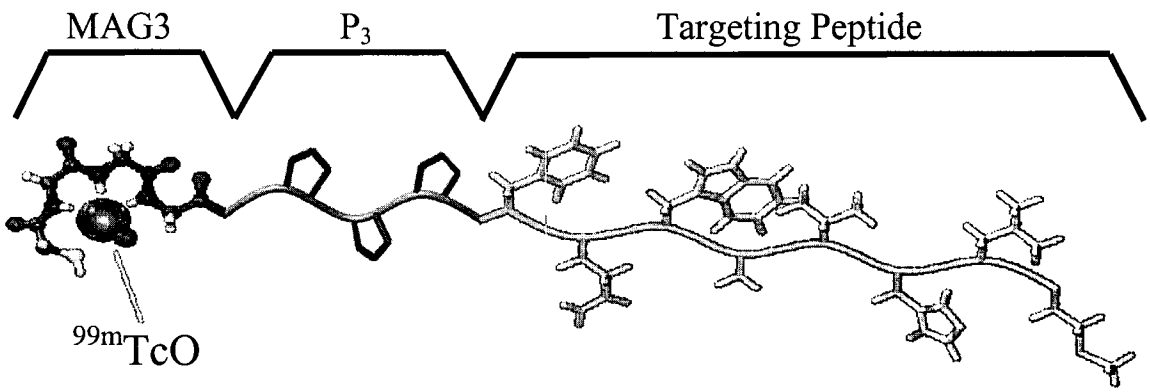


Figure 2.1. Illustration of [$^{99m}$TcO]MAG3-$P_3$-targeting peptide construct.

## 2.2. Materials and Methods

### 2.2.1. Reagents

All Fmoc amino acids, Rink-methylbenzhydrylamine (MBHA) resin, O-benzotriazole-N,N,N′,N′-tetramethyluronium hexafluorophosphate (HBTU), and piperidine were purchased from Chem-Impex International Inc. (Woodale, IL) and used without further purification. Sequencing grade N,N′-dimethylformamide (DMF), obtained from Fisher Scientific Canada Inc. (Edmonton, Canada), was assayed for free amine content by quantitative reaction with Sanger's reagent [14] and, if necessary, purified by passing over a biphasic alumina column prior to use. Trifluoroacetic acid (TFA) was purchased from Halocarbon Products Corporation (River Edge, NJ).

Acetonitrile (spectrophotometric grade) was purchased from BDH Inc. (Toronto, Canada). N-methyl morpholine (NMM), anisole, and thioanisole were purchased from Aldrich Chemical Co. (Milwaukee, IL). Dithiothreitol (DTT) was purchased from ICN Biomedicals Inc. (Aurora, OH). All other chemicals used in this study were of reagent grade and used without further purification. Sodium pertechnetate ($Na^{+}\ ^{99m}TcO_4^{-}$) was supplied by the Edmonton Radiopharmaceutical Centre (Edmonton, Canada). Fresh human plasma was obtained from the Canadian Red Cross Centre (Edmonton, Canada).

### 2.2.2. Instrumentation

Mass spectra were recorded using a Fisons VG Trio 2000 electrospray mass spectrometer (ES-MS) operating in positive mode at 78 $^{o}$C with an accelerating voltage of 3.5 kV, a cone voltage of 48 V and a scanning range of 500 to 1500 m/z. Analytical HPLC was carried out on a Beckman Gold Nouveau HPLC system fitted with a reversed-phase column (C-8, 5μ, 2.1 mm x 15 cm) and running a 2% B/min gradient (Solvent A: 0.1% aqueous TFA, Solvent B: 0.1% TFA in acetonitrile) at 0.5 ml/min. Amino acid analysis was performed at the Alberta Peptide Institute (Edmonton, Canada) using a Beckman System Gold amino acid analyzer using post-column ninhydrin derivatization. The samples were hydrolyzed in sealed glass ampoules for 1 h at 165 $^{o}$C with constant-boiling HCl containing 1% phenol. $^{1}$H NMR spectra were acquired using a Varian Unity 500 MHz NMR spectrometer.

### 2.2.3. Peptide Synthesis

Sequences for all the peptides used in this study are provided in Table 2.1. The peptides were assembled using a combination of manual and automated synthesis

(PerSeptive Biosystems Biosearch 9500), following standard Fmoc/HBTU methodology [15]. Specifically: the Rink-MBHA resin (ca. 260 mg; 0.77 meq/g; 0.2 mmol) was swollen in DMF, then thoroughly washed using DCM (3x10 ml) and DMF (5x10 ml). The C-terminal amino acid was activated with HBTU and NMM (in DMF) and allowed to react with the solid support. The remaining amino acids were assembled on the derivatized resin by repeated cycles of deprotection, activation, and coupling. Each deprotection step involved a double treatment with 20% piperdine in DMF (10 min total) followed by washing DCM (3x10 ml) and DMF (5x10 ml). Each activation step was performed by mixing the protected amino acid (0.8 mmol in 2.7 ml DMF) with HBTU (0.7 mmol in DMF) and a slight excess (1.6 mmol) of neat NMM for 5 min. The activated amino acid was then allowed to couple to the resin for 45 minutes with nitrogen bubbling. The peptide-resin was thoroughly washed with DCM (3x10 ml) and DMF (5x10 ml) after coupling. Upon completion of synthesis the N-terminal Fmoc group was removed, and the peptide-resin washed to prepare for condensation with S-benzoylmercaptoacetic acid.

Table 2.1. Peptide sequences used in this study. The sequences have been aligned to better display the common and modified regions.

| BFCA-Peptide | Sequence |
|---|---|
| Bz-MAG3-P0-(KLA)3 | Bz-mAc G G G — — — K L A K L A K L A $NH_2$ |
| Bz-MAG3-P1-(KLA)3 | Bz-mAc G G G P — — K L A K L A K L A $NH_2$ |
| Bz-MAG3-P2-(KLA)3 | Bz-mAc G G G P P — K L A K L A K L A $NH_2$ |
| Bz-MAG3-P3-(KLA)3 | Bz-mAc G G G P P P K L A K L A K L A $NH_2$ |
| Bz-MAG3-Bombesin | Bz-mAc G G G — — — Q R L G N Q W A V G H L M $NH_2$ |
| Bz-MAG3-P3-Bombesin | Bz-mAc G G G P P P Q R L G N Q W A V G H L M $NH_2$ |
| aM2 | Y C A R E P P T R T F A Y G $NH_2$ |
| Bz-MAG3-P3-aM2 | Bz-mAc G G G P P P Y C A R E P P T R T F A Y G $NH_2$ |
| Bz-MAG3-P3-aM2-a | Bz-mAc G G G P P P Y A A R E P P T R T F A Y G $NH_2$ |

### 2.2.4. Addition of S-benzoylmercaptoacetic Acid

Preparation of S-benzoylmercaptoacetic acid has been reported previously [16]. Synthesis of this material was performed on a 5 g scale. The product was characterized by ES-MS and $^{1}H$ NMR. Purity (>99%) was confirmed by reversed-phase analytical HPLC. A four-molar excess (with respect to the peptide-resin) of S-benzoylmercaptoacetic acid was activated and manually coupled to the free N-terminus of the peptide-resin using standard HBTU/NMM protocol [15]. The reaction proceeded to completion within 15 min as determined by the Kaiser ninhydrin assay [17]. This step completed the synthesis of the bz-MAG3 moiety to yield the final BFCA-peptide-resin. The peptide resin was washed thoroughly with DCM (3x10 ml), DMF (5x10 ml) and methanol (5x10 ml), then dried *in vacuo* overnight to prepare for cleavage.

### 2.2.5. Cleavage and Side-Chain Deprotection

The peptide-resin (ca. 200 – 300 mg) was placed in a disposable polypropylene cartridge fitted with a polyethylene frit. A 10 ml solution of cleavage cocktail: TFA:$H_2O$:DTT (95:2.5:2.5) was added and shaken gently for 2 h. The resin was then removed by filtration and washed with 2 ml TFA. The filtrate was evaporated *in vacuo*, then precipitated with cold ether (30 ml). After decanting the ether layer, the precipitated peptide was washed again with cold ether (2x20 ml), dissolved in dd$H_2O$, frozen, and lyophilized to yield the crude bz-MAG3-peptide.

### 2.2.6. Purification and Analysis

Crude BFCA-peptides were purified by HPLC (Waters – System 501) on a reversed-phase C-8 2.1x25 cm Zorbax 300 preparative column using a binary gradient of

aqueous 0.1% TFA (solvent A) and acetonitrile containing 0.1% TFA (solvent B) at a flow rate of 8.0 ml/min. The eluent was monitored at 210 nm and collected into fractions at one-minute intervals. The preparative column was equilibrated at a percent B composition expected to be approximately 10% below that required to elute the desired peak. A gradient of 0.2% B/min was then applied, UV absorbing fractions were collected and then characterized by analytical HPLC and ES-MS. Fractions of sufficient purity were combined and lyophilized to yield the a desired BFCA-peptides in excess of 95% purity.

### 2.2.7. Labeling with $^{99m}Tc$

The BFCA-peptides were labeled with $^{99m}Tc$ by reduction in the presence of SnCl2. Specifically, radiolabeling was achieved by mixing 25 μl [1 mg/ml in 50:50 $CH_3CN:H_2O$ (v/v)] of each BFCA-peptide with 100 μl of 0.1 M citrate-phosphate buffer, 300 μl tartrate (40 mg/ml aqueous solution), 100 μl $SnCl_2$ (4 mg/ml in 0.05 N HCl) and 100 μl $^{99m}TcO^{4-}$ (1 to 5 mCi) in saline. The labeling mixture was heated at 100 $^{o}C$ in a water-bath for 10 min and cooled to room temperature prior to radiochromatographic analysis. Labeling conditions were optimized for all BFCA-peptides by adjusting the citrate-phosphate buffer from pH 2 to 12 in increments of 0.5, and then analyzing the result by radio-HPLC. Labeling conditions were further optimized for the biologically active BFCA-peptides (αM2 and bombesin) by examining their radiolabeling characteristics using sodium dithionite (100 μl of 50 mg/ml aqueous $Na^{+}N_2S_2O_4^{-}$) as an alternative reducing agent, and sodium gluconate (100 μl of a 100 mg/ml aqueous

solution) as an alternate transfer ligand, and analyzing the radio-HPLC results from pH 2 to 12.

### 2.2.8. Radiochemical Purity

Radiochemical purity was determined primarily by analytical radio-HPLC. A reversed-phase HPLC column (C-18, 5μ, 3.9 x 150 mm, DeltaPak) was equilibrated in 0.1% aqueous 2.5%/min gradient (A, 0.1% aqueous TFA; B, 0.1% TFA in acetonitrile). The eluent was monitored for UV absorbance at 210 nm (Waters model 486) and for radioactivity by scintillation (Bioscan). The detectors were arranged in tandem to minimize the retention time difference for each profile. For the serum stability and cysteine challenge experiments, radiochemical purity was determined by radio-TLC using Whatman chromatography paper No. 1 with acetone and saline (0.9% NaCl) as mobile phases. When acetone is used as the mobile phase, the radiolabeled BFCA-peptide remains at the origin while free $^{99m}$Tc migrates with the solvent front. When saline is used as the mobile phase, the radiolabeled BFCA-peptide migrates with the solvent front while reduced and hydrolyzed $^{99m}$Tc remains at the origin. Labeling efficiency is calculated as 100% - [% (free $^{99m}$Tc) + % (reduced and hydrolyzed $^{99m}$Tc)] [18].

### 2.2.9. *In Vitro* Plasma Stability

To assess the *in vitro* stability of the complexes, a 100 μl aliquot of both $^{99m}$Tc complexed MAG3-$P_3$-peptides (αM2-a and bombesin) were incubated with 0.5 ml human plasma at 37 $^{o}$C for 18 h. The quantity of free versus bound $^{99m}$Tc was determined

by radio-TLC. As a control, the radiochemical purity of the [$^{99m}$Tc]MAG3-peptides was determined in saline (0.9% NaCl) at 30 min and 18 h after radiolabeling.

### 2.2.10. *In Vitro* Transchelation

To evaluate the chelation strength of a particular BFCA-peptide design, analytical methods need to indicate the relative strength of the metal-ligand bond. One such method is the cysteine challenge assay [19], which measures the ability of cysteine to transchelate, or remove $^{99m}$Tc from a given $^{99m}$Tc-ligand complex. The relative strength of the [$^{99m}$Tc]BFCA-peptide was determined by incubating the labeled BFCA-peptides with varying molar concentrations of cysteine. For these particular transchelation experiments, each $^{99m}$Tc-labeled peptide was mixed with excess cysteine at molar ratios of 1:100 and 1:500. The reaction mixtures (ca. 1 ml) were incubated at 37 $^{o}$C. Samples were removed at 1 h and 6 h intervals and analyzed by radio-TLC to determine the percentage of transchelated $^{99m}$Tc.

### 2.2.11. *In Vitro* Receptor Binding

The receptor-binding ability of the [$^{99m}$Tc]MAG3-$P_3$-peptides bombesin and αM2-a were evaluated on human PC-3 prostate carcinoma and MCF-7-III breast carcinoma cell lines using direct detection. Both cell lines were grown to confluence in 24 well plates in RPMI-1640 culture media with 10% FBS. Twenty-four hours prior to conducting the binding assays, the media was replaced with RPMI-1640 with 5% FBS.

Varying amounts of each radiolabeled peptide were incubated at 0 $^{o}$C with each line and washed with PBS to determine the total binding of the $^{99m}$Tc-peptide-complex.

In parallel, equal amounts of each $^{99m}$Tc-labeled peptide were incubated with the cells together with a 100-fold excess of corresponding unlabeled MAG3-$P_3$-peptide to determine non-specific binding. The difference between the total and non-specific binding was used to determine specific receptor binding. Each data point with these cancer cell lines represent mean ±S.D. of pentuplicates (n=5).

## 2.3. Results and Discussion

### 2.3.1. Chelator Selection

In this study, we chose to use the S-benzoyl protected derivative of mercaptoacetyltriglycine (MAG3) as the thiol-protected BFCA. MAG3 is a well-known, FDA-approved $N_3S$ amidothiol-based $^{99m}$Tc chelator and has been used as a renal imaging agent for a number of years [20-23]. Besides its achiral structure and polydentate binding character, MAG3 possesses many additional features that make it a nearly ideal preformed chelator, including: high labeling yield, excellent solution stability, high resistance to transchelation by cysteine, and facile synthesis by SPPS.

A critical factor to consider when designing a general SPPS strategy for assembling MAG3 into peptides lies in the choice of an appropriate protecting group for the chelator's reactive thiol. The ideal protecting group should be stable to conditions of solid-phase peptide synthesis, cleavage, and purification; remain stable during storage; and deprotect *in situ* during radiolabeling. The S-benzoyl protected derivative of MAG3 satisfies the requirements for long shelf life and *in situ* deprotection [23]. Although the benzoyl's thioester is known to be unstable in alkaline conditions, we speculated that it might survive exposure to the mildly basic conditions required for HBTU-based

activation and coupling, and therefore could be added to the peptide-resin as the final coupling step during SPPS. Our results show that S-benzoyl protected MAG3 can be successfully assembled into a peptide under these conditions. The S-benzoylmercaptoacetyl group proved to be completely stable to SPPS coupling conditions and TFA cleavage, as judged by analytical reversed-phase HPLC and ES-MS of the crude peptide product before and after its coupling to the growing peptide chain. In every case, the S-benzoylmercaptoacetylated peptides produced mass spectra containing the expected molecular ion masses (within an experimental error of one a.m.u.), with no evidence of any debenzoylated product or underivatized starting materials, even for couplings of over 2 h. Comparison of the HPLC traces before and after addition of S-benzoylmercaptoacetic acid confirmed its quantitative addition to the peptide N-terminus. To test the benzoyl group's stability towards SPPS Nα- deprotection conditions, 1 mg benzoyl-MAG3-peptide was placed in a vial containing 10 ml neat piperidine. Samples were withdrawn occasionally and examined by reversed-phase analytical HPLC and ES-MS. As expected, the benzoyl group was unstable in piperidine, with approximately 25% debenzoylation after 4 h. These results suggest that the benzoylmercaptoacetylation step should be restricted to the last step of the synthesis.

### 2.3.2. Linker Selection

In our initial attempts at preparing MAG3-based BFCA peptides, we attached the MAG3 chelator directly on to the N-terminus of our bioactive peptides. Analysis after $^{99m}$Tc labeling, all of the BFCA-peptides displayed poor radiochemical purity. We speculated that the source of this impurity was due to the misdirected chelation of $^{99m}$Tc with the targeting, or distal portion of the BFCA-peptide. This prompted us to investigate

the use of an appropriate linker to separate the BFCA from the biologically active peptide. Linker composition is an important consideration in the design of peptide based radiopharmceuticals, as they can modify the pharmacokinetic profile and receptor-binding capability of the final construct, either inadvertently or by design [6]. Linkers used successfully previously to improve radiochemical purity include 4-aminobutyric acid [10] and 6-aminocaproic acid [11]. We chose instead to use multiple proline residues as a linker, primarily for to amenability to SPPS, imide backbone structure, rigidity, biodegradability, and genetic codability. Fmoc-proline is an inexpensive, readily available, and routinely used protected amino acid for SPPS. Its relatively inflexible, imide backbone and non-reactive side chain is expected to have negligible technetium-chelating ability. The rigidity also helps to separate the chelator from the targeting peptide. Proline, being a natural amino acid, is biodegradable, yet its homopoylmeric nature suggests that it may resist premature degradation by serum proteases. Finally, because proline is genetically codable, the results of this study can be used to evaluate the suitability of MAG3-$P_3$ analogs for the preparation of recombinantly synthesized chelator-spacers for $^{99m}$Tc labeling of proteins.

One potential limitation when using prolines as a spacer is its relative bulk compared to other linkers, which can potentially dominate the peptide-radiopharmaceutical's pharmacokinetic properties as well as interfere with the receptor-binding capabilities when conjugated to very small targeting peptides. For very small peptides, less hindered spacers such as polyethylene glycol, or the aforementioned 4-aminobutyric acid and 6-aminocaproic acid linkers may be better alternatives.

The minimum number of proline residues required to isolate the MAG3 chelating moiety from the targeting peptide was determined by building proline linkers of increasing length onto the N-terminus of a model peptide with the sequence K-L-A-K-L-A-K-L-A-$NH_2$, appending the spacers with bz-MAG3, and characterizing the [$^{99m}$Tc]BFCA-peptide by radio-HPLC. The results of these studies are presented in Figure 2.1. The chromatograms display a clear trend of increasing radiochemical purity with increasing proline number, and suggest that a minimum spacer length of three proline residues are required in order to achieve >90% radiochemical purity.

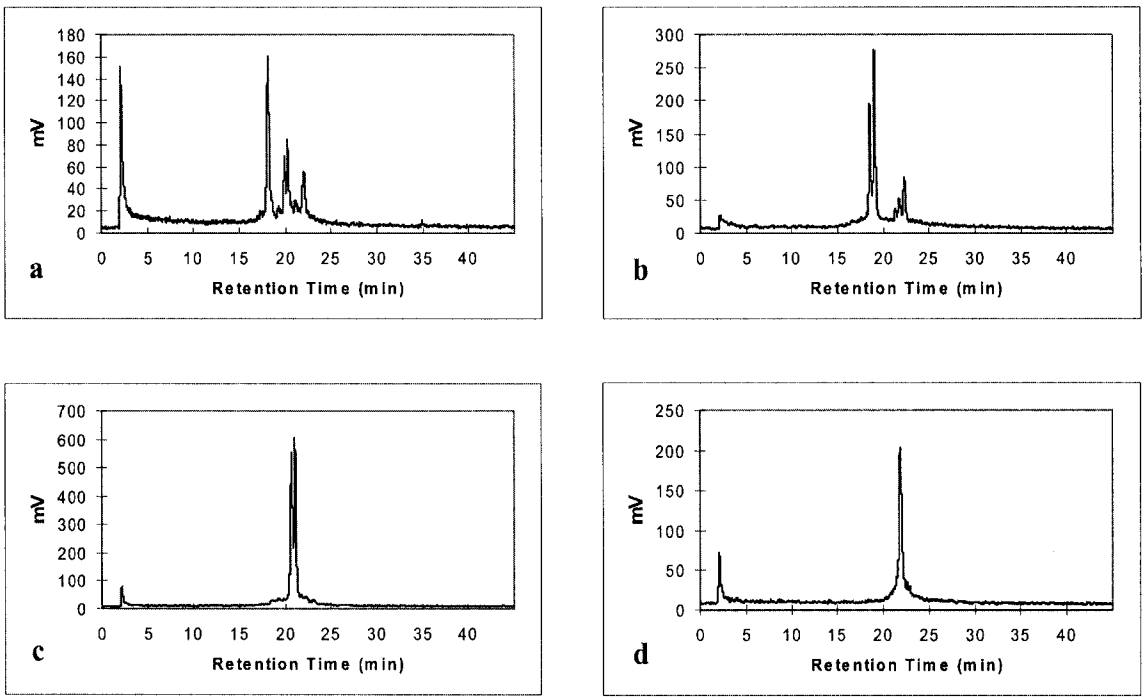


Figure 2.2. Effect of spacer length on radiochemical purity. BFCA-peptides were constructed with zero (a), one (b), two (c), and three (d) proline spacers between the bz-MAG3 BFCA and a model peptide with the sequence KLAKLAKLA-$NH_2$. The radiochromatograms for the $^{99m}$Tc-labeled constructs display a clear trend of increasing radiochemical purity with increasing number of prolines in the spacer.

### 2.3.3. Targeting Peptide Selection

To establish the generality of this technology, we prepared and labeled several bz-MAG3-$P_3$-peptides, using analogs of bombesin [12], and the αM2 sequence [13] as our representative targeting peptides. Bombesin is a 14-residue peptide (pE-Q-R-L-G-N-Q-W-A-V-G-H-L-M-$NH_2$) that binds to the gastrin-releasing peptide (GRP) receptor with an affinity in the low-to-sub-nanomolar range [31-34]. The GRP receptor is overexpressed in many tumours, including small-cell lung carcinoma (SCLC), glioblastoma, gastric cancer, as well as cancers of the pancreas, prostate, and breast [25-30]. αM2 is a 15-residue peptide (Y-C-A-R-E-P-P-T-R-T-F-A-Y-W-G) derived from the third heavy chain complementarity determining region (CDR 3H) of the ASM2 murine IgG1 monoclonal antibody [13]. The αM2 peptide binds with micromolar binding affinity (25 μM) to tumor-associated antigen polymorphic endothelial mucin core protein (MUC1), which is expressed on over 90% of all epithelial carcinomas [13]. Analogs of bombesin and the αM2 peptide have both recently been shown to label $^{99m}$Tc at their N-termini; either by conjugation with a BFCA, as in the case of DADT-lys$^3$-bombesin [34]; or using the natural chelating ability of the native sequence (αM2); without significantly affecting their receptor-binding ability. An additional advantage in using these two peptides is that their combined composition encompasses nearly the entire range of natural amino acids expected to interfere with $^{99m}$Tc chelation.

### 2.3.4. Radiochemical Purity Characterization

Radiochemical purity was judged primarily by radio-HPLC. It is important to note that although powerful in its ability to resolve many of the isomers generated during

the $^{99m}$Tc labeling of BFCA-peptide conjugates (epimers, diastereomers, and misdirected chelations from the targeting peptide), radio-HPLC is not an absolute measure of radiochemical purity. [$^{99m}$Tc]colloid formation and optical isomers cannot be resolved by conventional radio-HPLC. In determining the choice and length of linker group, the only isomeric species under consideration are indeed distinguishable by radio-HPLC, and we therefore restricted these aspects of the present study to this single analytical technique, with concurrent monitoring of the UV chromatogram at 220 nm to confirm that the observed radiochemical profiles had no corresponding UV profile and were in fact due to interaction with $^{99m}$Tc at the tracer level. A summary of the comparative radiochemical purity profiles under optimal labeling conditions for each [$^{99m}$Tc]BFCA-peptide is provided in Table 2.2. All the BFCA-peptides used in the present study were labeled by an exchange labeling approach. Radiochemical purity and yield were optimized by adjusting the pH of the reaction mixture and then observing the radiochromatographic profile. The radiolabeling characteristics of the biologically active BFCA-peptides bz-MAG3-$P_3$-bombesin and bz-MAG3-$P_3$-αM2 were also examined using different reducing agents (substituting $Na^+N_2S_2O_4^-$ for the more commonly used $SnCl_2$) and transfer ligand (replacing sodium tartrate with sodium gluconate). Interestingly, nearly all the BFCA-peptides showed optimal radiochemical purity when using the $SnCl_2$/tartrate labeling mixture at pH 12, the only exception being MAG3-$P_3$-bombesin. Optimal labeling conditions for this labeled peptide were found instead using sodium dithionite/gluconate at pH 8.

Table 2.2. Optimized labeling conditions and corresponding radio-HPLC characterization for the $^{99m}$Tc labeled peptides.

| BFCA-Peptide | $^{99m}$Tc Labeling Conditions | Radio-HPLC Characterization |
|---|---|---|
| MAG3-$(KLA)_3$ | $SnCl_2$/tartrate/pH 12 | multiple isomers, low yield |
| MAG3-$P_1$-$(KLA)_3$ | $SnCl_2$/tartrate/pH 12 | multiple isomers, high yield |
| MAG3-$P_2$-$(KLA)_3$ | $SnCl_2$/tartrate/pH 12 | two primary peaks, high yield |
| MAG3-$P_3$-$(KLA)_3$ | $SnCl_2$/tartrate/pH 12 | single peak, high yield |
| MAG3-Bombesin | $Na^+N_2S_2O_2^-$/gluconate/pH 8 | two primary peaks, high yield |
| MAG3-$P_3$-Bombesin | $Na^+N_2S_2O_2^-$/gluconate/pH 8 | single peak, high yield |
| aM2 | $SnCl_2$/tartrate/pH 12 | multiple isomers, low yield |
| MAG3-$P_3$-aM2 | $SnCl_2$/tartrate/pH 12 | one primary peak, low yield |
| MAG3-$P_3$-aM2-a | $SnCl_2$/tartrate/pH 12 | single peak, high yield |

The radio-HPLC chromatograms for bz-MAG3-Bombesin and bz-MAG3-$P_3$-Bombesin (Figure 2.2) illustrate the marked improvement in radiochemical purity achievable by using a triproline spacer. The radio-HPLC profile for bz-MAG3-bombesin, which lacks a spacer group, is characterized by two primary peaks of approximately equal intensity along with numerous leading and trailing peaks. In contrast, the radiochromatogram for bz-MAG3-$P_3$-bombesin contains over 95% radioactivity in a single peak. Both BFCA-peptides labeled quickly and with high yield (>90%), likely due to the high labeling efficiency of MAG3.

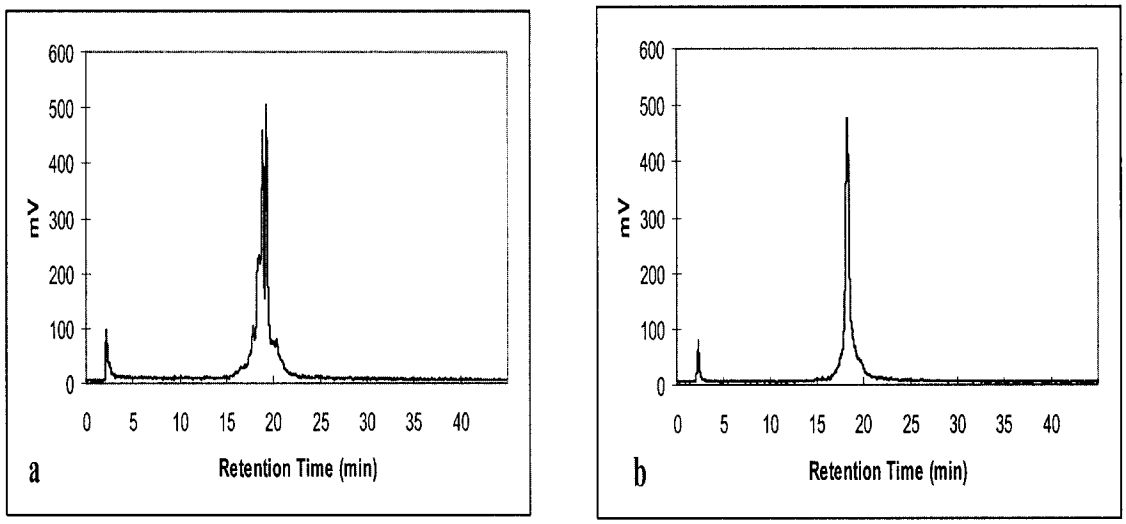


Figure 2.3. Optimized radio-HPLC profiles for MAG3-bombesin (a) and MAG3-$P_3$-bombesin (b). Addition of the triproline spacer considerably improves radiochemical purity.

The radiolabeling characteristics for the αM2 series of experiments are consistent with those of bombesin. αM2 contains a cysteine residue near its N-terminus, which imparts a natural chelating ability to this sequence, although the technetium-labeled product is quite impure when radiolabeling by this method is employed. Several species are visible in the radiochromatogram, including a significant amount of unbound $^{99m}$Tc, indicating poor radiochemical purity and yield. When bz-MAG3-$P_3$ is appended to the αM2 N-terminus, radiochemical purity improves substantially, with just one primary peak associated with the radiolabeled peptide. Curiously, all efforts to improve the radiochemical yield past ~50% for this sequence met with failure. We hypothesized that the poor radiolabeling efficiency might be due to interference from the native cysteine present in the sequence. To test this hypothesis, we constructed an analog of the αM2 sequence (αM2-a), substituting alanine for cysteine, then adding the bz-MAG3-$P_3$ BFCA-spacer to the peptide N-terminus. The radiolabeling characteristics for this sequence showed a considerable improvement over the native

sequence, with over 95% radioactivity present as a single peak. These results suggest that the presence of cysteine in the MAG3-$P_3$-peptide sequence may interfere with technetium chelation. Accordingly, the presence of cysteine would be a limitation in targeting peptides for technetium labeling by this method.

### 2.3.5. Stability in Plasma

Since the efficacy of a diagnostic test largely depends on the *in vivo* stability of the radiopharmaceuticals, one of the more important objectives of this study was to determine the stability of these radiolabeled peptides in plasma. The results of these experiments demonstrate that the [$^{99m}$Tc]MAG3-$P_3$-peptide complexes remained stable and did not show any significant breakdown when incubated with human plasma at 37 $^{o}$C for 18 h. A maximum of 20% dissociated $^{99m}$Tc activity was found for both the [$^{99m}$Tc]MAG3-$P_3$-peptides when compared with the radiochemical yield of original compound.

### 2.3.6. Cysteine Challenge

Transchelation of $^{99m}$Tc from peptides or proteins to endogenous cysteine is known to occur *in vivo* [35]. The strength of each [$^{99m}$Tc]peptide complex was evaluated by displacement of the bound radionuclide with cysteine. The incubation of radiolabeled peptide with 100-fold and 500-fold molar excess of cysteine at 37 $^{o}$C for 1 h and 6 h intervals allowed for an estimation of the extent of transchelation of the weakly bound $^{99m}$Tc. Samples were analyzed by radio-TLC and examined for any displacement of $^{99m}$Tc activity from the labeled peptide. After 1 h of incubation, it was found that a

maximum of 11% of the radioactivity could be transchelated when these peptides were challenged with a 500-fold molar excess of cysteine. Radiochromatographic analysis of the same samples after 6 h incubation indicated that, for [$^{99m}$Tc]MAG3-$P_3$-bombesin, a maximum of 15% of the $^{99m}$Tc activity was dissociated, and for [$^{99m}$Tc]MAG3-$P_3$-αM2-a, a maximum of 10% transchelation. These transchelation studies show that the incubation of [$^{99m}$Tc]BFCA-peptides with excess amount of cysteine can result in a gradual decomposition of radiolabeled peptide with the simultaneous formation of [$^{99m}$Tc]cysteine. In contrast, [$^{99m}$Tc ]MAG3 alone tends to remain stable under these conditions. Nevertheless, these transchelation studies show that the [$^{99m}$Tc ]MAG3 peptides are nearly as stable as [$^{99m}$Tc ]MAG3 alone [36].

### 2.3.7. In Vitro Receptor Binding

[$^{99m}$Tc]MAG3-$P_3$ peptides of bombesin and αM2-a were tested for their ability to bind two human tumor cell lines: PC-3 (prostate adenocarcinoma), and MCF-7-III (breast adenocarcinoma). A dose-dependent binding curve was found for both cell lines (a representative plot for [$^{99m}$Tc]MAG3-$P_3$-bombesin is shown in Fig 2.3). The binding of the two bioactive peptides was inhibited by the presence of an excess of its corresponding unlabeled competing peptide showing that the binding was specific. The nonspecific binding progressively increases at higher concentrations for both peptides. However, specific binding was demonstrable at lower concentrations. The double-reciprocal plot of the [$^{99m}$Tc]MAG3-$P_3$-bombsin specifically bound versus the amount of free peptide provides a $K_d$ of ~6.3 nM which is similar to data reported for [$^{125}$I]Tyr$^4$-bomesin [26]. Specific binding was clearly demonstrable for the

[$^{99m}$Tc]MAG3-$P_3$-αM2-a although saturation was not evident at the concentrations employed (Fig 2.3-b).

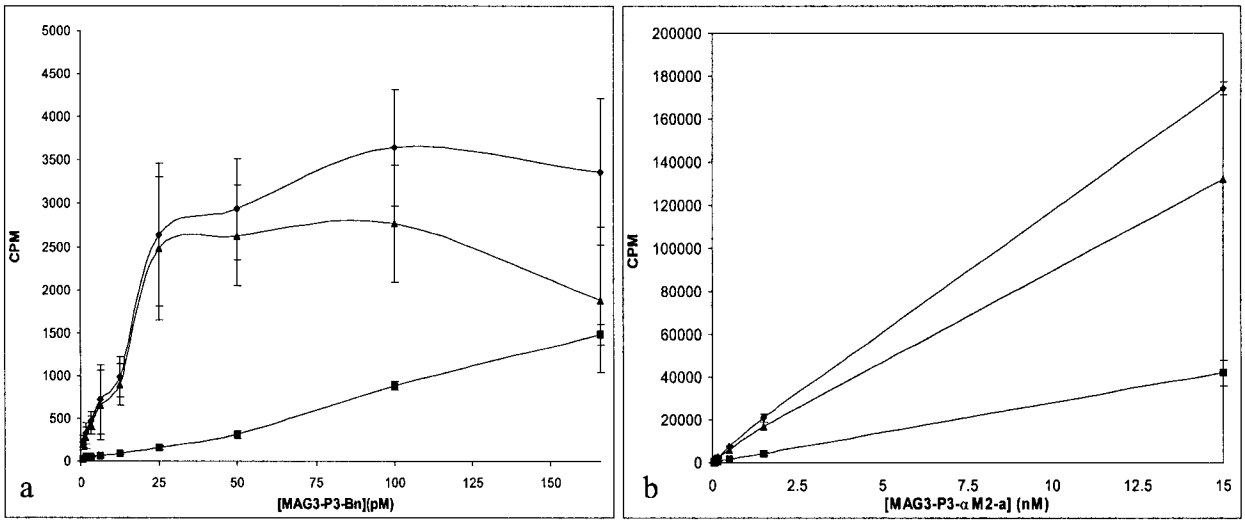


Figure 2.4. *In vitro* binding data for a) [$^{99m}$Tc]MAG3-$P_3$-bombesin with the MCF-7-III breast carcinoma cell-line, and b) [$^{99m}$Tc]MAG3-$P_3$-αM2-a with PC-3. Specific binding (triangles) is calculated as the difference between the total binding (diamonds) and non-specific binding (squares).

## 2.4. Conclusion

The combined use of benzoyl-protected MAG3 with a triproline spacer allows for the preparation of $^{99m}$Tc-based peptide radiopharmaceuticals with many desirable qualities. Synthesis by SPPS affords simultaneous peptide synthesis, linker addition, and chelator addition while reducing the number of synthetic steps and purification steps required to prepare the final product. The unreactive triproline linker not only simplifies the synthetic strategy but also makes the protocol extendable to genetically expressed peptides and proteins. In particular our results suggest that BFCA-spacers can be engineered into proteins to create BFCA-proteins with well-defined labeling characteristics for nuclear imaging purposes. Incorporation of MAG3 as the chelating

agent allows one to obtain all its associated advantages: FDA approval, low isomerism, stability in plasma, resistance to transchelation, and 15 years of clinical experience. Synthesis of benzoyl-protected MAG3-peptides imparts long shelf life and high efficiency labeling under mild conditions; thus making kit formulation feasible. Our studies indicate that the synthesis, stability, labeling protocols, and biological activity of peptides prepared and labeled by this method are all good, suggesting that these techniques are generally applicable and with the exception of cysteine, sequence independent.

## 2.5. References


1. Lister-James J., Moyer B.R., and Dean R.T. (1996) Small Peptides Radiolabeled with $^{99m}$Tc. *Q. J. Nucl. Med.* **40**:221-233.

2. Thakur M.L. (1995) Radiolabeled peptides: now and future. *Nucl. Med. Commun.* **16**:724-732.

3. Fischman A.J., Babich J.W., and Strauss H.W. (1993) A ticket to ride: peptide radiopharmaceuticals. *J. Nucl. Med.* **34**:2253-2263.

4. McAfee J.G. and Neumann R.D. (1996) Radiolabeled peptides and other ligands for receptors overexpressed in tumor cells for imaging neoplasms. *Nucl. Med. Biol.* **23**:673-676.

5. Deutsch E., Libson K., Vanderheyden J., Ketring A.R., and Maxon H.R. (1986) The chemistry of rhenium and technetium as related to the use of isotopes of these

elements in therapeutic and diagnostic nuclear medicine. *Int. J. Rad. Appl. Instrum. [B]* **1**:465-477.

6. Liu S., Edwards D.S., and Barrett J.A. (1997) $^{99m}$Tc Labeling of Highly Potent Small Peptides. *Bioconjugate Chem.* **8**:621-636.

7. Zamora P.O. and Rhodes B.A. (1992) Imidazoles as well as thiolates in proteins bind technetium-99m. *Bioconjugate Chem.* **3**:493-498.

8. Liu S., Edwards D.S., and Harris A.R. (1998) A novel ternary ligand system for $^{99m}$Tc-labeling of hydrazino nicotinamide-modified biologically active molecules using imine-N-containing heterocycles as coligands. *Bioconjugate Chem.* **5**:589-595.

9. Subhani M., Cleynhens B., Bormans G., Hoogmartens M., De Roo M., and Verbruggen A.M. (1989) Complexes of technetium-99m with mercaptoacetyltripeptides: labeling and characteristics and biodistribution in mice. *In* "Technetium and Rhenium in Chemistry and Nuclear Medicine 3" (M. Nicolini, G. Banoli, and U. Mazzi, eds.) pp. 661-666. Cortina International, Verona.

10. Pallela V.R., Thakur M.L, Chakder S., and Rattan S. (1999) $^{99m}$Tc-Labeled Vasoactive Intestinal Peptide Receptor Agonist: Functional Studies. *J. Nucl. Med.* **40**:352-360.

11. Harris T.D., Rajopadhye M., Damphousse P.R., Glowacka D., Yu K., Bourque J.P., Barrett J.A., Damphousse D.J., Heminway S.J., Lazewatsky J.L., Mazaika T., and Carroll T.R. (1996) Tc-99m-labeled fibrinogen receptor antagonists: design and synthesis of cyclic RGD peptides for the detection of thrombi. *Bioorg. Med. Chem. Lett.* **6**:1741-1746.

12. Anastasi A., Erspamer V., and Bucci M. (1972) Isolation and amino acid sequences of alytesin and bombesin: two analogous active tetradecapeptides from skin of European discoglossid frogs. *Arch. Biochem. Biophys.* **148**:443-446.

13. Sivolapenko G.B, Douli V., Pectasides D., Skarlos D., Sirmalis G., Hussain R., Cook J., Coutenay-Luck N.S., Merkouri E., Konstantinides K., and Epnetos A.A. (1995) Breast cancer imaging with radiolabeled peptide from complementarity-determining region of antitumour antibody. *The Lancet* **346**:1662-1666.

14. Stewart J.M. and Young J.D. (1984) *In* "Solid Phase Peptide Synthesis. 2nd Ed." pp. 83-84. Pierce Chemical Company, Rockford, Illinois.

15. Wellings D.A. and Atherton E. (1997) Standard Fmoc protocols. *Methods Enzymol.* **289**:44-67.

16. Brandau W., Bubeck B., Eisenhut M., and Taylor D.M. (1988) Technetium-99m labeled renal function and imaging agents: III. Synthesis of $^{99m}$Tc-MAG3 and biodistribution of by-products. *Appl. Radiat. Isot.* **39**:121-129.

17. Kaiser E., Colescott R.L., Bossinger C.D., and Cook P.I. (1970) Color test for detection of free terminal amino groups in the solid-phase synthesis of peptides. *Anal. Biochem.* **34**:595-598.

18. Chilton H.M. and Witcofski R.L. (1986) Nuclear Pharmacy: An Introduction to the Clinical Application of Radiopharmaceuticals. Lea & Febiger, Philadelphia, PA.

19. Rhodes B.A., Zamora P.O., Marek M.J., Sharma S.D., and Wall F.J. (1995) Direct $^{99m}$Tc labeling of proteins and peptides: Factors that alter radiochemical yields and *in*

*vivo* stability. *In* "Technetium and Rhenium in Chemistry and Nuclear Medicine 4" (M. Nicolini, G. Bandoli, and U. Mazzi, eds.) pp. 281-286. Bressanone, Italy.

20. Schaap G.H., Alferink T.H., de Jong R.B, Oe P.L., Roos J.C., and Donker A.J. (1988) $^{99m}$Tc-MAG3: Dynamic studies in patients with renal disease. *Eur. J. Nucl. Med.* **14**:28-31.

21. Taylor A. Jr., Eshima D., Christian P.E., and Milton W. (1987) Evaluation of Tc-99m Mercaptoacetyltriglycine in patients with impaired renal function. *Radiology* **162**:365-370.

22. Fritzberg A.R., Kasina S., Eshima D., and Johnson D.L. (1986) Synthesis and biological evaluation of technetium-99m MAG3 as a Hippuran replacement. *J. Nucl. Med* **27**:111-116.

23. Okarvi S., Adriaen P., and Verbruggen A.M. (1997) Comparison of the labeling characteristics of mercaptoacetyltriglycine (MAG3) with different S-protective groups. *J. Label. Compds. Radiopharm.* **39**:853-874.

24. Preston S.R., Miller G.V., and Primrose J.N. (1996) Bombesin-like peptides and cancer. *Crit. Rev. Oncol. Hematol.* **23**:225-238.

25. Alexander R.W., Upp J.R. Jr., Poston G.J., Gupta V., Townsend C.M. Jr., and Thompson J.C. (1988) Effects of bombesin on growth of human small cell lung carcinoma in vivo. *Cancer Res.* **48**:1439-1441.

26. Moody T.W., Mahmoud S., Staley J.S., Naldini L., Cirillo D., South V., Felder S., and Kris R. (1989) Human glioblastoma cell lines have neuropeptide receptors for bombesin/gastrin-releasing peptide. *J. Mol. Neurosci.* **1**:235-242.

27. Farre A., Ishizuka J., Gomez G., Parekh D., Koo J.Y., Townsend C.M., and Thompson J.C. (1993) Bombesin stimulates growth on colon cancer in mice and decreases their survival. *Surg. Oncol.* **2**:169-173.

28. Qin Y., Ertl T., Cai R.Z., Halmos G., and Schally A.V. (1994) Inhibitory effect of bombesin receptor antagonist RC-3095 on the growth of human pancreatic cancer cells in vivo and in vitro. *Cancer Res.* **54**:1035-1041.

29. Qin. Y., Halmos G., Cai R.Z., Szoke B., Ertl T., and Schally A.V. (1994) Bombesin antagonists inhibit in vitro and in vivo growth of human gastric cancer and binding of bombesin to its receptors. *J. Cancer Res. Clin. Oncol.* **120**:519-528.

30. Yano T., Pinski J., Szepheshazi K., Groot K., and Schally A.V. (1992) Stimulation by bombesin and inhibition by bombesin/gastrin releasing peptide antagonist RC-3095 of growth of human breast cancer cell lines. *Cancer Res.* **52**:4545-4547.

31. Reile H., Cai R., Armatis P., and Schally A.V. (1995) New antagonists of bombesin/gastrin-releasing peptide with C-terminal Leu $\psi(CH_2N)$Tac-$NH_2$. *Int. J. Onc.* **7**:749-754.

32. Edwards J.V., McLean L.R., Wade A.C., Eaton S.R., Cashman E.A., Hagaman K.A., and Fanger B.O. (1994) Potent pseudopeptide bombesin-like agonists and antagonists. *Int. J. Pept. and Prot. Res.* **43**:374-383.

33. Cai R., Quin Y., Ertl T., and Schally A.V. (1995) New Pseudononapeptide bombesin antagonists with C-terminal Leu $\psi(CH_2N)$Tac-$NH_2$ show high binding affinity to bombesin/GRP receptors on CFPAC-1 human pancreatic cancer cells. *Int. J. Onc.* **6**:1165-1172.

34. Baidoo K.E., Lin K.S., Zhan Y., Finley P., Scheffel U., and Wagner H.N. Jr. (1998) Design, Synthesis, and Initial Evaluation of High-Affinity Technetium Bombesin Analogues. *Bioconjugate Chem.* **9**:218-225.

35. Rusckowski M., Fogarasi M., Virzi F., Winnard P., and Hnatowich D.J. (1993) Investigations into the mechanism in tumor of transchelation of $^{99m}$Tc from antibodies to cysteine. *J. Nucl. Biol. Med.* **37**:176-180.

36. Stalteri M.A., Bansal S., Hider R., and Mather S.J. (1999) Comparison of the stability of technetium-labeled peptides to challenge with cysteine. *Bioconjugate Chem.* **10**:130-136.

# CHAPTER 3. APPLICATION OF SOLID PHASE PEPTIDE SYNTHESIS TO ENGINEERING PEO-PEPTIDE BLOCK COPOLYMERS FOR DRUG DELIVERY[1]

## 3.1. Introduction

Amphipathic block copolymers consist of a linear arrangement of alternating hydrophilic and hydrophobic segments. When exposed to polar solvents these block copolymers can self-assemble to form extraordinarily stable micellar suspensions consisting of a dense, hydrophobic core and a solvated outer shell [1]. Hydrophobic small molecule drugs can be incorporated into the hydrophobic core during micellization. The amphipathic block copolymer micelle, with its core/shell architecture, and its ability to transport lipophilic substances in aqueous media, is structurally and functionally similar to plasma lipoproteins [2,3]. Thus, researchers are actively investigating the use of biocompatible block copolymers as long-circulating delivery systems for hydrophobic small molecule drugs. Micellar drug microcontainers can, in principle, impart numerous desirable therapeutic advantages to existing drugs in that they: (a) protect the drug from enzymatic or other degradative mechanisms; (b) increase the solubility of poorly soluble hydrophobic drugs; (c) modulate the drug's pharmacokinetics; and (d) can accumulate at the target site. However, in developing a pharmaceutically useful polymeric micelle for drug delivery, many performance-related issues must be addressed, including

---

[1]Portions of this chapter appear in Surfaces and Colloids B: Biointerfaces: Van Domselaar G.H., Kwon G.S., Andrew L.C., and Wishart D.S. Application of Solid Phase Peptide Synthesis to Engineering PEO-Peptide Block Copolymers for Drug Delivery. *Coll. Surf. B: Bioint.* (in press).

drug-loading capacity, release kinetics, circulation time, biodistribution, static and dynamic stability, morphology, size, and size distribution [4]. To a large extent these properties are determined by block copolymer composition. The hydrophilic shell-forming block determines the micelle's pharmacokinetic parameters, biodistribution, and contributes significantly to the micelle's physical and biological stability of the micelle. On the other hand, the composition of the core-forming block determines the micelle's drug loading capacity, drug specificity, and contributes largely to the micelle's physico-chemical properties. With few notable exceptions [5-7] most research on block copolymer micelles for drug delivery has focused on the use of poly(ethylene oxide) (PEO) for the hydrophilic shell. PEO's high degree of hydration and large excluded volume induce repulsive forces which impart steric stability to the micelle, and extend circulation times by preventing opsonization, thereby avoiding clearance by the reticuloendothelial system [8]. In contrast to the near universal application of PEO for the hydrophilic shell-forming block, a somewhat larger variety of hydrophobic core-forming blocks have been investigated. Examples of core-forming block compositions include poly($\epsilon$-caprolactone) [9], poly(D,L-lactide) [6], poly(propylene oxide) [10], and poly(L-amino acids) and their derivatives [11-14].

Although biocompatible PEO-*b*-peptide block copolymer micelles show promise as drug carriers, their development and study has been slowed by the difficulty associated with their synthesis. Traditionally, block copolymer synthesis is performed by derivatizing one or both ends of the PEO block with an initiator, and then adding the PEO to a solution containing the monomeric L-amino acid N-carboxyanhydride which, upon polymerization, yields the block copolymer [2]. This synthetic route, although

reproducible and well established, requires strict control of reagent purity and stoichiometry in order to minimize polydispersity and byproduct formation. Moreover, this strategy is restricted to the formation of compositionally homogeneous copolymer hydrophobic blocks. Hence, for a given hydrophobic block composition, micelle nano-engineering is limited to "approximately" adjusting the relative and absolute lengths of the block copolymer segments.

We have hypothesized that the techniques of solid phase peptide synthesis (SPPS) may be adapted to the construction PEO-*b*-peptide block copolymers with precisely defined core lengths and core compositions, thus allowing the properties of the resulting micelles to be engineered in fine detail. To test this hypothesis, we used SPPS, followed by solution phase condensation (SPC) to prepare two series of block copolymers: one of fixed composition and varying length; the other of fixed length and varying composition. We then performed experiments to systematically study the relationships of core length and core composition to micelle size and thermodynamic stability in terms of free energy of micellization (CMC), micelle-unimer equilibrium, and micelle dissociation rates.

## 3.2. Experimental Section

### 3.2.1 Materials and Reagents

5000 molecular weight α-methyl-ω-proprionic acid-PEO (PEO-O-$CH_2$-$CH_2$-COOH) was obtained from Shearwater Polymers Inc. (Huntsville, AL). Rink amide methylbenzhydrylamine resin (Rink Amide MBHA), O-benzotriazole-N,N,N′,N′-

tetramethyluronium hexafluorophosphate (HBTU), piperidine, and Fmoc-amino acids were purchased from Chem Impex International Inc. (Woodale, IL) and used as received. HATU [(7-azabenzotriazol-1yl)-1,1,3,3,-tetramethyluronium hexafluorophosphate] was purchased from PerSeptive Biosystems (Framingham, MA). Sequencing grade dimethylformamide (DMF) and dichloromethane (DCM) were obtained from Fisher Scientific Canada. Trifluoroacetic acid (TFA) was purchased from Halocarbon Products Corporation (River Edge, NJ). N-methyl morpholine (NMM) was purchased from Aldrich Chemical Co. (Milwaukee, IL).

### 3.2.2 PEO-Proprionic Acid Characterization

PEO-proprionic acid was characterized for weight-average molecular weight (*Mw*), number average molecular weight ($M_n$,) and polydispersity index (*I*) by MALDI-TOF mass spectrometry. A 200 μM sample of PEO-proprionic acid in $ddH_2O$ was prepared and mixed 1:1 with a matrix solution consisting of 0.1 M dihydroxybenzoic acid dissolved in 1:1 MeOH and doped with 2 mM NaCl to promote ionization. Spectra were acquired on a PerSeptive Biosystems Voyager Elite MALDI-TOF mass spectrometer. *Mw*: 5223, *Mn*: 5180, *I*: 1.01.

### 3.2.3 Solid-Phase Peptide Synthesis, Cleavage, and Purification

A series of polytyrosine core-forming blocks, with composition Gly-$Tyr_n$, where n = 7, 9, 12, and 15 residues, and a series of constant length blocks with compositions Gly-$Phe_{15}$ (polyphenylalanine), Gly-$Leu_{15}$ (polyleucine), and Gly-Phe-Leu-Tyr-Trp-Phe-Leu-Tyr-Trp-Phe-Leu-Tyr-Trp-Phe-Leu-Tyr-Trp-Phe-Leu-Tyr (polyFLYW), were assembled using an ABI 430A automated peptide synthesizer on Rink amide MBHA resin using standard

Fmoc/t-butyl protected L-amino acids and HATU active-ester based coupling [15]. Upon completion of each peptide block synthesis the protected peptide-resin was transferred to a 20 ml disposable polypropylene cartridge fitted with a polyethylene frit. A 10 ml solution of cleavage cocktail: TFA:$H_2O$ (95:5) was added and the mixture shaken gently for 2 hours. The cleaved and deprotected peptide block was then filtered from the resin and the resin washed with 3x2 ml of TFA. The combined eluate was evaporated *in vacuo*, precipitated and washed with cold ether (3x20 ml), then dried *in vacuo* overnight to prepare for purification.

Each crude peptide was purified by RP-HPLC (Waters-System 501) on a reversed-phase $C_8$ 21x250 mm Zorbax 300 S.B. column with a binary gradient at a flow rate of 8.0 ml/min using aqueous 0.1% TFA and 0.1% TFA in acetonitrile as the mobile phase. The eluent was monitored at 220 nm and one-minute fractions were collected. UV absorbing fractions were analyzed by mass spectrometry using a Fisons VG Trio 2000 electrospray mass spectrometer (ES-MS). Fractions containing the correct mass and of sufficient purity were combined and lyophilized to yield the desired peptide block in excess of 90% purity, as judged by ES-MS analysis.

### 3.2.4 Block Copolymer Synthesis

PEO-*b*-peptide block copolymers were prepared using solution phase condensation (SPC). PEO-proprionic acid was coupled to each peptide block in solution at a 0.05 mmol scale. The PEO-proprionic acid carboxyl group was activated using a 0.9 molar equivalent of HATU and two molar equivalents of NMM in DMF. The PEO-proprionic acid was allowed to activate for 1 hour at room temperature on a shaker. The activated PEO (two molar equivalents with respect to the hydrophobic block) was

then coupled to the glycine N-terminal amine of the peptide block in DMF until a negative Kaiser test [16] was obtained (overnight at room temperature on a shaker). The crude block copolymer was dialyzed with three changes of DMF (overnight at room temperature with stirring using Spectra/Por 3500 MWCO dialysis membrane) to remove any unreacted peptide and small molecular weight contaminants. DMF was then removed from the polymer by evaporation *in vacuo*. Unreacted PEO was removed from the block copolymer by preparative HPLC using the same conditions as for crude peptide purification (described earlier). The UV absorbing fractions were collected, lyophilized, desiccated, and stored at 4 °C. The segment condensation coupling efficiency was determined by $^1$H NMR analysis (relative integrated peak area) of the block copolymer in DMSO-$d_6$.

### 3.2.5 Determination of CMC

The critical micelle concentration (CMC) was determined by light scattering according to a previously published procedure [17]. Block copolymer micelles of each of the seven different PEO-*b*-peptide block copolymers were prepared by a gradient dialysis approach [18]. The block copolymer (20 ml) was dissolved in DMF (5 ml) and 10 ml of dd$H_2O$ was added dropwise over 2 h. The solution was dialyzed into three changes of 1 L dd$H_2O$ over 24 h. The micelle solution was filtered through a 0.22 μm nylon membrane (Fisher, Pittsburgh, PA) and lyophilized. Lyophilized micelles (12 mg) were accurately weighed and dissolved into 12 ml 0.1 M $PO_4^{3-}$, pH 7.2. A series of doubling dilutions, from 1.0 mg/ml to $1.0 \times 10^{-4}$ mg/ml, were prepared in triplicate from this stock solution. Light scattering was measured with a SPEX Fluoromax spectrofluorometer using both an excitation wavelength and an emission wavelength of 600 nm, a bandpass

width of 1 nm, a step increment of 0.5 nm, and an integration time of 1.0 s. The intensity of scattered light was plotted against polymer concentration to determine the concentration at which the intensity sharply increases, indicating the formation of micelles.

### 3.2.6 Electron Microscopy Examination

Lyophilized micelles were reconstituted in $ddH_20$ (ca. 1 mg/ml). Samples of the aqueous micelle suspensions were examined by negative-stain transmission electron microscopy (TEM). One drop of the micelle sample was placed on a 300-mesh copper membrane coated disk, followed by one drop of 1% phosphotungstic acid in water (pH 7.0) (the negative stain). After 30 seconds excess liquid was blotted from the disk with filter paper and the sample loaded onto a sample holder. The sample was then examined using a Hitachi Transmission Electron Microscope H-7000 at an accelerating voltage of 75 keV. Micelle size and size distribution was determined directly from the TEM images.

### 3.2.7 Micelle Dissociation Rates

Accurately weighed samples of lyophilized block copolymer micelles were reconstituted in 0.1 M phosphate buffer (pH 7.2) at concentrations above their critical micelle concentration (ca. 1.0 to 2.0 mg/ml). An accurately measured aliquot was removed from each and diluted to a concentration below the CMC (from ca. 0.02 to 0.001 mg/ml) and incubated at 37 °C in a dry bath. 100 µl Samples were withdrawn periodically and subjected to chromatographic analysis using a Rainin HPLC system consisting of a Rainin HPXL solvent delivery system, a Rainin Dynamax

UV-Visible absorption detector. Samples were applied to an Ultrahydrogel 2000 column and matching guard column at a flow rate of 0.8 ml/min and 0.1 M phosphate buffer (pH 7.2) as the mobile phase. The column was calibrated with size exclusion standards: blue dextran (2 000 000 Da), proteins (600 000 Da to 17 000 Da), and sodium azide (65 Da). The eluent was monitored at an appropriate wavelength for detection of the hydrophobic block.

## 3.3. Results and Discussion

Although recent reports have emerged describing the construction of PEO-*b*-peptide block copolymers [19], to our knowledge, this is the first reported application of solid phase peptide synthesis towards the preparation of PEO-*b*-peptide block copolymer micelles. Given the ease with which custom peptides can be prepared or purchased (through commercial and non-commercial peptide synthesis facilities) we believe this hybrid SPPS-SPC approach provides a convenient and cost-effective alternative to the conventional NCA-based ring-opening polymerization strategy. Indeed, a person only needs to order peptides and to have access to an HPLC and a few commercial reagents to prepare these block copolymers – they don't have to be peptide chemists.

The key advantages of SPPS over classical polymerization techniques are the ability to apply combinatorial chemistry to the polymer's construction, and the ability to precisely control core length. Hence, the flexibility of nano-engineering micelle-based drug delivery systems can be extended considerably. In the present study, these properties are exploited to study micellization behavior. Other examples of the possible

applications of this technology include: incorporation of crosslinking residues (such as cysteine) into the core-forming block to produce rigid cores; construction of multipartite systems with separate blocks for core formation, drug binding, and shell formation; and incorporation of peptide-based cleavage substrates into the polymer chain to promote site-specific micelle degradation and drug release.

This SPPS technique was applied to the construction of a set of PEO-*b*-peptide block copolymers with fixed lengths and varying compositions. PEO-*b*-polyleucine contains a hydrophobic, aliphatic core. PEO-*b*-polytyrosine and PEO-*b*-polyphenylalanine contain hydrophobic, aromatic cores. PEO-*b*-polyFLYW is unique among this series, in that it contains a heterogeneous distribution of both aliphatic and aromatic residues. It was designed to study the effect of defined sequence heterogeneity on block copolymer micellization, in analogy to globular proteins, which contain a heterogeneous structure, and form core/shell type particles with glassy cores under physiological conditions [20]. A second set of block copolymers, composed of a polytyrosine peptide block, was constructed with varying lengths (7, 9, 12, and 15 residues) to examine the effect of core-block size on micellization.

### 3.3.1 Synthesis and Characterization

A diagram describing structures of the various block copolymer constructs is provided in Figure 3.1. The peptide block compositions and lengths were controlled by altering the number of SPPS cycles and the order of addition of protected L-amino acids. All seven peptide blocks were appended at the N-terminus with a single glycine residue to aid in the conjugation efficiency of PEO to the peptide block. Glycine is a relatively hydrophilic, unhindered amino acid and is known to disrupt secondary structure

formation. These properties combine to help expose the N-terminal amino group and therefore increase coupling efficiency [21].

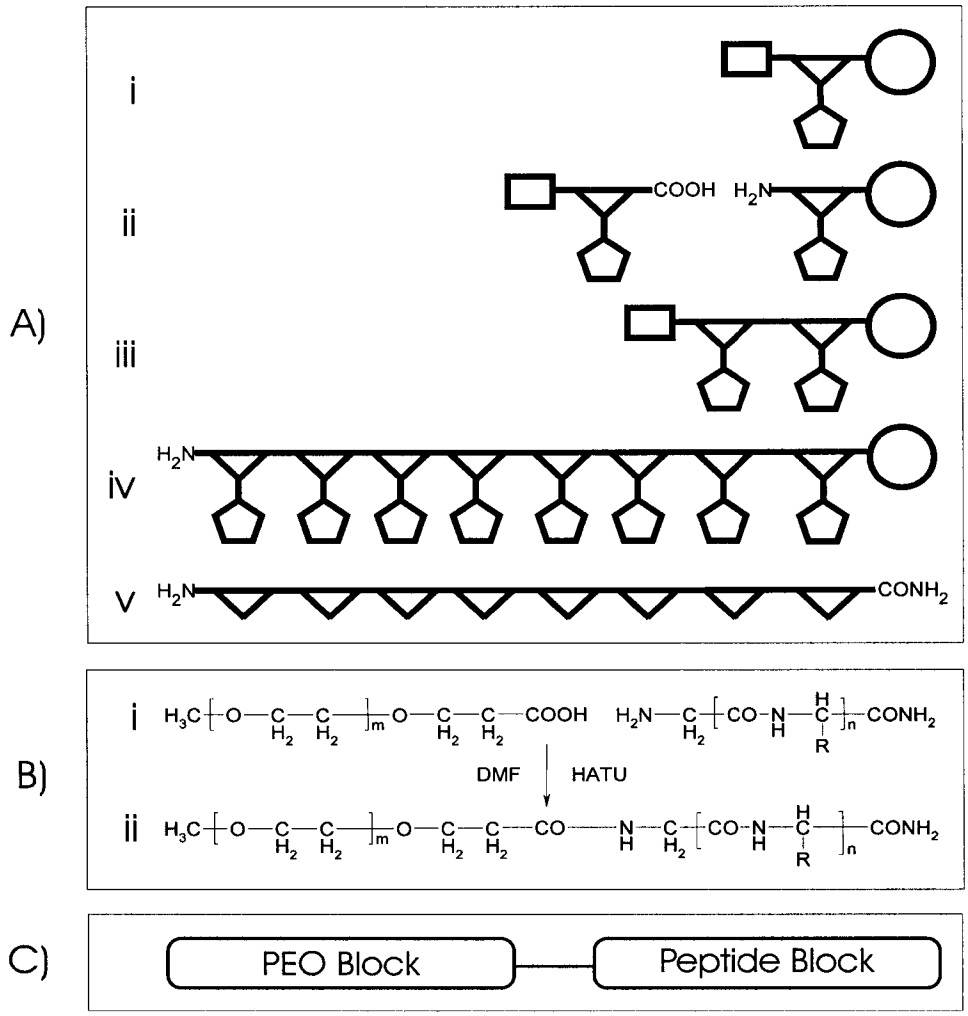


Figure 3.1. A) Schematic diagram depicting the construction of the construction of the peptide block by SPPS: (i) Amino acids (triangle), bearing side-chain protection (hexagon) and $N^{\alpha}$–amino protection (square) are attached to the insoluble support (circle). (ii) The Nα-protecting group is removed. (iii) The incoming amino acid is activated with HATU and coupled to the growing peptide-resin. (iv) Repeated cycles of deprotection, activation and coupling yield the complete peptide-resin. (v) The sidechain protecting groups and the peptide-resin linkage are removed by exposure to TFA. B) Formation of the PEO-*b*-peptide: (i) PEO-proprionic acid is condensed to peptide by amide bond formation (ii). C) Schematic diagram of the amphipathic PEO-peptide block copolymer.

The crude peptide blocks were purified by conventional preparative RP-HPLC to obtain purity levels in excess of 90%, as judged by ES-MS analysis, for all the constructs prepared in this study (data not shown). The remaining fractions consisted of (typically one-residue) deletion products; hence, peptide blocks prepared by SPPS can be considered for all intents and purposes to be monodisperse. This ability to precisely control peptide block length can in turn be exploited to tailor micellization properties such as CMC and dissociation rates, as we demonstrate here.

Early attempts in our lab to attach PEO to resin-bound peptides resulted in low coupling efficiencies, due to the inability of PEO to effectively penetrate the peptide-resin (unpublished results). Instead, the conjugation of each block in the PEO–*b*-peptide block copolymer was accomplished by solution-phase condensation of PEO-proprionic acid with the peptide N-terminal amine. The solvents and reagents used in the conjugation step are identical to those used for amino acid coupling during SPPS and result in the efficient formation of a chemically stable amide bond, making this a convenient and attractive conjugation strategy. Coupling of PEO to peptide was complete after 24 h, as measured by the Kaiser ninhydrin assay for free amines [16]. Purification was achieved by dialysis to remove small molecular weight contaminants and unreacted peptide, followed by RP-HPLC to remove unreacted PEO. $^{1}$H NMR analysis of the purified PEO-*b*-peptide block copolymer in deuterated DMSO revealed the expected peak intensity ratio of PEO methyl protons at 3.55 ppm to amino acid side-chain protons to an accuracy of over 80% (Table 3.1).

Table 3.1. PEO-*b*-peptide block copolymer $^{1}H$ NMR integration results.

| Block Copolymer | Integration | | PEO:PLAA Integration Ratio | | Integration Ratio (Percent Found/Expected) |
|---|---|---|---|---|---|
| | PEO | PLAA | Expected | Found | |
| PEO-*b*-polytyrosine$_7$ | 93.73 | 6.27 | 15.53 | 14.94 | 96.20 |
| PEO-*b*-polytyrosine $_9$ | 93.83 | 6.17 | 12.88 | 15.20 | 118.0 |
| PEO-*b*-polytyrosine $_{12}$ | 90.77 | 9.23 | 9.66 | 9.83 | 101.7 |
| PEO-*b*-polytyrosine $_{15}$ | 89.32 | 10.68 | 7.73 | 8.36 | 108.2 |
| PEO-*b*-polyphenylalanine $_{15}$ | 83.62 | 16.38 | 6.18 | 5.11 | 82.68 |
| PEO-*b*-polyleucine$_{15}$ | 84.71 | 15.29 | 5.15 | 5.54 | 107.6 |
| PEO-*b*-G-polyFLYW | 96.32 | 3.68 | 29.0 | 26.17 | 90.24 |

### 3.3.2 Critical Micelle Concentration

The critical micelle concentration (CMC) is the minimum concentration of copolymer that will result in micelle formation. This parameter is an important indicator of the stability of a micelle: the lower the CMC value the more stable the micelle. Light scattering was used to determine the CMC values of the various PEO-*b*-peptide micelles (Table 3.2 and Figure 3.2). At concentrations below the CMC the change in light scattering intensity with a corresponding change of concentration is minimal. At and above the CMC, the block copolymer unimers self-assemble into micelles, resulting in a dramatic change in the sensitivity of light scattering to concentration. The CMC of the PEO-b-peptide constructs is taken as the intersection between the two essentially linear sections of the intensity-concentration curve.

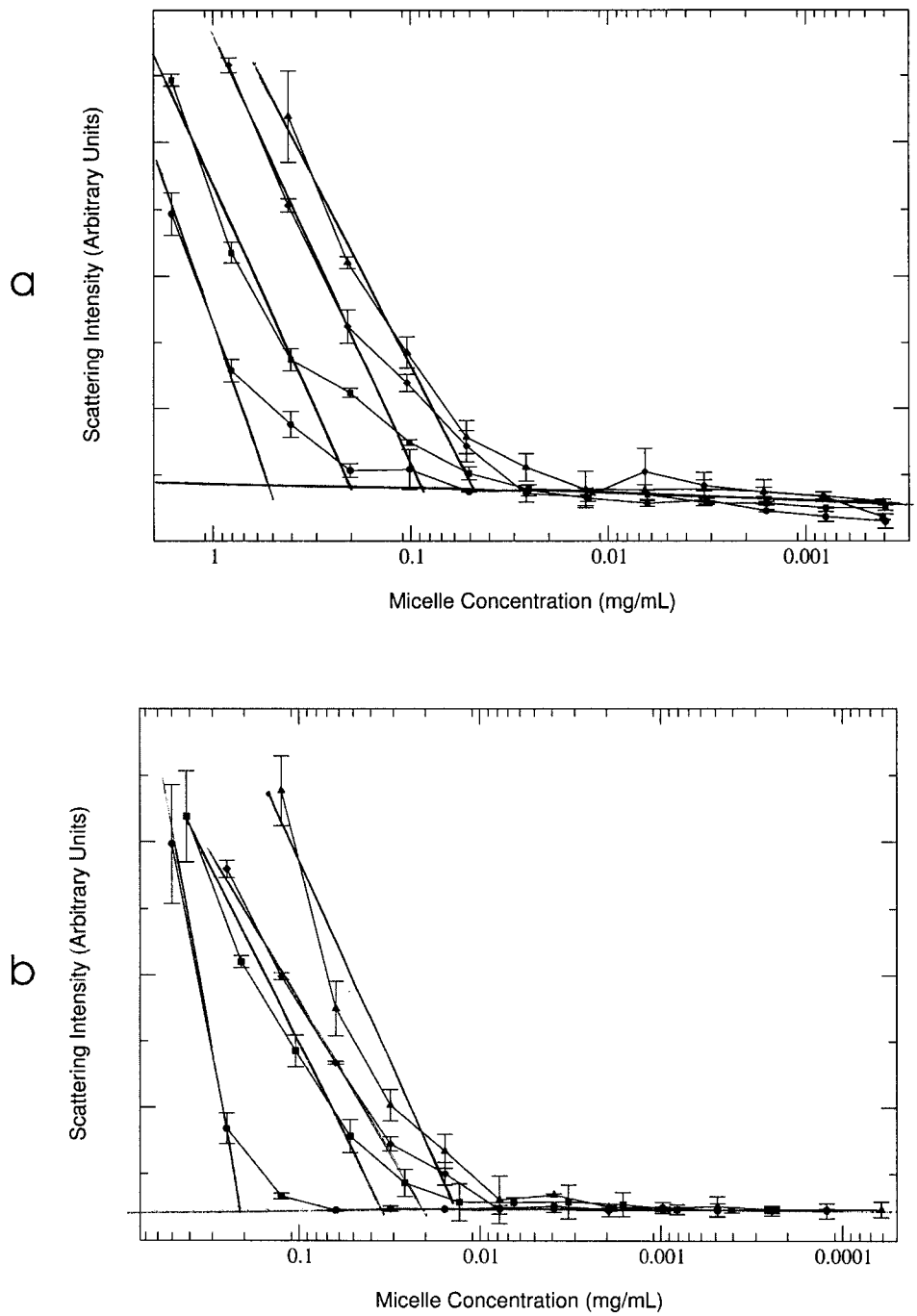


Figure 3.2. CMC determination by light scattering. (a) PEO-*b*-polytyrosine with core lengths of 7 residues (circles), 9 residues (squares), 12 residues (diamonds), and 15 residues (triangles). (b) Fixed core length series (15 residues) with core compositions of polyleucine (triangles), polyphenylalanine (diamonds), polytyrosine (squares), and polyFLYW (circles).

Table 3.2. Micelle characteristics.

| Block Copolymer | HPLC Elution Time (min) | | CMC (mg/ml) | Size (nm) | Peptide Hydropathy[†] |
|---|---|---|---|---|---|
| | Unimers | Micelles | | | |
| PEO-*b*-polytyrosine$_7$ | 15.59±0.04 | n.d. | 0.46 | 24.5 ±0.90 | 0.960 |
| PEO-*b*-polytyrosine $_9$ | 15.62±0.05 | n.d. | 0.19 | 26.3±0.30 | 0.960 |
| PEO-*b*-polytyrosine $_{12}$ | 15.60±0.05 | 12.25±0.02 | 0.080 | 26.8±0.40 | 0.960 |
| PEO-*b*-polytyrosine $_{15}$ | 15.92±0.09 | 10.04±0.02 | 0.050 | 28.3±0.7 | 0.960 |
| PEO-*b*-polyphenylalanine$_{15}$ | 15.74±0.02 | n.d. | 0.019 | 38.6±0.3 | 1.790 |
| PEO-*b*-polyleucine$_{15}$ | 17.20±.0.02 | 11.50±0.05 | 0.014 | 24.0±1.2 | 1.700 |
| PEO-*b*-polyFLYW | 15.61±0.02 | n.d. | 0.20 | 63.7±0.5 | 1.675 |

[†] Based on Fauchere-Pliska hydrophobicity values [26].

The CMC values for the variable length PEO-*b*-polytyrosine block copolymers decreased (indicating greater stability) as the length of the hydrophobic block increased, consistent with both theory [22] and observation [23]. The range of values (0.5 mg/ml - 0.05 mg/ml) compare favorably with those reported for other PEO-*b*-poly(amino acid) block copolymers under investigation as drug delivery vehicles [24,25].

The relationship between peptide block composition and CMC is not as clear as for peptide block length. The observed CMC values for the fixed length, variable composition series were compared against their predicted hydrophobicity, using the scale of Fauchere and Pliska [26]. The CMC values associated with the homopolymeric PEO-*b*-peptides correlated reasonably with their predicted hydrophobicities; however, the CMC value obtained for the heterogeneous core was strikingly high compared to the value expected from its predicted hydrophobicity. Considering that three of the four amino acids comprising the polyFLYW peptide are represented in the compositions of its

homopolymer counterparts, it seems likely that this discrepancy is due to sequence heterogeneity. Chothia showed that the "effective" hydrophobicity of peptides and proteins are influenced by their secondary structure, which in turn are influenced by their primary sequence and the polarity of the surrounding medium [27]. Cammas *et al.* [28,29] studied the conformation of PEO-*b*-poly(β-benzyl L-aspartate) in organic solvents, but did not relate the effect of conformation on micellization thermodynamics. We speculate that the sequence variability within the polyFLYW core translates into a more disordered secondary structure than for the homopolymeric series, and that this disorder results in a greater exposure of the peptide's relatively polar main chain to the surrounding medium, thus decreasing hydrophobicity and increasing the observed CMC.

### 3.3.3 Micelle Size Distribution

Block copolymer micelle shape, size and size distribution was examined by TEM analysis (Figure 3). Spherical, uniform micelles, with diameters typical of those reported for other polymeric micelles, were observed for all seven micelle compositions (see Table 3.2) [6,25,30,31]. Micelle diameters within the size range are considered desirable for drug-delivery, that is, they are large enough to escape renal excretion, yet small enough to avoid elimination by the RES. As seen for other PEO-*b*-peptide block copolymer micelles, this size range, coupled with the non-immunogenic PEO shell imparts a 'stealthy' quality to the micelle, allowing it to circulate *in vivo* for extended periods of time [12].

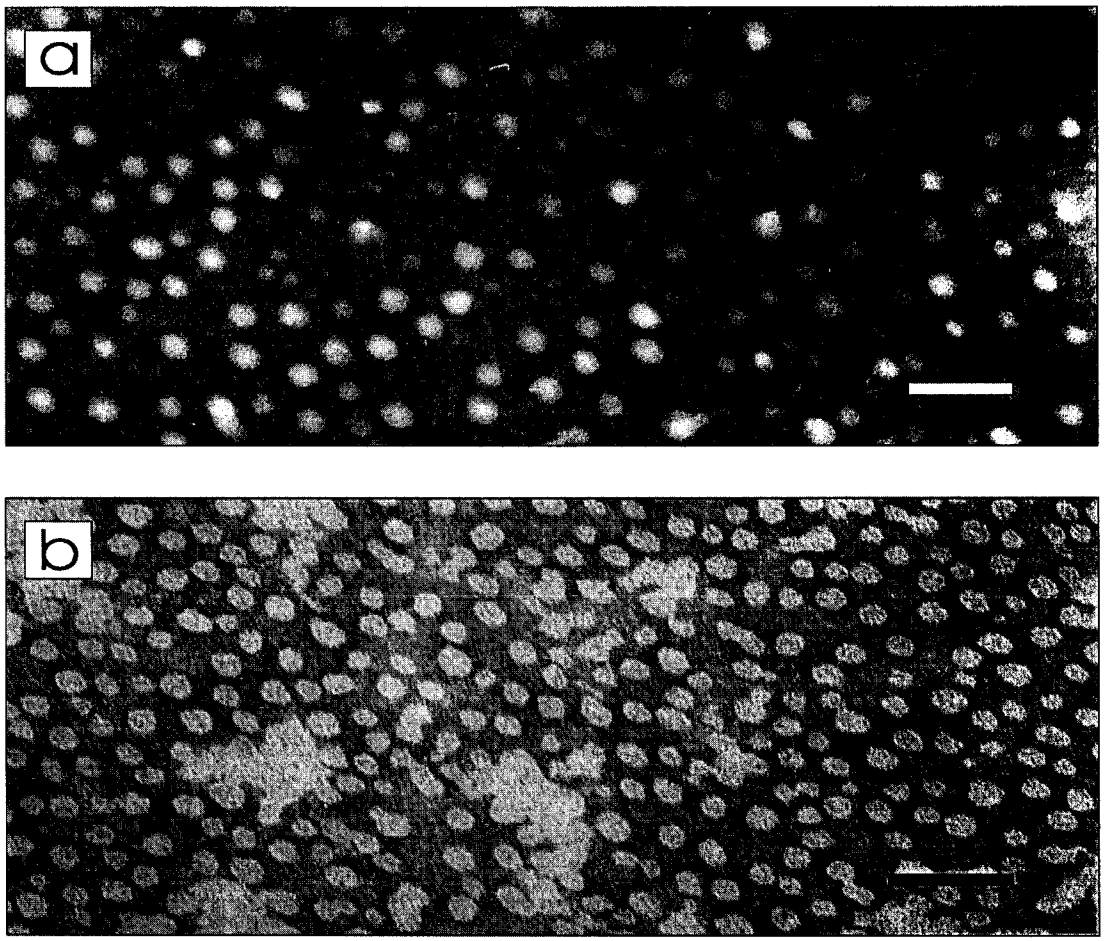


Figure 3.3. TEM images for a) PEO-b-polytyrosine$_7$, b) PEO-b-polytyrosine$_9$, c) PEO-b-polytyrosine$_{12}$, d) PEO-b-polytyrosine$_{15}$, e) PEO-b-polyleucine, f) PEO-b-polyFLYW, and g) PEO-b-polyphenylalanine. The scale for all images is 100 nm.

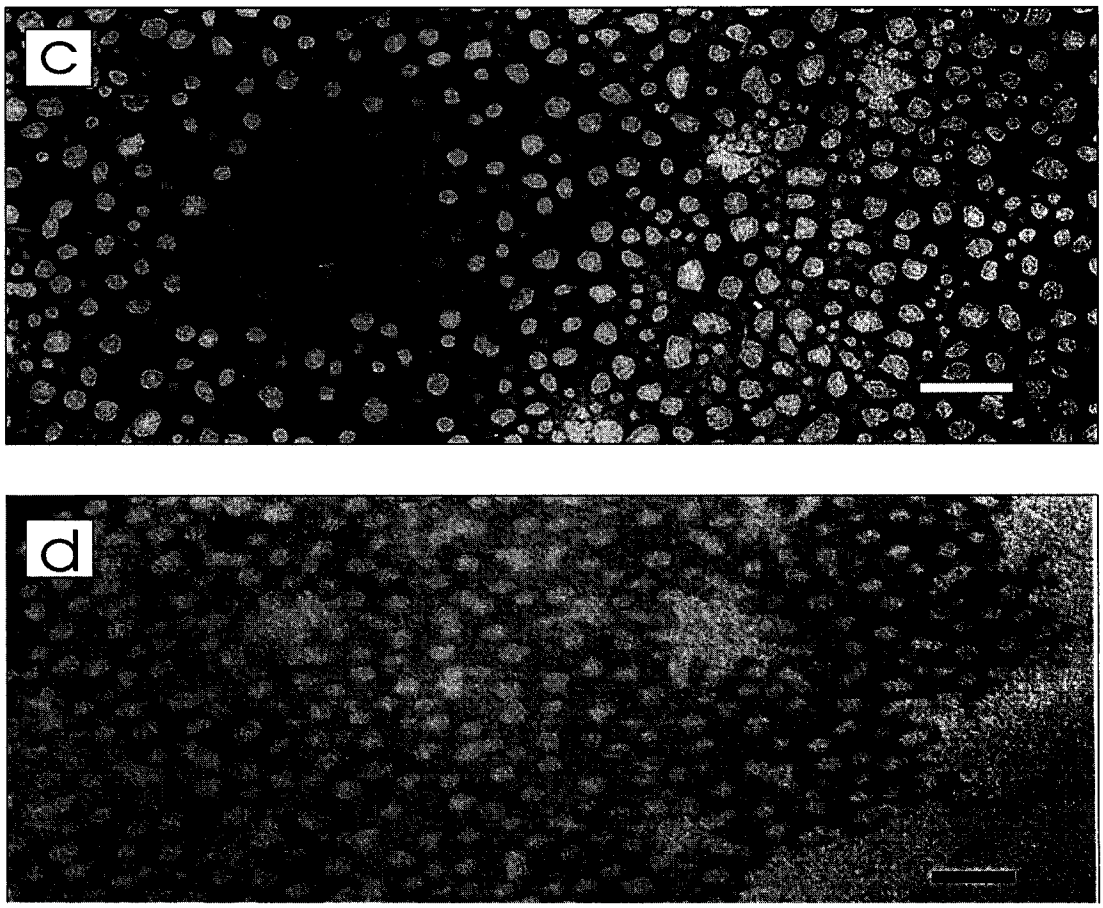


Figure 3.3. TEM images c) PEO-b-polytyrosine$_{12}$, d) PEO-b-polytyrosine$_{15}$. The scale for all images is 100 nm.

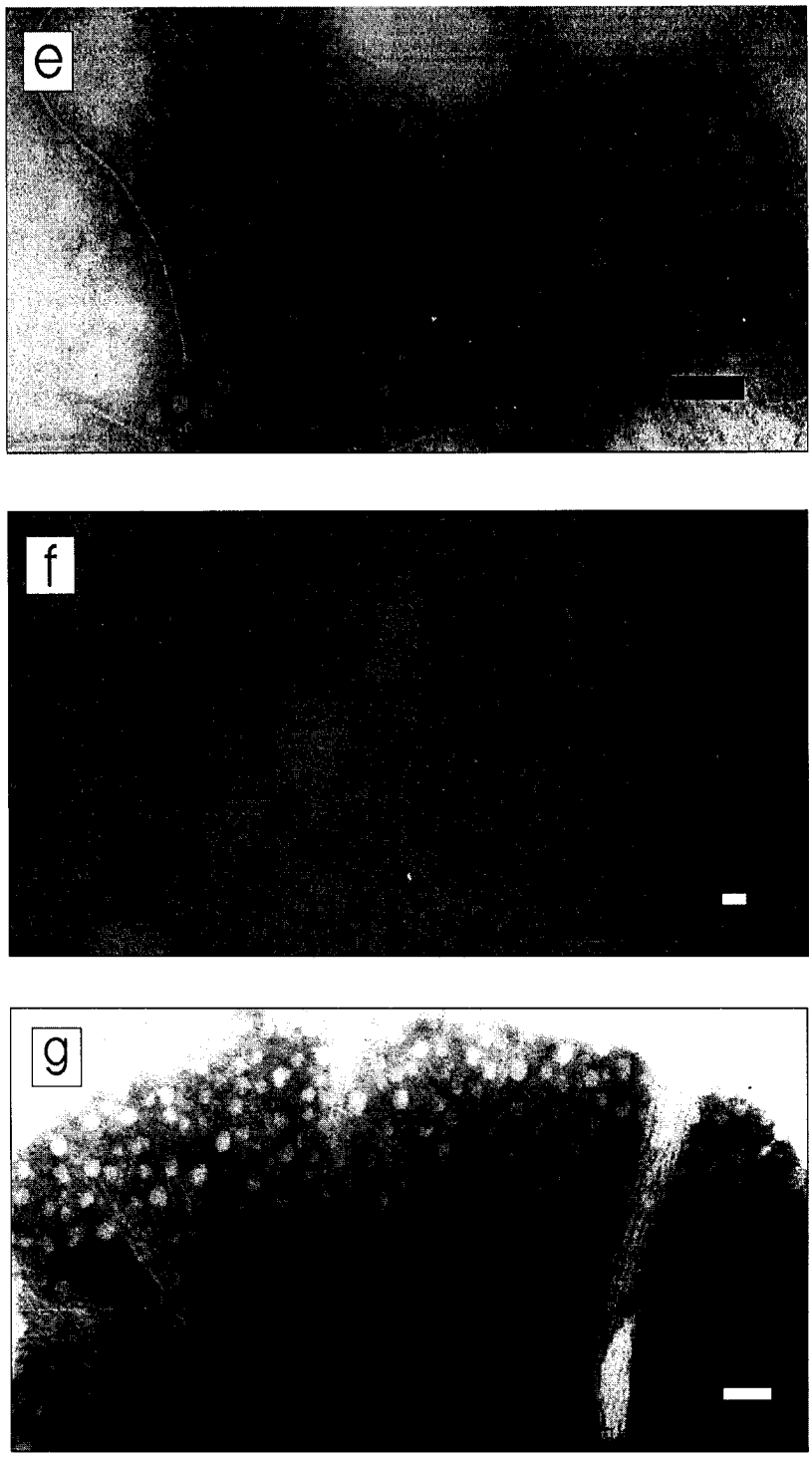


Figure 3.3. e) PEO-b-polyleucine, f) PEO-b-polyFLYW, and g) PEO-b-polyphenylalanine. The scale for all images is 100 nm.

Micelle diameters were observed to increase slightly with increasing peptide block length. In contrast, the micelle diameters for the fixed size series were much more varied. The PEO-*b*-polyFLYW construct showed the greatest deviation, with a diameter over twice the average diameter of the other homopolymeric peptide cores. The reason for this deviation is not clear, however, it seems likely that, as with the CMC, the heterogeneous core composition is a major contributing factor.

### 3.3.4 Micelle Dissociation Rates

A micelle's dynamic stability is an important measure of its utility for drug delivery. Upon introduction to the blood compartment, micelles are diluted to concentrations below the CMC, making them thermodynamically unstable. In contrast to low molecular weight surfactant micelles, which dissociate quickly (on the order of milliseconds), block copolymer micelles have been shown to have much longer dissociation rates at concentrations below their CMC (hours or days) [32]. A major factor influencing micelle dissociation rate is the viscosity of the micelle core. $^{1}$H NMR studies on block copolymer micelles with long dissociation rates reveal a solid-like core [33].

Micelle dissociation rates were studied by size exclusion (SEC) HPLC. Using molecular weight markers, the excluded volume was found to occur at 10.02 minutes (post injection) and the void volume was found to occur at 15.27 minutes. This information was used to monitor the dissociation of micelles into unimers over time (Table 3.1 and Figure 3.4). The size varying PEO-*b*-polytyrosine series showed a clear and strong dependence of core length with dynamic stability. Both the seven and nine residue polytyrosine cores dissociated immediately upon dilution below their CMC. At

12 residues, the presence of micelles was observable up to 48 h after dilution. The 15 residue PEO-*b*-polytyrosine demonstrated far greater stability, with less than 30% dissociation after 7 days. These observations are consistent with the idea of a critical molecular weight below which (at a given temperature) the polymer exists as a melt, and above which the polymer exists in the solid, glassy state. For PEO-*b*-polytyrosine, it appears that a minimum chain-length of 12 residues is necessary to form micelles with long-term stability at 37 °C.

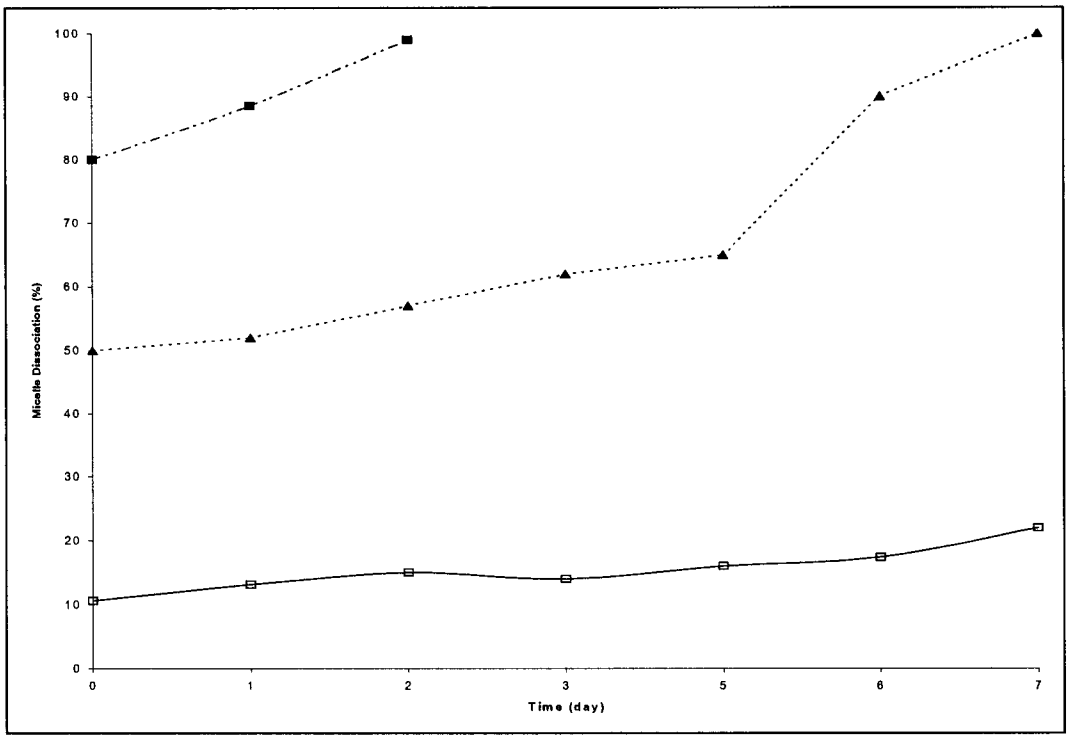


Figure 3.4. Dissociation rates for PEO-*b*-peptide micelles PEO-*b*-polytyrosine$_{12}$ (closed squares), PEO-*b*-polytyrosine$_{15}$ (open squares), and PEO-*b*-polyleucine$_{15}$ (closed triangles). Micelle dissociation percent is defined as the ratio of the area under the curve of the block copolymer micelle to that of the free unimer.

Of the various fixed-size constructs investigated, only PEO-*b*-polytyrosine and PEO-*b*-polyleucine showed long-term stability below their CMC. Both PEO-*b*-polyFLYW and PEO-*b*-polyphenylalanine were not stable below the CMC. This

apparent instability of PEO-*b*-polyphenylalanine is unexpected, considering that the chemical structure of phenylalanine is very similar to that of tyrosine (tyrosine has a *para*-hydroxyl group whereas phenylalanine does not), yet the 15-residue PEO-*b*-polytyrosine micelles are the most stable of all the micelles examined in this study. The reason for this discrepancy is not entirely clear, however, it is possible that the increased size of the tyrosine side-chain over phenylalanine, coupled with its ability participate in intermolecular hydrogen bonding, may be sufficient to account for the difference in observed dissociation rates. Regardless, these results suggest that micelle stability is a complex function of core composition, and cannot be predicted on the basis of hydrophobicity alone.

## 3.4. Conclusion

Block copolymer micelles hold much potential as non-toxic, non-immunogenic, controlled-release systems for hydrophobic drugs. We have developed a simple and versatile SPPS-SPC method for the construction of PEO-*b*-peptide block copolymers that greatly expands the preparative capabilities of these polymers. To demonstrate its utility and versatility we employed this technique in the construction of a number of PEO-*b*-peptide block copolymers with precisely defined sequence compositions and sizes. This allowed us to investigate the relationship of core size and composition to micelle formation and stability. The results of these investigations showed that one construct in particular, $PEO_{5000}$-b-poly(tyrosine)$_{15}$, possessed many of the desired qualities for a block copolymer-based micelle drug delivery system, including small CMC, long term dynamic stability, small size, narrow polymer polydispersity and narrow micelle polydispersity.

These results suggest that this method may used in the construction of many block copolymers for drug delivery.

## 3.5. References


1. Kratochvil P. and Tuzar Z. (1992) Self-association of block copolymers in solution: copolymer micelles. *Polymer Preprints* **41**:135-138.

2. Kwon G.S. and Kataoka K. (1995) Block copolymer micelles as long-circulating drug vehicles. *Adv. Drug Deliv. Rev.* **16**:295-309.

3. Kataoka K., Kwon G.S., Yokoyama M., Okano T., and Sakurai Y. (1993) Block copolymer micelles as vehicles for drug delivery. *J. Control. Rel.* **24**:119-132.

4. Allen C., Maysinger D., and Eisenberg A. (1999) Nano-engineering block copolymer aggregates for drug delivery. *Colloids and Surfaces B: Biointerfaces* **16**:3-27.

5. Kabanov A.V., Chekhonin V.P., Alakhov V.Y., Batrakova E.V., Lebedev A.S., Melik-Nubarov N.S., Arzhakov S.A., Levashov A.V., Morozov G.V., Severin E.S., *et al.* (1989) The neuroleptic activity of haloperidol increases after its solubilization in surfactant micelles. Micelles as microcontainers for drug targeting. *FEBS Lett.* **258**:343-345.

6. Hagan S.A., Coombes G.A., Garnett M.C., Dunn S.E., Davies M.C., Illum L., and Davis S.S. (1996) Polylactide-poly(ethylene glycol) copolymers as drug delivery

systems. 1. Characterizaton of water dispersible micelle-forming systems. *Langmuir* **12**:2153-2161.

7. Inoue T., Chen G., Nakamae K., and Hoffman A.S. (1998) An AB block copolymer of oligo(methyl methacrylate) and poly(acrylic acid) for micellar delivery of hydrophobic drugs. *J. Control. Rel.* **51**:221-229.

8. Abuchowski A., van Es T., Palczuk N.C., McCoy J.R., and Davis F.F. (1977) Effect of covalent attachment of polyethylene glycol on immunogenicity and circulating life of bovine liver catalase. *J. Biol. Chem.* **252**:3582-3586.

9. Kim S.Y., Shin G.I., Lee Y.M., Cho C.S., and Sung Y.K. (1998) Methoxy poly(ethylene glycol) and ε-caprolactone amphiphilic block copolymeric micelle containing indomethacin. I. Preparation and characterization. *J. Control. Rel.* **51**:1-11.

10. Miller D.W., Batrakova E.V., Waltner T.O., Alakhov V.Y., and Kabanov A.V. (1997) Interactions of pluronic block copolymers with brain microvessel endothelial cells: evidence of two potential pathways for drug absorption. *Bioconjugate Chem.* **8**:649-57.

11. Yokoyama M., Miyauchi M., Yamada N., Okano T., Sakurai Y., Kataoka K., and Inoue S. (1990) Characterization and anticancer activity of the micelle-forming polymeric anticancer drug adriamycin-conjugated poly(ethylene glycol)-poly(aspartic acid) block copolymer. *Cancer Res.* **50**:1693-1700.

12. Kataoka K., Masumoto T., Yokoyama M., Okano T., Sakurai Y., Fukushima S., Okamoto K., and Kwon G.S. (2000) Doxorubicin-loaded poly(ethylene

glycol)-poly(β-benzyl-L-aspartate) copolymer micelles: their pharmaceutical characteristics and biological significance. *J. Control. Rel.* **64**:143-153.

13. Jeong Y.I., Cheon J.B., Kim S.H., Nah J.W., Lee Y.M., Sung, Y.K., Akaike T., and Cho C.S. (1998) Clonazepam release from core-shell type nanoparticles in vitro. *J. Control. Rel.* **51**:169-178.

14. Katayose S. and Kataoka K. (1998) Remarkable increase in nuclease resistance of plasmid DNA through supramolecular assembly with poly(ethylene glycol)-poly(L-lysine) block copolymer. *J. Pharm. Sci.* **87**:160-163.

15. Fields C.G., Lloyd D.H., Macdonald R.L., Otteson K.M., and Noble R.L. (1991) HBTU activation for automated Fmoc solid-phase peptide synthesis. *Pept. Res.* **4**:95-101.

16. Kaiser E., Colescott R.L., Bossinger C.D., and Cook P.I. (1970) Color test for detection of free terminal amino groups in the solid-phase synthesis of peptides. *Anal. Biochem.* **34**:595-598.

17. Tancrede P., Barwicz J., Jutras S., and Gruda I.B. (1990) The effect of surfactants on the aggregation state of amphotericin B. *Biochim-Biophys. Acta.* **1030**:289-295.

18. Li Y. and Kwon G.S. (1999) Micelle-like structures of poly(ethylene oxide)-*block*-(2-hydroxyethyl aspartamide)-methotrexate conjugates. *Colloids and Surfaces B: Biointerfaces* **16**:217-226.

19. Pechar M., Ulbrich K., Subr V., Seymour L.W., and Schach E.H. (2000) Poly(ethylene glycol) multiblock copolymer as a carrier of anti-cancer drug doxorubicin. *Bioconjugate Chem.* **11**:131-139.

20. Onuchic J., Luthey-Schulten Z., and Wolynes P. (1997) Theory of Protein Folding *Ann. Rev. Phys. Chem.* **48**:545-600.

21. Lu Y. and Felix A. (1993) Pegylated peptides – solid phase synthesis of $N^{\alpha}$-pegylated peptides using Fmoc strategy. *Pept. Res.* **6**:140-146.

22. Munch M. and Gast A. (1998) Block copolymers at interfaces. I. Micelle formation. *Macromolecules* **21**:1360-1366.

23. Alexandridis P. and Hatton T.A. (1995) Poly(ethylene oxide)-block-Poly(propylene oxide)-*block*-Poly(ethylene oxide) Copolymer Surfactants in Aqueous Solutions and at Interfaces: Thermodynamics, Structure, Dynamics, and Modelling. *Colloids Surfaces A: Physicochem. Eng. Aspects* **96**:1-46.

24. Kwon G.S., Naito M., Yokoyama M., Okano T., Sakarai Y., and Kataoka K. (1993) Micelles based on AB block copolymers of poly(ethylene oxide) and poly( β-benzyl L-aspartate). *Langmuir* **9**:945-949.

25. La S.B., Okano T., and Kataoka K. (1996) Preparation and characterization of the micelle-forming polymeric drug indomethacin-incorporated poly(ethylene oxide)-poly(β-benzyl-L-aspartate) block copolymer micelles. *J. Pharm. Sci.* **85**:85-90.

26. Fauchere J.L. and Pliska V. (1983) Hydrophobic parameter-$\pi$ of amino acid side-chains from the partitioning of N-acetyl amino acid amides. *Eur. J. Med. Chem.* **18**:369-375.

27. Chothia C. (1976) Nature of accessible and buried surfaces in proteins. *J. Mol. Biol.* **105:**1-12.

28. Cammas S., Harada A., Nagasaki Y., and Kataoka K. (1996) Poly(ethylene oxide)-*co*-($\beta$-benzyl-L-aspartate) block copolymers: influence of the poly(ethylene oxide) block on the conformation of the poly($\beta$-benzyl-L-aspartate) segment in organic solvents. *Macromolecules* **23**:3227-3231.

29. Harada A., Cammas S., and Kataoka K. (1996) Stabilized $\alpha$-helix structure of poly(L-lysine)-*block*-poly(ethylene glycol) in aqueous medium through supramolecular assembly. *Macromolecules* **29**:6183-6188.

30. Cao T., Munk P., Ramireddy C., Tuzar Z., and Webber S.E. (1991) Fluorescence studies of amphiphilic poly(methacrylic acid)-*block*-polystyrene-*block*-poly(methacrylic acid) micelles. *Macromolecules* **24**:6300-6305.

31. Zareie H.M., Kaitian X., and Piskin E. (1996) STM images of PDLLA-PEG copolymer micelles. *Colloids and Surfaces A: Physicochem. Eng. Aspects* **112**:19-24.

32. Halperin A. and Alexander S. (1989) Polymeric micelles – their relaxation kinetics. *Macromolecules* **22**:2403-2412.

33. Nakamura K., Endo R., and Takeda M. (1977) Study of molecular-motion of block copolymers in solution by high-resolution proton magnetic resonance. *J. Polym. Sci. Polym. Phys. Ed.* **15**:2095-2101.

# CHAPTER 4. MONTE CARLO SIMULATIONS OF MICELLE FORMATION BY NONIONIC BLOCK COPOLYMERS

## 4.1. Introduction

Amphipathic block copolymers are linear polymeric molecules consisting of a hydrophobic and a hydrophilic segment. Under the proper conditions of temperature, concentration, solvent selectivity, and polymer composition, these copolymer unimers can self assemble into extraordinarily stable micellar suspensions. This phenomenon has prompted researchers to investigate the use of biocompatible block copolymers as delivery systems for hydrophobic small molecule drugs [1]. Although this method of drug delivery appears promising, development has been slowed by the significant trial-and-error involved in identifying block copolymer–drug combinations with adequate properties for drug-delivery including: drug-loading capacity, release kinetics, circulation time, biodistribution, static and dynamic stability, morphology, and size [1]. The field of block copolymer micelle modeling holds some promise in reducing the time and effort involved in optimizing block copolymer micelle properties for drug delivery by predicting which combinations of block size and composition are required to stably formulate and with sufficient capacity the hydrophobic small molecule drug.

Two distinct approaches exist for modeling micelle formation: analytical modeling [2-7], and computer simulations [8-13]. Prominent in the area of analytical modeling are the self-consistent field theory (SCF) and mean-field theory (MFT). An introduction and review of analytical modeling of nonionic micelle formation appears in Section 1.4 of Chapter 1. These models describe the free energy change associated with

transferring a completely solvated system of polymers into a micelle. By including a number of phenomenological parameters associated with micelle formation, these analytical models have achieved considerable predictive accuracy, although most make assumptions on micelle shape and size, do not include intermicellar interactions, and can be quite complex to carry out. In contrast, computer simulations utilizing stochastic algorithms such as the Monte Carlo algorithm, make no *a priori* assumptions about micelle size or shape, provide considerable information on intermicellar interactions, and are simple to compute.

Cifra and co-workers were among the first to attempt computer simulations of nonionic copolymers, although limitations on computing power limited these simulations to two dimensions [8]. These same researchers later produced the first three dimensional simulation of copolymer interactions [9]. Rodrigues and Mattice [10] expanded on the early work of Cifra *et al.* [8,9] to produce a popular model for simulating micelle formation of nonionic micelles. With advancements in computing power, Mattice's group was able to sufficiently increase the lattice volume to the point where CMC determinations became feasible[11]. Today micelle simulations are being used to study environmental influences, such as behaviour near interfaces [12], in confined regions [13], and in the presence of solubilizing agents [14].

The computational resources required to perform simulations on a large group of copolymers with molecular-level detail currently is impractical. Instead, investigators have adopted *lattice-based* simulations. Lattice-based simulations allow only a rough level of molecular and intermolecular detail, however, they have been used successfully to describe supramolecular aggregation phenomena and have provided considerable

insight into the nature of micelle formation. In lattice-based simulations of nonionic copolymers, a three-dimensional simple cubic lattice represents a discretized space. Periodic boundary conditions are applied in all three directions in order to simulate a constant volume fraction of polymer within the lattice without compromising mass transfer. Each node in the lattice may be occupied by a solvent molecule, or copolymer "unit." No lattice node may be doubly occupied. Each unit interacts with its neighbors via a predetermined interaction energy, $E_{ij}$ where $i$ and $j$ represent the various components within the matrix, specifically, head unit, tail unit, or solvent. The interaction energies are independent of each other, and extend only to the *von Neumann* neighborhood; i.e. the 6 sites (in 3 dimensional lattices) immediately surrounding the node under investigation.

Several methods exist for translating the unimers through the matrix. These include the Verdier-Stockmayer kink-jump move [15], the configuration-bias method [16], and the reptation move. For the current study, only reptation moves of the unimers were considered [17]. Reptation is a method of repositioning a polymer 'molecule' within a simulation by randomly choosing one end of a (randomly chosen) polymer chain, examining the von Neumann neighborhood for a vacant lattice site and, if found, repositioning the terminal polymer segment to that new node, while the remaining polymer segments "follow through".

By far the most popular method for minimizing the energy of polymer systems is the Monte Carlo method using the Metropolis sampling method [17]. A sufficiently randomized, homogenous system is defined as the initial configuration of the system, and the corresponding initial system energy is determined. A new "trial" configuration is

generated by reptation. The energy of the new system is then determined and compared with the old energy. If the new system's energy is less than or equal to that of the old system, then the new configuration is accepted unconditionally, otherwise the new system is accepted with probability $e^{-\Delta E/kT}$, where $\Delta E$ is the net change in energy, $T$ is the absolute temperature, and $k$ is the Boltzmann constant. This procedure, defined as an *iteration,* is repeated until equilibrium has been achieved.

This work presents a lattice model of nonionic micelle interaction. System parameters such as unimer number, array volume were chosen based on (although not exactly reproducing) values reported for other micelle-forming simulations. The interaction energies necessary for stable micelle formation were determined experimentally. The interaction energies between head, tail, and solvent were determined experimentally. The effect of hydrophobic block length was also examined and compared with the results obtained experimentally in Chapter 3 of this thesis.

## 4.2. Methods

### 4.2.1. Hardware and Software

The Monte Carlo simulation model was programmed in ANSI C and compiled on a Sun SparcStation using the GNU C compiler (gcc). For visual inspection, the coordinate data was converted into Persistance of Vision (POV) format using Perl 5.8. Pov-Ray 3.0 was used to generate ray-traced images of the lattice. GnuPlot was used to monitor the system energy during simulations. All simulations were carried out on a 175 MHz Sun SparcStation or a 1.7 GHz Linux Intel workstation. A typical simulation of

$1x10^7$ iterations required approximately 60 cpu hours to complete on the SunStation, or approximately 6 h on the Linux/Intel workstation. Following completion of the simulations, the coordinate data was analyzed for unimer aggregation into micelles using Perl 5.8.

4.2.2. Model

A flowchart describing the procedure for the nonionic micelle formation simulations by Monte Carlo energy minimization appears in Figure 4.1. Simulations were carried out on a 40x40x40 cubic lattice containing 200 block copolymer unimers initially composed of 10 hydrophilic "head" units and 10 hydrophobic "tail" units. This gives a volume fraction of 0.025, which is expected to be above the CMC, yet below the concentration necessary to achieve phase separation.[14] The unoccupied nodes in the lattice are considered to be polar solvent, selective for the hydrophilic head segment. Periodic boundary conditions and volume exclusion conditions were applied. The interaction energies were assigned as follows:

Table 4.1 Interaction Energies for polymer head unit (h), tail unit (t), and solvent (s).

| $E_{hs}$ | $E_{hh}$ | $E_{ht}$ | $E_{tt}$ | $E_{ts}$ |
|---|---|---|---|---|
| $-\varepsilon$ | 0 | $+\varepsilon$ | $-\varepsilon$ | $+\varepsilon$ |

where $\varepsilon$ is a dimensionless interaction parameter. The magnitude of $\varepsilon$ was fixed within a given simulation, but adjusted between simulations in order to determine the optimal interaction energy for micelle formation. The assignment of sign and magnitude for the interaction energies are based upon what is reasonably expected for a system of amphipathic copolymers in a selective solvent, and are similar to those reported in the literature [8-13].

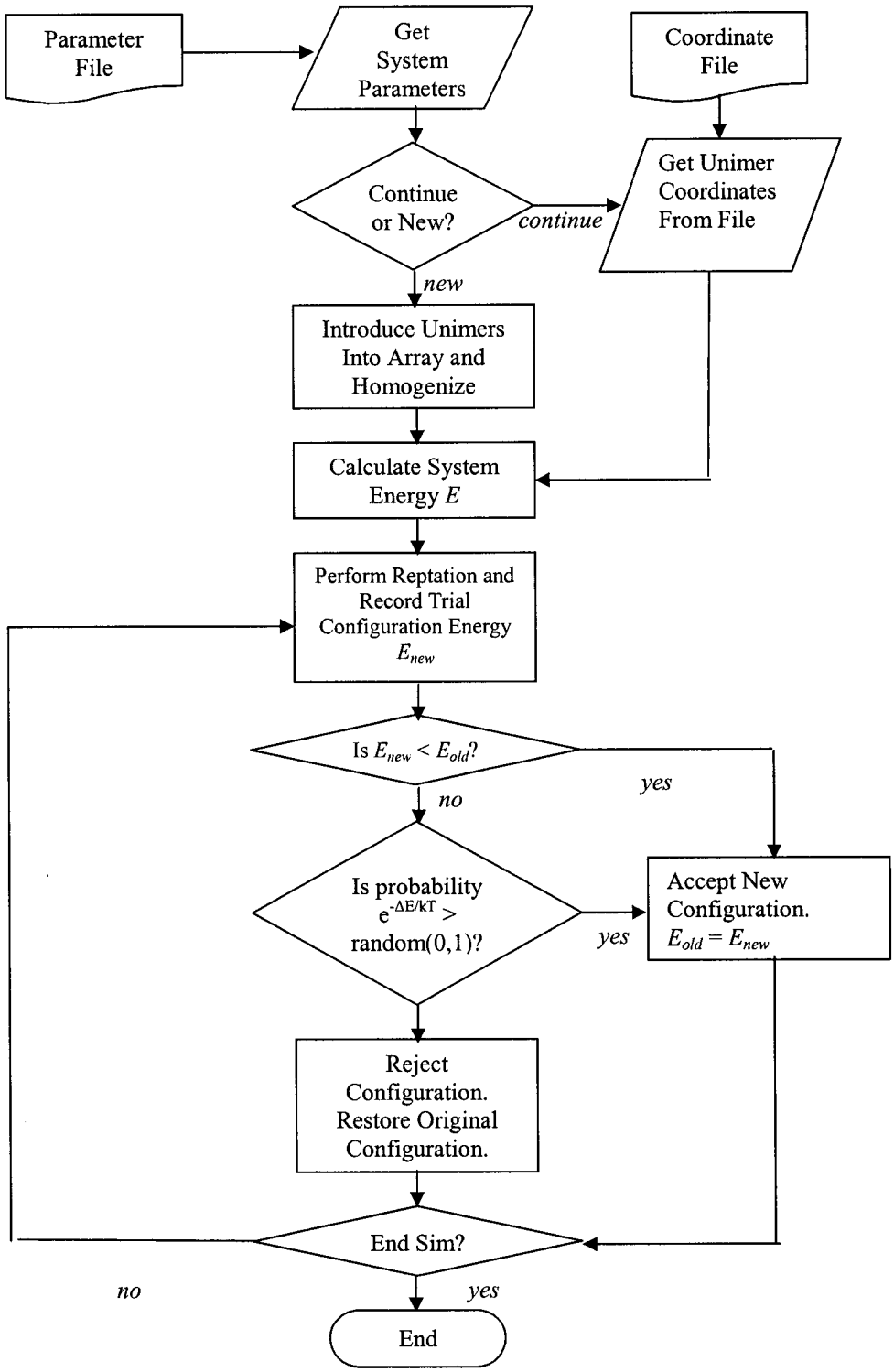


Figure 4.1. Flow Chart describing Monte Carlo simulations of nonionic block copolymer formation.

Reptation moves were used to convert one system configuration into another. Trial configurations were accepted or rejected according to the Metropolis rules, as described previously.

Unimers were introduced in a regular, evenly spaced fashion (Figure 4.2-a). In order to ensure sufficient homogenization of the system, $0.5x10^6$ iterations were performed with the interaction energies turned off (Figure 4.2-b). The interaction energies were then turned on, and the system is allowed to equilibrate. The system energy was recorded at 100 iteration intervals. Unimer coordinates were written out to a file every 1000 iterations. The system was considered equilibrated when the average slope of the energy curve remained steadily at zero.

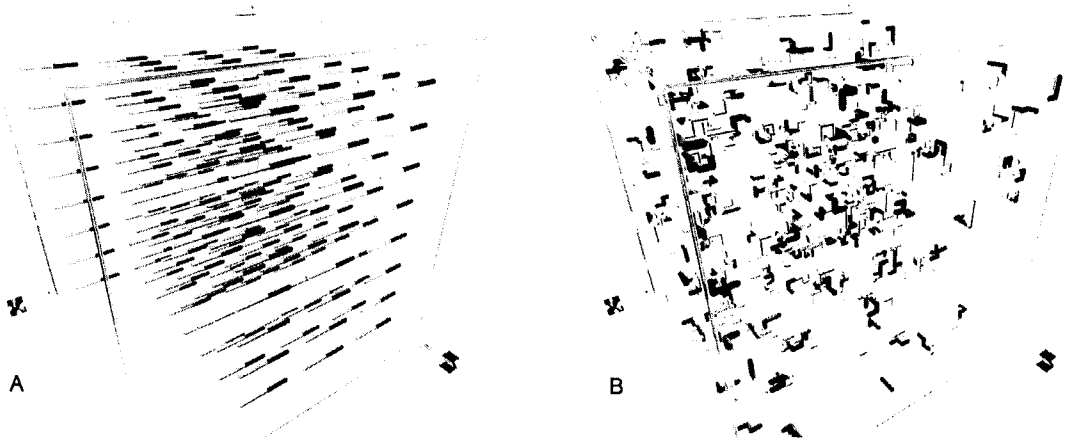


Figure 4.2 A) System initial state and B) system state after 500 000 reptations with interaction energies turned off. Hydrophobic blocks appear black; hydrophilic blocks appear gray.

## 4.3. Results and Discussion

In order to determine the optimal interaction energies for micelle formation, a number of initial simulations were performed using a range of intermolecular energy

magnitudes, $\varepsilon = 0.05 - 0.60$. This range of values spans the range of interaction energies reported in the literature [9-11]. In each case, the system was homogenized by performing $0.5 \times 10^6$ iterations with the interaction energies off. A subsequent $9.5 \times 10^6$ iterations were then performed with the interaction energies on. The system energy was monitored continuously and used to aid in evaluating the overall state of the system. A system snapshot at $1 \times 10^7$ iterations was rendered in order to visually inspect the state of each simulation. Upon determining the optimal interaction energy, a second set of simulations were performed, sytematically adjusting the hydrophobic block length, from 1 to 10 nodes. As a control, a simulation was run for $1 \times 10^7$ iterations with $\varepsilon = 0$.

4.3.1. Determination of Optimal Interaction Energy

In order to determine the effect of interaction energy on micellization properties, a series of simulations were performed from $\varepsilon = 0.05$ to $\varepsilon = 0.60$, in increments of 0.05 $\varepsilon$. The system energy profiles for these simulations are provided in Figure 4.3. Bar charts representing the micelle size distribution ($N_{agg}$) for each simulation appear in Figure 4.4. A plot of the average micelle number for each simulation appears in Figure 4.5. The distribution profile for the control is presented in Figure 4.6.

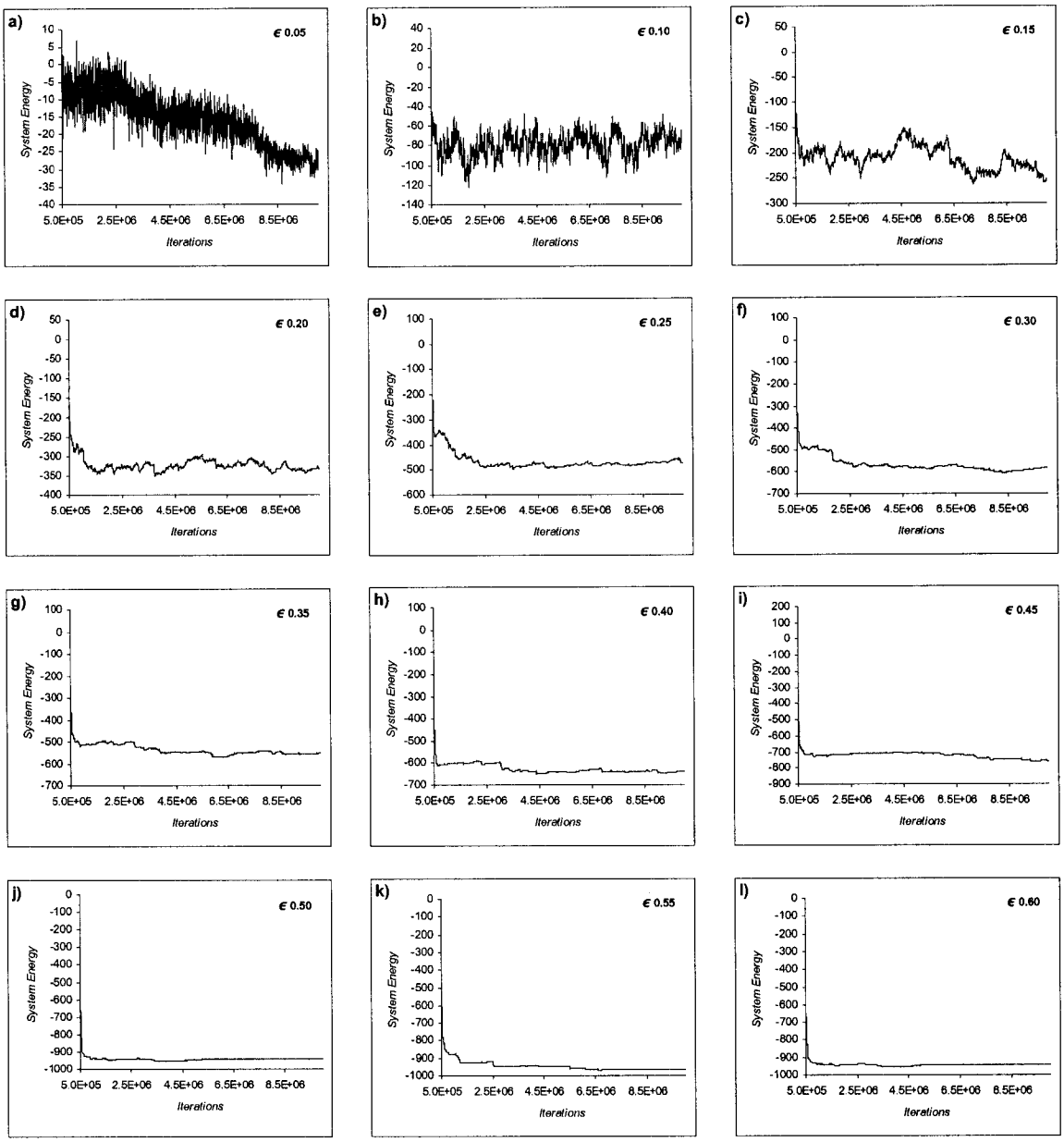


Figure 4.3. Micelle simulation system energy profiles for $\epsilon = 0.05$ (a) to $\epsilon = 0.60$ (l).

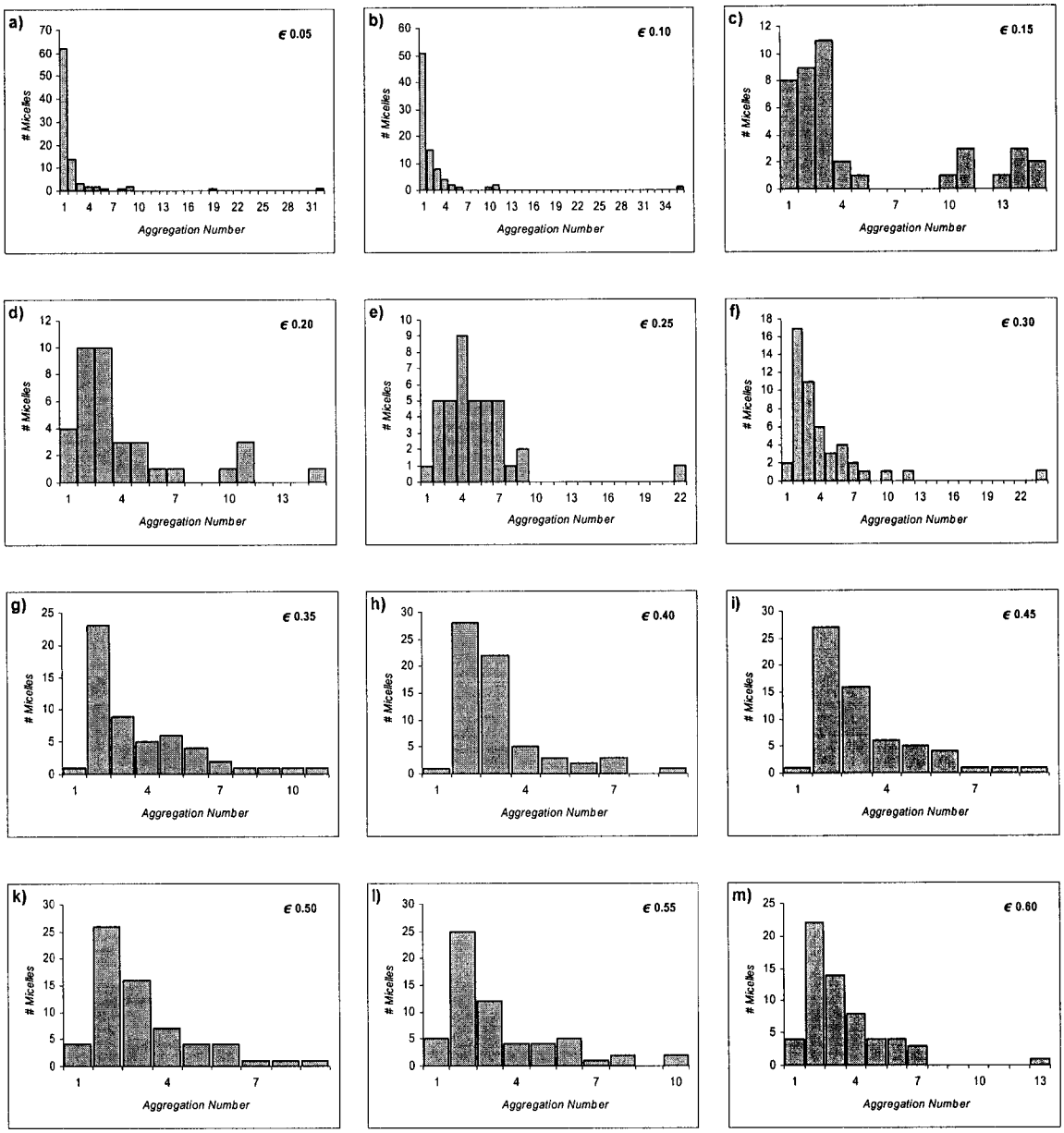


Figure 4.4. Micelle number distribution profiles for $\epsilon = 0.05$ (a) to $\epsilon = 0.60$ (l).

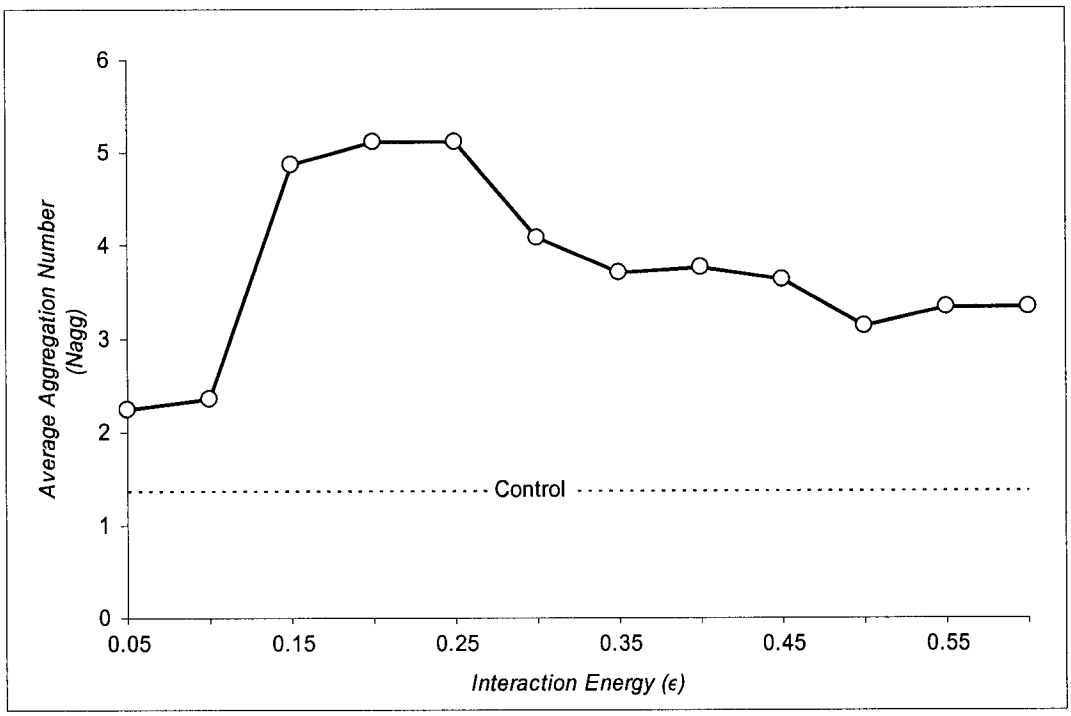


Figure 4.5. Average micelle aggregation number as a function of interaction energy.

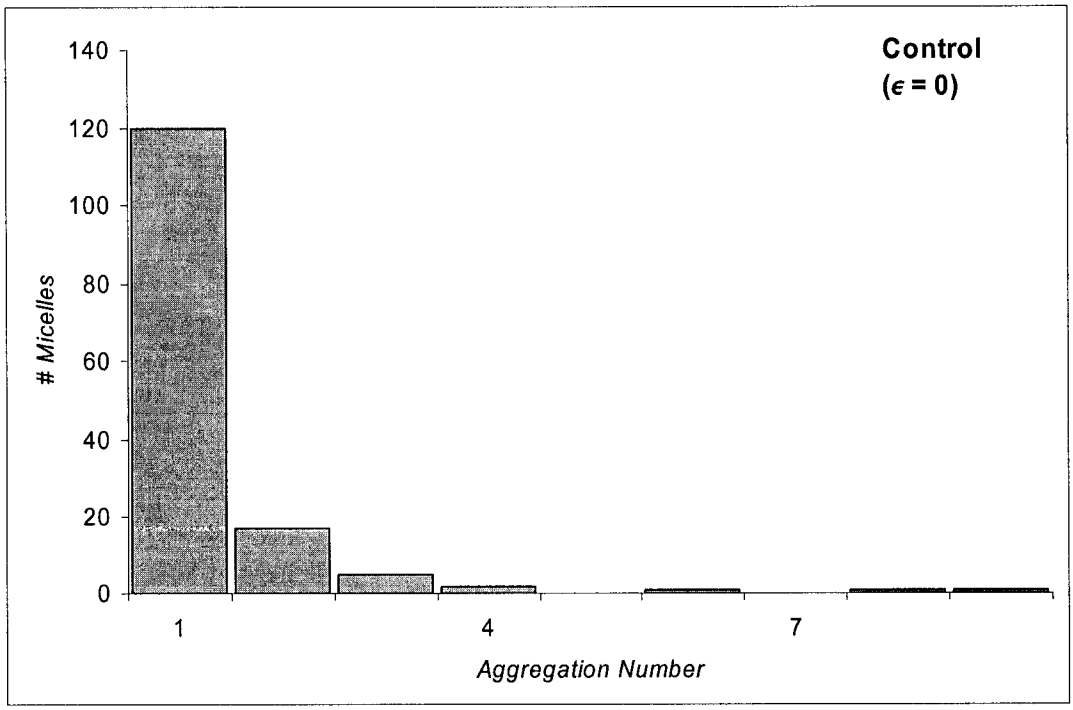


Figure 4.6. Micelle distribution profile for the control simulation.

Simulations with low interaction energies ($\varepsilon = 0.05$ and $\varepsilon = 0.10$) are characterized by a high number of unaggregated unimers (Figures 4.4-a and 4.4-b) and low average $N_{agg}$ (Figure 4.5), similar to that of the control, although the amount of unimer is reduced by around 50% in favor of dimer. The system energy profiles show a large amount of fluctuation in the overall system energy (Figures 4.3-a and 4.3-b). These observations suggest that low interaction energies produce systems where the unimers exist in a free and dynamic exchange. It is likely that these simulations represent micelle systems above the critical micelle temperature (CMT).

As $\varepsilon$ increases from 0.15 to 0.30, $N_{agg}$ rises sharply, from 2 to 5 polymers/micelle (Figure 4.5). The system energy profiles for these systems gradually descend in energy for approximately $2.5 \times 10^6$ iterations then level off with little relative fluctuation in system energy (Figures 4.3-c-f). The micelle distribution profiles (Figures 4.4-c-f) show a marked reduction in free unaggregated unimer. This behaviour resembles the behaviour observed for micelles in "closed association" [19]. Unlike micelles in open association with liquid-like cores, micelles in closed association have solid, or glassy cores. Micelles with glassy cores do equilibrate between micelle and unaggregated unimer; rather, they act like a sink for the unimer, trapping the polymers in the micelle through a combination of entanglement and large entropy change [19]. It is likely therefore that these simulations represent micelle systems below the CMT and below the glass transition temperature ($T_g$).

In systems of real nonionic polymer systems, the temperature at which the transition from unimers to micelles occurs is sharply defined. The transition from unimers to micelles is similarly sharp in these simulations, occuring within a single

increment of $\varepsilon$, which is equivalent to a small decrease in temperature.(Figure 4.5). Within this range of $\varepsilon$, the micelle size distribution profiles increasingly appear to adopt a gaussian distribution. Again this observation agrees well with the observations obtained from dynamic light scattering measurements on real nonionic block copolymer micelle systems (see for example [20].

The micelle simulations with high energies ($\varepsilon > 0.3$) represent that of a metastable "frozen" state [21]. The energy profiles for these systems initially descend rapidly and then quickly level out (Figure 4.3-e-l). The $N_{agg}$ values fall from 5 to approximately 3 for this series (Figure 4.5). There is a strong bias to form micelles with $N_{agg} = 2$ (Figure 4.4-e-l). It is likely that for these systems, the drop in energy upon two micelles contacting each other is so great that they become frozen in place. As a result, the system is unable to escape to a true minimal energy configuration within $1x10^7$ iterations. This observation suggests that interaction energies above 0.3 are not representative of real micelle systems. These observations agree with the findings of others researching Monte Carlo simulations of nonionic block copolymer micelles [22].

For nearly all the micelle systems with energies of 0.3 and less, the micelle distribution is bimodal with a large number of micelles of small $N_{agg}$ and a small number of micelles (1 or 2) with high $N_{agg}$. This behaviour is consistent with real micelle systems at high concentration, where the micelles can form large lamellar (sheet-like) aggregates in addition to spherical aggregates. Formation of lamellae is also encouraged when the size of the hydrophobic block is equal or exceeds that of the hydrophilic block [21], which is indeed the case for the simulations presented here.

From analysis of the micelle simulation data it is clear that the optimal interaction energy for micelle formation lies at $\varepsilon = 0.25$. At this value of $\varepsilon$, the system energy profile (Figure 4.3-e) shows a gradual descent to minimum value, indicating that the system is at its true minimum. The micelle distribution profile (Figure 4.4-e) has a Gaussian bimodal distribution indicative of spherical micelles with a small amount of lamellar aggregate, low amount of unaggregated unimer, and maximal average $N_{agg}$ (Figure 4.5) all point to this interaction energy as the best representative of real micellar systems with glassy cores at concentrations above the CMC. The system snapshot after $1.0x10^7$ iterations (Figure 4.7) confirms the formation of micelles with a hydrophobic core and a hydrophilic shell. Based on these findings, this interaction energy was used to study the effect of adjusting micelle core-forming block size to micellization properties.

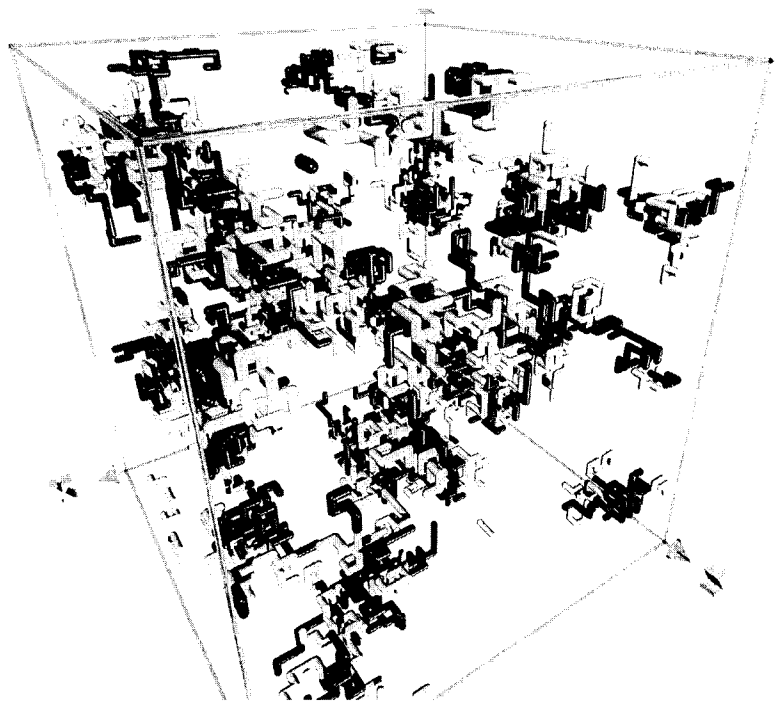

Figure 4.7. 3D Rendering of micelle simulation for $\varepsilon = 0.25$. The rendering represents the state of the system after $1.0x10^7$ iterations. Core-forming blocks appear black. Shell-forming blocks appear grey.

From the perspective of the core-forming block, adjusting the interaction energy is equivalent to adjusting hydrophobicity (increasing negative interaction energies is equivalent to increasing the core-forming blocks "hydrophobicity". In Chapter 3 of this thesis, SPPS was used in a similar fashion to study the effects of core hydrophobicity and micellization properties. In contrast with the clear relationships found between interaction energy and micellization, no clear trends could be identified between the estimated hydrophobicity of the core-forming block and micellization properties. The difference likely is due to the fact that these simulations allow for the adjustment of hydrophobicity (interaction energy) in isolation from all other properties. In Chapter 3, the difference core hydrophobicities were obtained by using different core compositions (L-leucine, L -phenylalanine, and L -tyrosine). The differences inherent in the side-chain structures undoubtedly influence the overall micellization properties of the block copolymer. This complicating factor prevents any lucid comparison between the results obtained in Chapter 3 and the results obtained by these simulation studies.

### 4.3.2. Effect of Hydrophobic Block Size on Micellization

A second set of simulations were conducted using the optimal interaction energy $\epsilon$ of 0.25. Hydrophobic block length was adjusted from 1 node to 10 nodes. The system energy profiles for these systems are presented in Figure 4.8. The size distribution profiles are provided in Figure 4.9. A plot of the average micelle aggregation number appears in Figure 4.10.

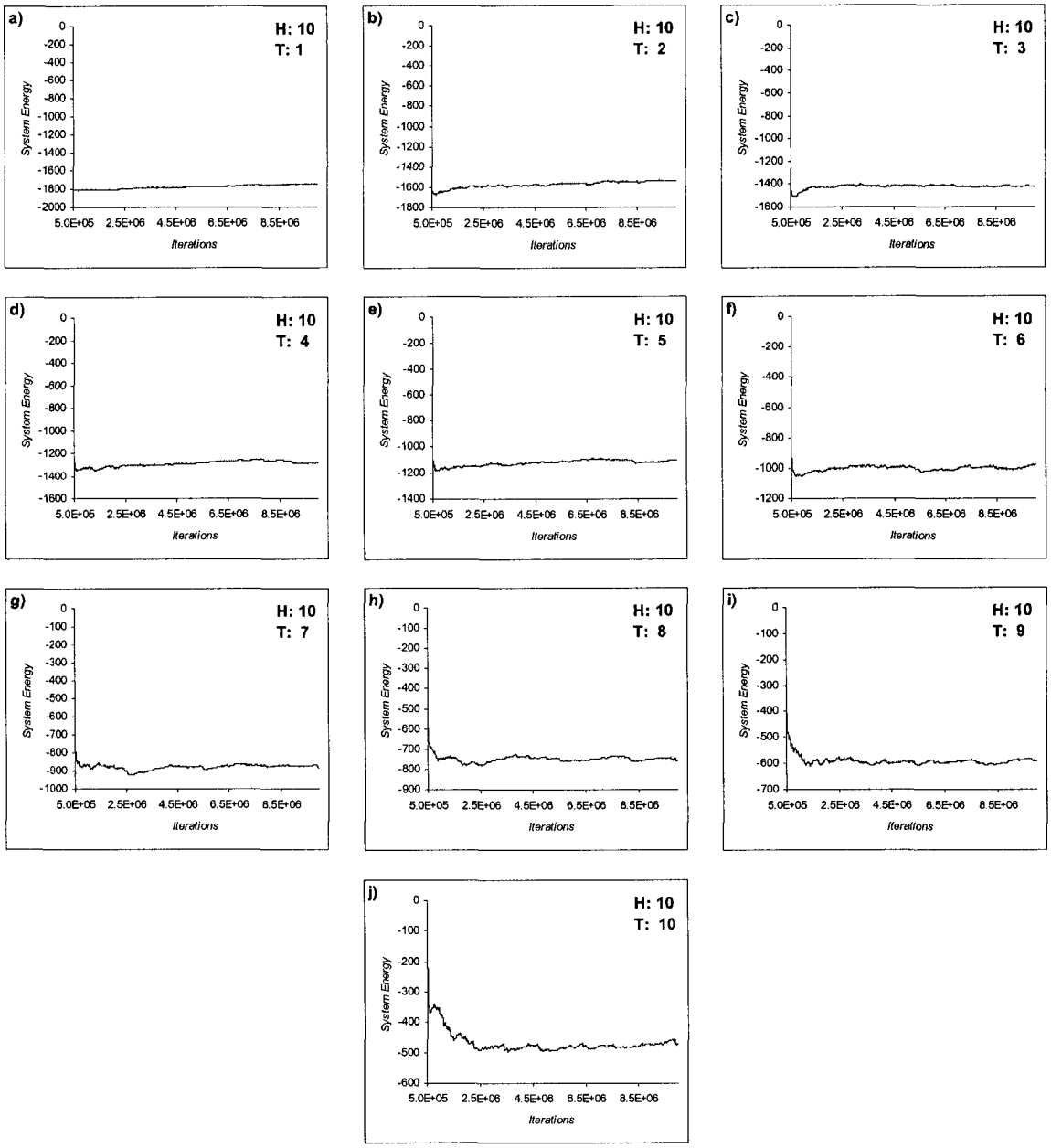


Figure 4.8. Micelle simulation system energy profiles for polymers with 10 hydrophilic head (H) units and varying [1(a) to 10 (l)] tail (T) units.

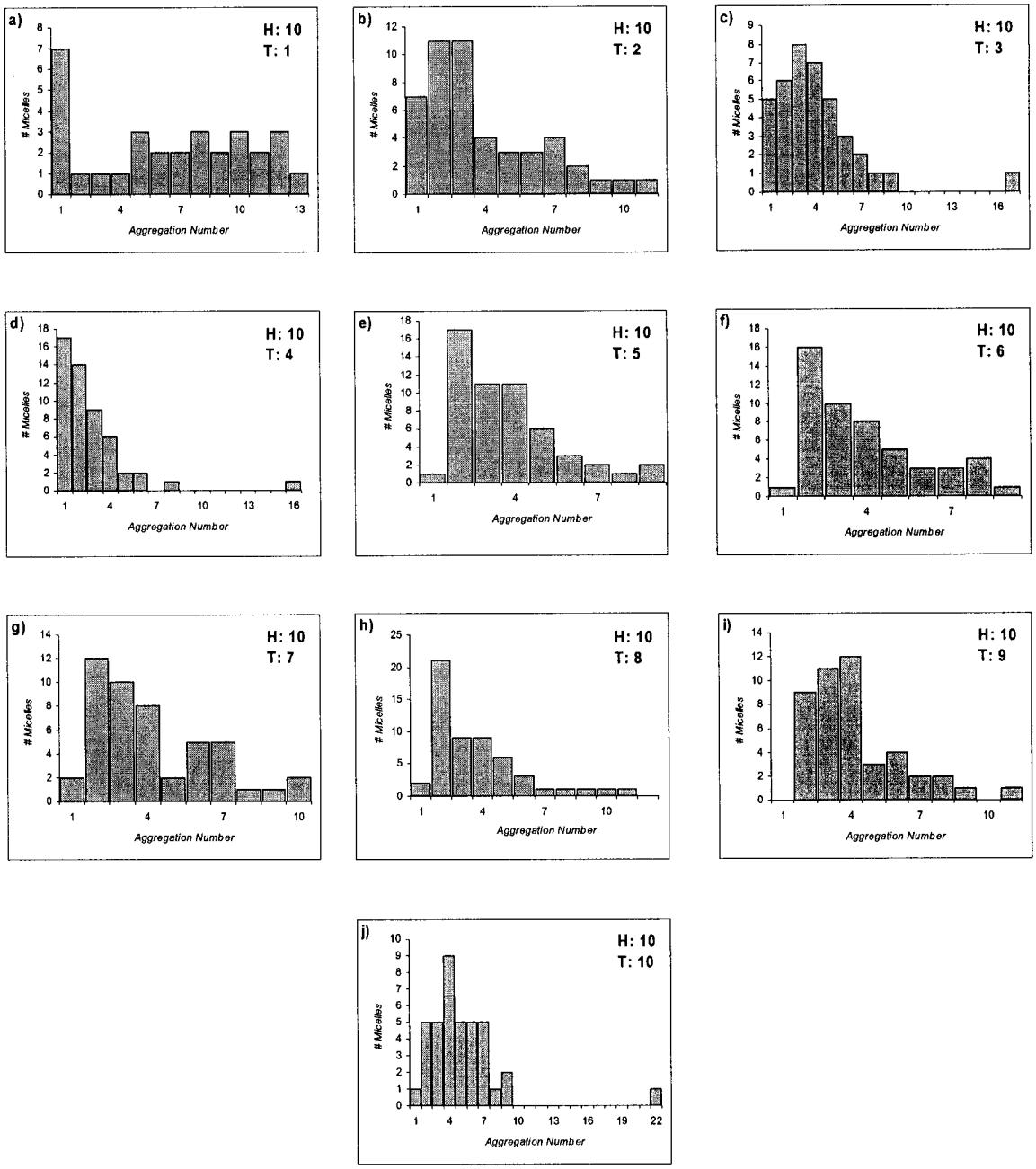


Figure 4.9. Micelle number distribution profiles for polymers with 10 hydrophilic head (H) units and varying [1(a) to 10 (l)] hydrophobic tail (T) units.

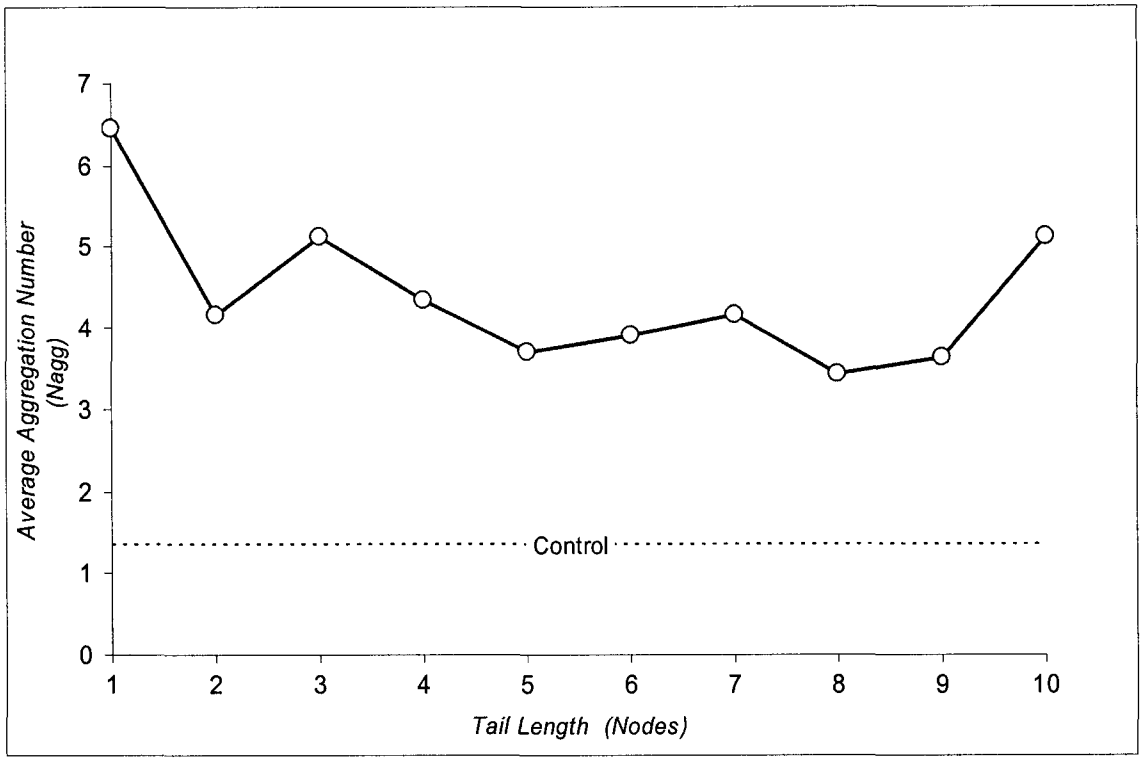


Figure 4.10. Average micelle aggregation number as a function of tail length for polymers with 10 hydrophilic head (H) units and varying [1(a) to 10 (l)] hydrophobic tail (T) units.

The system energy profiles for the hydrophobic block size-varying simulations (Figure 4.8) indicate that for small hydrophobic blocks, the contribution to the overall system energy upon micellization is small compared the contribution of the hydrophilic-block—solvent interaction. The profiles for these simulations therefore appears essentially linear for tail lengths less than 7 units. As the tail block size increases, the contribution to overall energy also increases, and a small descent in system energies is discernable. For systems with less than 10 hydrophobic blocks, the descent is rapid, reaching equilibrium within $0.5 \times 10^6$ iterations (Figure 4.8-g – 4.8-i).. It is only for the micelle simulation with 10 hydrophobic blocks that the system appears to gradually descend to a minimum over approximately $2 \times 10^7$ iterations.

The micelle distribution profiles for simulations with 2 to 9 tail units exhibit a decreasing number of unimer and dimer with increasing number of tail units. There is also a trend towards an increasingly Gaussian distribution with increasing number of tail units. The average micelle number remains essentially constant at between approximately 3 and 4 polymers/micelle. An interesting exception occurs for the simulation with a single tail unit, which displays essentially equal numbers of micelles with aggregation numbers between 2 and 13 polymers / micelle (Figure 4.9-a). There is a strikingly high average aggregation of 6.5 for this simulation (Figure 4.10), the highest of all the simulations conducted in this study. These behaviours imply that the micelles are becoming increasingly stable with increasing tail number, due likely to the increased number of contacts between neighboring hydrophobic blocks and increased entanglement. As the number of neighbor contacts increase, the amount of energy required to escape from a micelle increases, making dissociation more difficult. As the the entanglement of polymers increases, the 'escape route' from a micelle becomes more convoluted and decreases the polymers chances at dissociating. The simulation with a single tail unit is not subject to entanglement and needs only a single reptation move to dissociate from the micelle. As a consequence, this simulation is unique from the others and this is reflected in the observed behaviours.

Overall the average aggregation numbers are low compared to real polymer micelle systems, which typically have greater than 10 polymer units per micelle. This is a reflection of the course grid size and the reptation movement. In the simulations, the 'path' that a unimer may take through the systems is limited to the nodes in the cubic

lattice. As micelles form the entry and exit paths to the micelles become reduced, effectively trapping the micelles at the observed low aggregation numbers.

In Chapter 3 of this thesis, block copolymers composed of PEO as the hydrophilic block, and poly (L-tyrosine) and the hydrophobic block, where constructed with block lengths of 7, 9, 12, and 15 residues, and examined for their micellization behaviour. As with these simulations, micelle stability increased with increasing block length, as judged by the CMC. Micelle static stability also increased, as judged by the micelle dissociation rate at concentrations below the CMC, with a dramatic increase in micelle stability for PEO-poly(L-tyrosine) with 15 amino acid units. The corresponding experiment for the Monte Carlo simulations has yet to be performed, so it is premature to draw any parallels between micelle dynamic stability for the real and *in silico* experiments. Dynamic stability *in silico* could be observed by increasing the volume of the lattice to a size expected to be below the CMC and monitoring the dissociation of micelles back into unimers. This experiment could provide valuable the necessary information to 'calibrate' the simulations to real systems of block copolymer micelles.

## 4.4. Conclusion

A model was developed for micelle formation using Monte Carlo simulations on a cubic lattice. The effect of intermolecular interaction energy were simulated and shown to reproduce empirically observed behaviors for real colloidal systems of nonionic block copolymers. Successful simulation of the metastable states associated with "hot" and "cold" systems and the transition state between freely exchanging unimers and polydisperse supramolecular aggregate suggests that this simulation this model may be

extended for use in the eventual simulation of micelle behaviours relevant to drug delivery systems. Observation of the effect of hydrophobic block length on tail behaviour showed a qualitative agreement with the observations of real colloidal systems of nonionic block copolymer micelles. Further experimentation *in silico* may allow for a calibration between Monte Carlo simulations and real systems of block copolymer micelles.

## 4.5. References


1. Kwon G.S. and Kataoka K. (1995) Block copolymer micelles as long-circulating drug vehicles. *Adv. Drug Deliv. Rev.* **16**:295-309.

2. Zoeller N., Lue L., and Blankshtein D. (1997) Statistical-Thermodynamic Framework to Model Nonionic Micellar Solutions. *Langmuir* **13**:5258-5275.

3. Zoeller N., and Blankshtein D. (1995) Development of user-friendly computer programs to predict solution properties of single and mixed surfactant systems. *Ind. Eng. Chem. Res.* **34**:4150-4155.

4. Scheutjens J.M. and Fleer G.J. (1979) Statistical theory of the adsorption of interacting chain molecules. 1. Partition function, segment density distribution, and adsorption isotherms *J. Phys. Chem.* **83**:1619-1635.

5. Hurter P.N., Scheutjens J.M., and Hatton T.A. (1993) Molecular modeling of micelle formation and solubilization in block copolymer micelles. 1. A self-consistent mean-field lattice theory. *Macromolecules* **26**:5592-5601.

6. Nagarajan R. and Ruckenstein E. (2000) Molecular Theory of Microemulsions. *Langmuir* **16**:6400-6415.

7. Leibler L. (1983) Theory of critical micelle concentration for solutions of block copolymers. *J. Chem. Phys.* **79**:3550-3557.

8. Cifra P., Karasz F.E., and MacKnight W.J. (1988) Distribution of interactions in binary polymer mixtures: a Monte Carlo simulation study. *Macromolecules* **21**:446-451.

9. Cifra P., Karasz F.E., and MacKnight W.J. (1989) Computer simulation of copolymer-copolymer and copolymer-homopolymer mixtures with a single interaction energy. *Macromolecules* **22**:3649-3653.

10. Rodrigues K. and Mattice W.L. (1991) Simulation of the Steric Stabilization of Polymer Colloids by Diblock Copolymers. *J. Chem. Phys.* **94**:761-766.

11. Wang Y. and Mattice W.L. (1993) Simulation of the Formation of Micelles by Diblock Copolymers under Weak Segregation. *Langmuir* **9**:66-70.

12. Sommer J.U., Peng G., and Blumen A. (1996) Copolymers at interfaces: Scaling and Monte Carlo studies. *J. Phys. II France* **6**:1061-1066.

13. Giessler K.H., Rauch F., and Stamm M. (1994) Influence of confinement on the order of diblock copolymer films. *Europhysics Lett.* **27**:605-610.

14. Talsania S.K., Wang Y., Rajagopalan R., and Mohanty K.K. (1997) Monte Carlo Simulations for Micellar Encapsulation. *J. Colloid and Interface Sci.* **190**:92-103.

15. Verdier P.H. and Stockmayer W.H. (1962) Monte Carlo Calculations on the Dynamics of Polymers in Dilute Solution. *J. Chem. Phys.* **36**:227-230.

16. Mackie A.D., Onur K., and Panagiotopoulos A.Z. (1992) Phase equilibria of a lattice model for an oil–water–amphiphile mixture. *J. Chem. Phys.* **104**:3718-3725.

17. de Gennes P.G. (1971) Reptation of a polymer chain in the presence of fixed obstacles. *J. Chem. Phys.* **55**:572-579.

18. Metropolis N., Rosenbluth A.W., Rosenbluth M.N., and Teller A.H. (1953) Equation of state calculations by fast computing machines. *J. Chem. Phys.* **21**:1087-1091.

19. Kratochvil P. and Tuzar Z. (1992) Self-association of block copolymers in solution: copolymer micelles. *Polymer Preprints* **41**:135-138.

20. Nakanishi T., Fukushima S., Okamoto K., Suzuki M., Matsumura Y., Yokoyama M., Okano T., Sakurai Y., and Kataoka K. (2001) Development of the polymer micelle carrier system for doxorubicin. *J. Control. Rel.* **74**:295-302.

21. Mortensen K. (1998) Structural properties of self assembled polymeric micelles. *Curr. Opin. Colloid Interface Sci.* **3**:12-19.

22. Garardi M. and Figueiredo W. (2000) Transition in three-dimensional micellar systems.

# CHAPTER 5. CONCLUSION

Solid phase peptide synthesis has a great deal to offer the field of drug delivery. SPPS allows each subunit in the polymer to be individually selected and incorporated into the polymeric structure, thus giving the polymer construct a well-defined and finely tailored chemical composition. Furthermore, the amino acid building blocks used in SPPS are a natural fit in a field that stresses biocompatibility. The wide range of chemical properties inherent in the collection of readily available amino acids for SPPS lends flexibility to the design of drug delivery systems. These advantages have been demonstrated in the design and synthesis of two very different types of delivery systems: 1) labeled peptides for radioimaging and 2) block copolymer micelles for the delivery of small hydrophobic drugs. Computer modeling of micelle formation for drug delivery promises to reduce the amount of time and effort involved in producing drug-polymer compositions with adequate drug delivery properties.

## 5.1. The Bz-MAG3-P3 Chelator-Spacer

As detailed in Chapter 2 of this thesis, a chelator-spacer system was described for $^{99m}$Tc-based peptide receptor radioimaging. The bifunctional chelator was designed based on mercaptoacetyltriglycine, which is well known for its excellent stability, high labeling yield, and strong resistance to transchelation. Synthesis of the triglycyl portion of MAG3 by SPPS is straightforward. The protecting group for the mercaptoacetyl's sulfhydryl is required to survive the conditions of SPPS, cleavage, and purification, remain stable during storage, and deprotect *in situ* during radiolabeling. Our studies

show that a simple benzoyl protecting group satisfies all of these requirements when the addition of benzoylmercaptoacetic acid is restricted to the last step of the synthesis.

Proline was chosen as a spacer group to separate the bz-MAG3 chelator and the targeting peptide. A minimum of three prolines in the linker was found to minimize the potential for chelation interference from the targeting peptide. Several bz-MAG3-$P_3$-peptides were synthesized entirely by SPPS and shown to possess high labeling efficiency, high resistance to transchelation, and minimal loss of receptor targeting ability.

From this work several important conclusions can be drawn. Foremost is that the synthesis, stability, labeling protocols, and biological activity of peptides prepared and labeled by this method meet the requirements for radiopharmaceutical peptides. This observation suggests that these techniques can be applied to the construction of many other targeting peptides for radiopharmaceutical imaging. Because SPPS is a simple, general and readily available synthetic technique, there is a tremendous advantage in using an all-SPPS strategy to construct BFCA-peptides for radiopharmaceutical imaging. Secifically, the amount of expertise and labor required to develop these constructs is significantly reduced. This fact can be exploited to test a greater number of candidate targeting peptides in a shorter amount of time.

The work described in Chapter 2 focused on the use of triproline as a spacer group to separate the chelator from the targeting peptide, however, the synthetic method developed here can accommodate other spacers as well. 4-aminobutyric acid and 6-aminocaproic acid are available as Fmoc-protected amino acids and can be used as flexible, low molecular weight spacers, although there is potential for chelation interference from the amide proton. Fmoc-protected heterobifunctional PEG derivatives

are also commercially available and may be used as potential linkers. PEO is nonimmunogenic and can extend the circulation time of the radiolabeled BFCA-peptide, although the large molecular weight (3400 a.m.u.) relative to the targeting peptide may make this option less desirable than the lower molecular weight alternatives.

This work also has implications for the production of radiolabeling proteins and peptides produced by recombinant methods. By replacing the mercaptoacetyl group with the natural amino acid cysteine, the sequence Cys-Gly-Gly-Gly-Pro-Pro-Pro could be genetically introduced to larger peptides and proteins, thus providing a chelator-spacer system for labeling with $^{99m}$Tc. Although this method likely would not have the same high labeling efficiency as MAG3-$P_3$, it would be a significant improvement over direct labeling and may be preferred over the preformed chelate approach.

## 5.2. PEO-*b*-Peptide Block Copolymer Micelles

In Chapter 3 a simple and versatile SPPS-SPC method was described for the construction of PEO-*b*-peptide block copolymers. To demonstrate its utility and versatility we employed this technique in the construction of a number of PEO-*b*-peptide block copolymers with precisely defined sequence compositions and sizes. All constructs investigated demonstrated the ability to micellize in aqueous solvents. A systematic study of block copolymer core composition and size yielded a block copolymer construct with suitable properties for drug loading.

These initial studies show SPPS to be a powerful and flexible method for constructing block copolymers for drug delivery. This flexibility can be exploited to

enhance micelle drug delivery in numerous important ways, such as polymer crosslinking, incorporation of drug conjugation sites, incorporation of enzyme-specific cleavage sites, complete block copolymer synthesis by SPPS, and attachment of peptide-based targeting moieties for receptor targeting.

### 5.2.1. Polymer Crosslinking

Crosslinking of the block copolymer micelle core can be useful in situations where an extended release of drug is desired. In these cases, drug release ideally is limited by diffusion as opposed to micelle degradation. Crosslinking can be easily accomplished by the judicious incorporation of two or more cysteine residues into the core-forming polymer backbone to create a telechelic core-forming block. Upon micelle formation and drug loading, the micelle-drug formulations could be subjected to oxidizing conditions. Crosslinking is effected by disulfide bridge formation between the different cysteine sulfhydryls.

### 5.2.2. Incorporation of Drug Conjugation Sites

Conjugation of drugs into the core-forming block backbone has been studied in some detail [1,2]. A number of these systems already use poly(L-amino acids) for the core-forming block. Hydrophobic drugs can be conjugated to the polymer backbone through the amino acid reactive side chain. Most of these systems rely on poly(L-amino acids) based on L-aspartic acid and L-glutamic acid. SPPS expands the range of available amino acids available for drug conjugation to include for example L-cysteine, L-lysine, and a host of specialty amino acids. SPPS allows these reactive side chain residues to be incorporated selectively. Unreactive hydrophobic amino acids could also be included to

drive the micellization process, thereby separating the micellization and drug conjugation requirements. This potentially would allow less hydrophobic drugs to be incorporated into the micelle and still effect micellization and drug delivery.

### 5.2.3. Enzymatic Substrate Incorporation

For drug-conjugated polymers, the polymer-drug linker plays a crucial role in drug release and must be optimized to allow for facile release and activation at the drug target. Drug conjugation to the core forming block of the micelle is typically carried out through a hydrolytically sensitive covalent bond such as an amide or ester bond. This conjugation methods risks the chance of premature hydrolysis of the linker and can lead to disappointing results. One attractive alternate strategy involves the incorporation of enzyme specific cleavage sites between the drug and the polymer. This strategy has been studied previously using N-(2-hydroxypropylmethacrylamide) (HPMA) conjugated to doxorubicin through a -Gly-Phe-Leu-Gly- peptidyl linkage [3]. The drug is cleaved by the lysosomal thiol-dependant protease cathepsin B following endocytic uptake of conjugate from the tumour interstitium. SPPS can easily accommodate this strategy by incorporating orthogonally protected amino acids into the peptide polymer backbone and building the cleavage site onto the amino acid side chain. This strategy can be used for engineering peptide drugs directly into the polymer as well. It is conceivable that peptide drugs can be introduced directly into the polymer by building the peptide into the interfacial region between the hydrophilic block and the hydrophobic block. By flanking the peptide sequence with enzyme-specific cleavage sites, a multipartite polymer could be created that should theoretically possess micellization and drug delivery properties similar to conventional drug-block copolymer conjugates.

### 5.2.4. Peptide-Based Targeting

The addition of targeting ligands to the micelle surface has been proposed to impart active targetability to block copolymer micelles. To date there exists only two published study on creating block copolymer micelles with surface-coated peptides [4,5]. SPPS could be used to construct block copolymer micelles with targeting surface peptides as well. The primary difficulty here lies in the addition of large PEO blocks to the polymer bead during SPPS, as their size is significantly larger than the average pore size of standard resins available for SPPS. This problem can be overcome by a combined approach, using a macroporous SPPS resin with multiple condensations of smaller (e.g. 2500 a.m.u.) Fmoc-derivatized heterobifunctional PEO blocks. The Fmoc-PEO allows for the addition of the targeting peptide to the $\omega$-terminus of PEO. In this way the entire targeting block copolymer can be constructed completely by SPPS.

## 5.3. Nonionic Block Copolymer Modeling

The systematic experimental analysis of block copolymer micelle behavior described in Chapter 3 yielded interesting and useful results, however the amount of time and effort involved in this type of study placed heavy demands on time and effort. To address this issue, a preliminary investigation was conducted to see if computer simulations could be applied to design block copolymer constructs for drug delivery. A modeling program was written to simulate nonionic block copolymer micelle formation using Monte Carlo energy minimization on a cubic lattice. The modeling system successfully reproduced observed behaviours for real world colloidal systems such as

metastable states and critical micellization temperature. It is possible that these simulations could be extended to examine other properties relevant to drug delivery such as behaviour in sink conditions and stability differences between unloaded and drug-loaded micelles. The approximate nature of these Monte Carlo simulations restricted these analyses to qualitative interpretation only, and this is a set-back for predicting which block copolymer compositions may provide the optimal drug delivery properties. Further experimentation may allow for a rough calibration between these simulation and real world simulations. As simulation sophistication and computing power increase, the level of detail attainable by these *in silico* investigations of block copolymer micellization behaviour may eventually reach the point where quantitative predictions can be obtained.

## 5.4. References


1. Gros L., Ringsdorf H., and Schupp H. (1981) Polymeric antitumour agents on a molecular and on a cellular level? *Angnew. Chem. Int. End. Engl.* **20**:305-325.

2. Kwon G.S. (1998) Diblock copolymer nanoparticles for drug delivery. *Crit. Rev. Ther. Drug Carrier Syst.***15**:481-512.

3. Satchi R., Connors T.A., and Duncan R. (2001) PDEPT: Polymer-directed enzyme prodrug therapy. I. HPMA copolymer-cathepsin B and PK1 as a model combination. *Brit. J. Cancer* **85**:1070-1076.

4. Kataoka K. (1998) The reactive polymeric micelle based on an aldehyde-ended poly(ethylene glycol)/poly(lactide) block copolymer. *Macromolecules* **31**:1473-1479.

5. Yamamoto Y., Nagasake Y., Kato M., and Kataoka K. (1999) Surface charge modulation of poly(ethylene glycol)-poly(D,L-lactide) block copolymer micelles: conjugation of charged peptides. *Colloids and Surfaces B: Biointerfaces* **16**:135-146.